UNIVERSIDADE DE LISBOA
FACULDADE DE CIÊNCIAS
DEPARTAMENTO DE FÍSICA

Clinical Validation of an Optical Surface Detection System for Stereotactic Radiosurgery with Frameless Immobilization Device in CNS Tumors

Cristiana Margarida Nunes Soares Oliveira Santos

Mestrado Integrado em Engenharia Biomédica e Biofísica
Perfil de Radiações em Diagnóstico e Terapia

Dissertação orientada por:
Professor Doutor Nuno Miguel de Pinto Lobo e Matela
Professor Especialista Filipe Martins Garcia Cidade de Moura

2022

Em memória dos meus avôs, Aníbal e Cândido

"We are very, very small, but we are profoundly capable of very, very big things."
— Stephen Hawking

Acknowledgements

I would like to share my gratitude with the entire team of the Radiotherapy Department of Hospital CUF Descobertas, especially to the Clinical Director Dr. Gonçalo Fernandez, for making this investigation possible. Thanks to all radiation therapists and physicists for their availability and time, making this experience more enriching, and for all the support I was given throughout the project.

I am particularly grateful to the exceptional Prof. Filipe Moura, who was always present throughout my academic journey, as a teacher and mentor, having played an important role in my Bachelor's degree and now in my Masters. To you, my dear colleague and friend, a thank you is not enough. I will be eternally grateful for the opportunities he has given me, on several occasions, and for supporting and challenging me always to be the best version of myself. The professional I became has a large part to do with his work ethic. He taught me that all goals are attainable with willpower, perseverance and humility.

I want to thank the distinguished Prof. Nuno Matela for accepting the invitation and for guiding my work on this master thesis. All the suggestions and incentives he provided me played an important role in this project. My gratitude goes especially for his availability, kindness and support with all students that reach for his help throughout the overall academic journey.

To my best friends; for the nights of laugh, enjoyments and adventures. Being always by my side.

Nevertheless, the most important acknowledgment goes to my family which is the foundation, stability and key for my success. I would like to thank my parents, Teresa and Paulo, for always supporting me and respecting my decisions, I will permanently look forward them and be grateful for everything they have given me. They are my everything.

To my grandmothers, Olívia and Ideliberta, who raised me and taught me so much about life, I hope they can stay as many years as possible by my side, watching me growing continuously, and sharing their love and affection. Their life stories were the encouragement to overcome myself.

Last but not least, a special thanks to my best friend and partner, Daniel, who has been by my side from the beginning of this journey and so many others. For always making me see the better picture in things. Your words of encouragement, understanding, love and patience, will be forever in my heart. For all the happy moments we shared. Thank you.

Agradecimentos

Em primeira instância, gostaria de compartilhar a minha gratidão com toda a equipa do Serviço de Radioterapia do Hospital CUF Descobertas, especialmente ao Diretor Clínico, Dr. Gonçalo Fernandez, por tornar esta investigação possível. Obrigado a todos os radioterapeutas e físicos pela sua disponibilidade e tempo, tornando esta experiência mais enriquecedora, e por todo o apoio que me foi facultado durante todo o projeto.

Um agradecimento ao excecional Prof. Filipe Moura, que esteve sempre presente durante todo o meu percurso académico, como professor e mentor, tendo desempenhado um papel importante na minha Licenciatura e agora no Mestrado. A ti, meu caro colega e amigo, um obrigado não é suficiente. Serei eternamente grata pelas oportunidades que me presenteou, em diversas ocasiões, e por apoiar-me e desafiar-me sempre a ser a melhor versão de mim mesma. A profissional que me tornei tem em grande parte que ver com a sua ética de trabalho. Ensinou-me que todos os objetivos são alcançáveis com força de vontade, perseverança e humildade.

Quero fazer um agradecimento ao exímio Prof. Nuno Matela, por ter aceitado o convite e por orientar o meu trabalho nesta dissertação de mestrado. Todas as sugestões e incentivos que me forneceu tiveram um papel importante neste projeto. Quero agradecer particularmente pela sua disponibilidade, amabilidade e apoio como docente a todos os alunos que procuram a sua ajuda durante o percurso académico.

Aos meus melhores amigos; por todo o percurso conjunto que partilhamos. Sempre a meu lado.

Não obstante, o reconhecimento mais importante de todos é dado à minha família, que é o alicerce; a estabilidade e a chave do meu sucesso. Gostaria de agradecer aos meus pais, Teresa e Paulo, por me apoiarem sempre e respeitarem as minhas decisões. São eles por quem me guio e serei eternamente grata por todas as oportunidades que me proporcionaram. São o meu ‘tudo’.

Às minhas avós, Olívia e Ideliberta, que me criaram e ensinaram tanto sobre a vida. Espero que possam ficar ainda muitos anos a meu lado, vendo-me crescer pessoalmente e profissionalmente, compartilhando o seu amor e carinho. As suas histórias de vida foram um grande incentivo para mim.

Por último, mas não menos importante, um agradecimento especial ao meu melhor amigo e companheiro, Daniel, que esteve ao meu lado desde o início desta jornada e de tantas outras. Por sempre me fazer ver a realidade das coisas. Pelas palavras de encorajamento, pela compreensão, amor e paciência, que ficarão para sempre em meu coração. Por todos os momentos felizes que compartilhamos. Obrigado.

Abstract

Stereotactic Radiosurgery (SRS) has been consolidated in recent years as the treatment of choice in selected central nervous system (CNS) tumors. With the introduction of stereotactic approach in clinical practice, accurate immobilization and motion control during treatment becomes fundamental. During SRS treatments, the common practice is to immobilize CNS patients in a cushion molded head support, with specific open-face thermoplastic masks. To verify and correct internal isocenter uncertainties before and during treatment, X-Ray volumetric imaging (XVI) is performed - image guided radiation therapy (IGRT).

An alternative to mid-treatment imaging is optical surface detection (OSD) imaging – a non-invasive, non-radiographic form of image guidance – to monitor patient intra-fraction motion. This imaging technique has shown to properly position, accurately monitor, and quantify patient movements throughout the entirety of the treatment – surface guided radiation therapy (SGRT).

The aim of this investigation is to test the viability of the implementation of a maskless immobilization approach, using only a vacuum mouthpiece suction system for head fixation in patients with CNS tumors who will undergo SRS treatment under the guidance of an OSD system coupled with 6-Degree of Freedom (6-DOF) robotic couch for submillimeter position correction. This master thesis addresses the five technical performance tests conducted on the Linear Accelerator components – XVI, HexaPOD couch and OSD system in the Radiotherapy Department of Hospital CUF Descobertas.

The results obtained lecture the best acquisition orientation to perform image verification; if the HexaPOD couch is correctly calibrated to the XVI radiation isocenter to assure submillimeter corrections; OSD system performance regarding phantom surface detection since some immobilization components can block the signal reading; which coplanar and non-coplanar angles occur most signal inconsistencies due to camera pod occlusion; what is the overall OSD system accuracy and what is the best non-coplanar angle arrangement to perform an SRS treatment with OSD system monitoring.

Keywords: Stereotactic Radiosurgery; Surface Guided Radiation Therapy; Optical Surface Detecting System; Frameless Immobilization; CNS Tumors.

Resumo

A Radiocirurgia Estereotáxica é uma modalidade terapêutica de alta precisão que se tem consolidado nos últimos anos como o tratamento de seleção em casos selecionados de tumores benignos e malignos do sistema nervoso central. A sua principal vantagem prende-se com a possibilidade de administrar uma dose altamente conformada e localizada no tumor, resultando numa redução do tecido cerebral normal irradiado, minimizando o risco de consequências do tratamento a longo prazo. Para a realização de técnicas especiais como o tratamento hipofracionado, são necessários dois pré-requisitos fundamentais: imobilização precisa do doente e monitorização intra-fração no tratamento. Com a introdução da abordagem estereotáxica na prática clínica, uma imobilização precisa torna-se imprescindível nos dias decorrentes, uma vez que a configuração do doente em cada fração do tratamento de radioterapia é afetada por inúmeras incertezas. As abordagens de radiocirurgia mais recentes fazem uso de sistemas de imobilização não invasivos para o doente. Para a realização desta técnica, a prática clínica comum prende-se em posicionar os doentes com patologia do sistema nervoso central num apoio de cabeça específico, constituído por uma almofada de vácuo ajustada à anatomia cervical do doente com uma máscara termoplástica adaptada à face do mesmo, ou uma máscara termoplástica de face aberta com um sistema de sucção a vácuo dental que permite a correta fixação do palato do doente e respetiva imobilização do mesmo. Antes da realização do tratamento é imprescindível a realização de imagens, sendo que as mesmas permitem efetuar as correções necessárias tendo em consideração as estruturas internas do doente e por conseguinte, aplicar os desvios para atingir a posição ideal de tratamento. Este tipo de realização de imagem designa-se radioterapia guiada por imagem, que utiliza um sistema de localização específico por meio de imagem volumétrica através de Raios-X, que visa verificar e corrigir incertezas do isocentro com precisão submilimétrica. Este tipo de modalidade pode ser realizado até três vezes durante o tratamento – antes, durante e após, de modo a verificar as estruturas internas tendo em consideração a alta dose administrada.

Uma alternativa à imagem volumétrica através de Raios-X é a imagem reconstruída através da deteção ótica da superfície, que permite realizar um varrimento tridimensional (3D) da superfície do doente, permitindo monitorizar o movimento intra-fração – durante todo tratamento. Recentemente, os sistemas óticos de deteção de superfície tornaram-se fidedignos como uma forma não invasiva e não ionizante de monitorizar o doente. As combinações de técnicas de imagem ótica através de laser em tempo real permitem posicionar adequadamente os doentes, monitorizar com precisão e quantificar o movimento dos mesmos durante todo o tratamento, denominada – radioterapia guiada por superfície. Foi comprovado que esta técnica pode ser realizada com segurança e precisão submilimétrica em patologias da cabeça e pescoço e sistema nervoso central, utilizando máscaras de imobilização de face aberta. A irradiação precisa de um tumor só é possível se a magnitude das incertezas do equipamento e as que ocorrem durante a administração do tratamento forem conhecidas e contabilizadas. Desse modo, é fundamental realizar testes e quantificar a precisão de um sistema para definir um protocolo de tratamento antes de implementar uma nova técnica.

O objetivo desta investigação prende-se em testar a viabilidade da hipótese que consiste em implementar uma abordagem de imobilização sem máscara, apenas com um sistema de imobilização a vácuo do palato, que permitirá a total imobilização da cabeça em doentes com tumores do sistema nervoso central que serão submetidos a radiocirurgia, sob a monitorização de um sistema ótico que permite a deteção da superfície do doente, concomitantemente à utilização de uma mesa robótica que permite fazer correções submilimétricas do mesmo em seis graus de liberdade.

Para validar a hipótese relativa à implementação de um sistema ótico de deteção de superfície concomitantemente à utilização de um sistema de imobilização a vácuo do palato durante a radiocirurgia, esta dissertação de mestrado aborda os cinco testes técnicos realizados ao sistema XVI, mesa HexaPOD e o sistema ótico de deteção de superfície do Serviço de Radioterapia do Hospital CUF Descobertas, com todos os dados registados no presente estudo. Os fantomas utilizados no estudo foram o fantoma QUASAR™ Penta-Guide, um fantoma de cabeça antropomórfico e um busto. O fantoma Penta-Guide possui um design simples e inovador que facilita a verificação intuitiva do alinhamento espacial e coincidência de isocentros entre os sistemas de imagem volumétrica e de superfície guiada. O fantoma de cabeça antropomórfico foi construído manualmente para reproduzir a estrutura interna e externa da cabeça humana. Todos os testes foram realizados no acelerador Linear Elekta Versa HD (Elekta AB, Estocolmo, Suécia), equipado com uma mesa robótica com um sistema HexaPOD™ com seis graus de liberdade e um sistema XVI para realização de tomografia computadorizada de feixe cónico. Inicialmente realizou-se uma tomografia computorizada a cada fantoma e busto, através de uma Tomografia Computorizada - Discovery Radiotherapy (RT) Scanner (da GE Healthcare, EUA). Posteriormente as imagens dos fantomas foram transferidas para o sistema de planeamento de tratamento - Monaco (Elekta AB, Estocolmo, Suécia). Um plano foi construído para cada fantoma e busto no sistema Monaco, tendo sido localizado o isocentro no centro de cada fantoma e busto. Todas as imagens de tomografia computorizada foram transferidas para o sistema XVI.

Os testes realizados foram:

- 1º Teste – Avaliação do Erro Sistemático do Cone Beam Computed Tomography (CBCT) - XVI – Clockwise (CW) e Counter Clockwise (CC);
- 2º Teste – Avaliação do Erro Mecânico entre a mesa HexaPOD e o XVI durante rotações de mesa;
- 3º Teste – Desempenho do Sistema Ótico de Deteção de Superfície em Ângulos Coplanares;
- 4º Teste – Desempenho do Sistema Ótico de Deteção de Superfície com Rotações de Mesa;
- 5º Teste – Avaliação do Erro Posicional entre o Sistema Ótico de Deteção de Superfície e a mesa HexaPOD em Ângulos Não Coplanares.

Os resultados obtidos no 1º teste mostram que o XVI tem um erro sistemático que ocorre sempre com a mesma variação e magnitude independentemente do tipo de aquisição - CW ou CC, correspondendo a um desvio de -0,3 mm no eixo translacional longitudinal. Em relação ao eixo rotacional, o XVI apresentou um erro sistemático de 0,1° no sentido roll em todas as aquisições CW, e 0,3° no sentido roll em todas as aquisições CC. Os resultados demonstram que não há diferenças significativas em realizar um CBCT em CW ou CC neste estudo. No 2º teste a maior diferença entre a mesa HexaPOD e o XVI ocorreu no eixo longitudinal, com um erro mecânico de 0,4±0,1 mm na rotação da mesa de 30°; 45°; 285°; 300° e 345° respetivamente. Este resultado corrobora a literatura quanto à precisão do sistema HexaPOD, sendo o mesmo referido como 0,5±1 mm para um IC de 95%. Além disso, os resultados estão dentro da tolerância de 1 mm sugerida pela AAPM TG142, que tem em consideração a coincidência do isocentro de radiação e isocentro mecânico. Relativamente ao 3º teste, o desempenho do sistema ótico depende diretamente da não oclusão das câmaras presentes na sala. Nos ângulos em que o acelerador linear oclui uma ou duas câmaras devido ao detetor XVI, ampola de Raio-X do XVI ou cabeça da gantry, existe uma menor leitura da superfície do fantoma, e consecutivamente, uma monitorização mais imprecisa. Os valores do Couch Relative – os deslocamentos de isocentro necessários – confirmam ser maiores nos ângulos oblíquos anteriores, correspondendo a um deslocamento do vetor translacional de 0,4 mm no angulo oblíquo anterior esquerdo - 45º, e 0,3 mm no angulo oblíquo anterior direito - 315º. O 4º teste consistiu na rotação da mesa com a gantry a 0º. Este teste teve dois objetivos; o primeiro foi avaliar se o erro do sistema ótico

varia em magnitude em relação à rotação da mesa; o segundo foi testar o desempenho do sistema ótico na deteção da superfície do fantoma antropomórfico durante as rotações da mesa. Os erros de maior magnitude foram observados nas rotações direitas da mesa, 30°, 60° e 90°, respetivamente. Este resultado prova que o sistema ótico demonstra um melhor desempenho na deteção da superfície do fantoma com a câmara central e lateral esquerda. O erro com maior magnitude do sistema ótico no eixo lateral foi detetado com a mesa a 90° correspondendo a um deslocamento de 1,2 mm; no eixo longitudinal foi detetado também com a mesa a 90º correspondendo a um deslocamento de -1,1 mm, e no eixo vertical com a mesa a 300° correspondendo a um deslocamento de 0,4 mm. No 5º teste, as correções sugeridas pelo sistema ótico com base na superfície do fantoma demostram variar independentemente da angulação da gantry e da rotação da mesa. Contrariamente, os deslocamentos de isocentro calculados pela mesa HexaPOD parecem ser reprodutíveis em cada rotação da mesa independentemente da angulação da gantry. Os dois sistemas mostram uma concordância global dentro de 1 mm em todos os eixos translacionais, para a maioria das rotações da mesa e angulações da gantry. As maiores discrepâncias entre os dois sistemas ocorreram com a angulação da gantry a 45º para as maiores rotações de mesa, principalmente no eixo lateral.

Palavras-Chave: Radiocirurgia Estereotáxica; Radioterapia Guiada por Superfície; Sistema Ótico de Deteção de Superfície; Imobilização Não-Invasiva; Tumores do Sistema Nervoso Central

Table of Contents

List of Figures

List of Tables

List of Equations

Acronyms

2D – Two Dimensional

3D – Three Dimensional

3D-CRT – Three-Dimensional Conformal Radiation Therapy

4D – Four Dimensional

6-DOF – Six Degrees of Freedom

AAPM – American Association of Physicists in Medicine

AP – Antero-Posterior

BAT – B-Mode Acquisition and Targeting

CA – Couch Absolut

CBCT – Cone Beam Computed Tomography

CCD – Charged-Coupled Device

CC – Counterclockwise

CI – Conformity Index

cm – Centimeter

cm^3 – Cubic Centimeter

cm/s – Centimeter per Second

CNS – Central Nervous System

CR – Couch Relative

CT – Computed Tomography

CTV – Clinical Tumor Volume

CW – Clockwise

$D_{2\%}$ - Near-Minimum Dose

$D_{50\%}$ - Half-Maximal Dose

$D_{98\%}$ - Near-Maximum Dose

DIBH – Deep Inspiration Breath Hold

$D_{near\text{-}max}$ – Near-Maximum Dose

$D_{near\text{-}min}$ – Near-Minimum Dose

DRRs – Digitally Reconstructed Radiographies

FDG – Fluorodeoxyglucose

FFF – Flattening Filter Free

FOV – Field of View

FSRT – Fractionated Stereotactic Radiotherapy

GI – Gradient Index

GTV – Gross Tumor Volume

Gy – Gray

HD – High Definition

H&N – Head and Neck

ICRU - International Commission on Radiation Units and Measurements

IGRT – Image Guided Radiation Therapy

IMRT – Intensity Modulated Radiation Therapy

IRLED – Infrared Light-Emitting Diode

IS – Inferior-Superior

ITV – Internal Target Volume

keV – Kiloelectron Volt

Kg – Kilogram

kV- Kilovoltage

kV-CBCT – Kilo-Voltage Cone Beam Computed Tomography

LED – Light-Emitting Diode

LINAC – Linear Accelerator

m^2 – Square Meter

MaxFOF – Maximum Field of View

MeV – Megaelectron Volt

mGy – Microgray

MLC – Multi-Leaf Collimator

mm – Millimeter

MRI – Magnetic Resonance Imaging

nm – Nanometer

MV – Megavolt

OARs – Organs at Risk

OBI – On-Board Imaging

OSD – Optical Surface Detection

PCU – Patient Control Unit

PE – Positional Error

PET – Positron Emission Tomography

PIV – Prescribed Isodose Volume

PIV_{half} - Volume Encompassed by The Isodose Hypersurface With The Prescribed Dose

PRVs – Planning Organ at Risk Volumes

PTV – Planning Target Volume

PTV_{PIV} - Volume Of The Target Receiving The Prescribed Dose

QA – Quality Assurance

QC – Quality Control

RL – Right-Left

RT – Radiotherapy

RTMs – Relative Table Movements

SBRT – Stereotactic Body Radiotherapy

SGRT – Surface Guided Radiation Therapy

SRS – Stereotactic Radiosurgery

TG142 – Task Group Nr 142

TNM – Tumor Staging (T= Tumor; N= Nodes; M=Metastasis)

T+R – Translational + Rotational

TPS – Treatment Planning System

V_{12} – Volume receiving > 12 Gy

$V_{D\%}$ - Volume Receiving a Dose %

VD – Vector Displacement

VMAT – Volumetric Modulated Arc Therapy

WBRT – Whole Brain Radiotherapy

WHO – World Health Organization

XVI – X-ray Volumetric Imaging

Symbols

λ – Wave Length

$\frac{\mu}{\rho}$ – Mass Attenuation Coefficient

σ - Standard Deviation

μ - Mean

1. Introduction

1.1 Motivation

Radiation therapy is a core modality of cancer treatment that makes use of many complex machines and techniques which require extreme precision and accuracy to deliver high-dose radiation treatments. To enhance our ability to achieve this goal, new techniques have been developed and implemented for routine clinical use over the past two decades. These include SRS, a high-precision treatment conducted to treat specific small lesions where the standard surgery cannot be performed. With the development of new treatments, also new immobilization devices and imaging modalities such as SGRT have emerged, due to the demand for precise immobilization and constant monitoring of patients during treatment. The motivation that led to this project is the fact that the research presented, which comprises the use of various systems concomitantly, has not been validated yet in the literature. RT research in Portugal plays an essential role in forging evidence-based practice to ensure the high-quality treatment provided to patients. Therefore, investigation remains an essential process to explore different techniques and approaches before implementing new treatments, and to make sure actual practices are administrated in the best possible way.

It is important to develop studies like this regarding the use of new technologies to implement new protocols and to upgrade our standard techniques in clinical practice.

1.2 Problematic

In modern oncology, the selection of treatment and therapeutic depend on several factors such as type of cancer; localization; size and stage of progression. Surgery, chemotherapy, and RT are the most common and widely used treatment methods.[1] Within the modality of RT, there are several techniques that can be implemented depending on the type of cancer. In radiotherapy, the term IGRT refers to the use of various imaging methods to verify and correct possible setup errors in patient position during treatments. Technological developments and implementations in the last two decades, including the introduction of CBCT, have significantly enhanced the accuracy and precision of dose administration to the target volumes, minimizing radio-induced toxicity to organs at risk (OARs).[2] The conventional cancer treatment consists of 25 to 40 radiotherapy fractions. The extra radiation exposure resulting from the use of these imaging systems to check patient positioning and organ motion before and during treatment delivery is no longer negligible the more irradiation a patient receives.[3] With the advance of IGRT, treatments became more accurate, nevertheless, dose delivery is still under investigation with the aim to minimize that additional exposure, while maintaining image quality.

With the introduction of stereotactic approach in clinical practice, SRS treatments are reduced to a single fraction or in some schemes to two to five fractions - as fractionated stereotactic radiotherapy (FSRT). Since these treatments have a much higher dose being administered per fraction, resulting in a subsequent margin reduction, precision in patient setup and continuous motion control during treatment become essential in daily clinical activities.[1] As such, these treatments must be monitored to a submillimetric level, where recently, newly developed OSD systems have been introduced.[4,5] They have been investigated over an extended period of time, but it was only after the development of recent technology that these tools could be further developed into accurate, high-resolution sensors and cameras.[5] Currently, SGRT is a technology that enables a continuous

monitorization of the patient surface during treatment and is a helpful tool for accurate patient positioning in 6-DOF without any additional radiation exposure. The combination of an OSD system and a 6-DOF couch system for position detection and correction requires validation tests before using the two systems concomitantly. Therefore, is critical to quantify the accuracy of each system regarding the isocenter localization, at different clinical settings.

1.3 Objectives

SGRT can be safely used in Head & Neck (H&N) and CNS treatment sites, providing a monitorization of the patient surface with submillimetric accuracy, before and during treatment delivery, with the utilization of advanced open-face immobilization masks.

This study has two objectives; the first is to test the viability of the implementation of a maskless immobilization approach with only a vacuum mouthpiece suction system for head fixation in patients with CNS tumors who will undergo SRS treatment under the guidance of an OSD system coupled with 6-DOF robotic couch for submillimetric position correction. The combination of all these systems concomitantly has not been validated in the literature since most SRS treatments are performed with full closed or open-face thermoplastic masks, without OSD system monitorization. For this purpose, system validation is necessary to assess if all systems can be implemented concomitantly.

This project addresses the technical performance tests performed to test the viability of the objective mentioned above. The three systems in this study – XVI, HexaPOD couch and OSD system - were tested in extreme configurations. Isocenter alignment accuracy between imaging systems and mechanical systems was the major key to be assessed in this thesis since all systems must be correctly calibrated to achieve precise treatment delivery. To test the viability of using all systems concomitantly, five technical performance tests were performed in the Radiotherapy Department of Hospital CUF Descobertas.

- 1st Test – CW and CC XVI-CBCT Systematic Error Assessment;
- 2nd Test – HexaPOD Couch and XVI Mechanical Error Assessment during Couch Rotations;
- 3rd Test – OSD System Performance in Coplanar Angles;
- 4th Test – OSD System Performance with Couch Rotations;
- 5th Test – PE Agreement between OSD System and HexaPOD Couch at Non-Coplanar Angles.

With the results obtained it will be possible to answer what is the best acquisition orientation – CW or CC - to perform a CBCT image before an SRS treatment; if the HexaPOD couch is correctly calibrated to the XVI radiation isocenter to assure submillimeter corrections; performance of the OSD system on phantom surface detection since the HexaPOD frame and the Fraxion mouthpiece vacuum system can block the signal reading and interfere in the monitorization; which coplanar and non-coplanar angles occur most signal inconsistencies due to camera pod occlusion; what is the overall OSD system accuracy and what is the best non-coplanar angle arrangement to perform an SRS treatment with OSD system monitoring.

If the results presented in this study are viable, the second objective is to propose a protocol for SRS treatments with the OSD system as a monitoring tool on clinical workflow in the Radiotherapy Department.

2. Background

2.1 CNS Tumors

A tumor is developed by a set of multi-factorial disorders involving complex modifications in the genome, imposed by interactions between host and environment. Under usual circumstances, immature stem cell populations in body tissues can undergo one of three changes: (1) they can differentiate to mature forms as constituent component cells of the tissue of residence; (2) they can self-replicate; or (3) they can suffer apoptosis. With mutation, a (4) change can take place: the genesis of a new neoplastic form.[6] Indeed, mutations that dysregulate the pathways that control normal stem-cell renewal cause a diverse range of cancers,[7,9] which indicates that cancer can be considered a disease of unregulated self-renewal mechanism in which mutations convert normal stem-cell renewal pathways into engines for neoplastic proliferation.[10] The resultant unusual cell mass in the body grows and affects normal tissues in their surroundings, and sometimes it also spreads to the other sites in the body – metastasis.[11] According to the most accepted model for cancer appearance, mutations in tumor suppressors and oncogenes are the major factor leading to cancer development.[12]

For simplicity, CNS tumors are classified as gliomas or non-gliomas. The most common gliomas are astrocytomas, oligodendrogliomas and ependymomas, glioblastoma being the most fatal. Uncommon astrocytoma variants, including pilocytic astrocytoma, pleomorphic xanthoastrocytoma, and subependymal giant cell astrocytoma, tend to be well circumscribed and may be excised with curative intent. Unfortunately, most gliomas are characterized by diffuse infiltration of white matter tracts, making surgical extirpation impossible. Nongliomas consist of typically benign tumors, such as meningiomas and pituitary adenomas, as well as malignant tumors, such as primitive neuroectodermal tumors – medulloblastomas, primary CNS lymphomas, and the rarely occurring CNS germ cell tumors. While other malignant brain tumors, benign tumors may be as well devastating, due to interactions with areas controlling vital functions.[13,14]

Regarding its classification, the histology and location of CNS tumors are more important categories to take in consideration rather than classifying it amidst Tumor, Nodes and Metastasis (TNM) staging. CNS has no lymph nodes associated and there are few tumors that metastasize outside the CNS.

In 2021, the classification of brain tumors by the World Health Organization (WHO) underwent a reappraisal,[15] focused on the improvement of differential diagnosis through the combined use of histological; molecular biomarkers; tumor taxonomy and genetic indicators.[15] The fifth edition of the WHO classification of tumors of the CNS is the sixth version of the international standard for the classification of brain and spinal cord tumors and builds on the updated fourth edition that appeared in 2016.[16,17]

For CNS tumor nomenclature, WHO follows the recommendations of the 2019 cIMPACT-NOW Utrecht meeting to make nomenclature more consistent and simpler. To standardize WHO classification, the term “type” is used instead of “entity” and “subtype” is used instead of “variant.”[17]

2.2 Computed Tomography for Radiotherapy Planning

In clinical practice, the treatment process starts with patient image acquisition. The patient setup is configured in this phase, with a purpose to be reproducible in every radiotherapy fraction. The patient is asked to lay on the CT couch, with his body being placed in the treatment position, prone or supine. The position of the head, arms, and legs is defined according to the treatment area being irradiated. The patient is then aligned correctly through coronal, sagittal and axial lasers present in the CT room. Often immobilization devices such as headrests, thermoplastic masks, or body cushions will be customized specifically and individually to maintain the body in the same exact position every day.[18] For a reproducible alignment of the patient afterward in the treatment room, small tattoo "dots" are marked on the area subjacent that requires treatment. This helps with the treatment position localization and ensures that the deviation shifts are calculated properly each day. In certain pathologies, depending upon the area of scanning and treatment, specific protocols are followed that require a previous organ preparation, as such, have a full bladder and empty bowel and rectum for a pelvis treatment.

In the last decades, the CT scan become a powerful diagnostic medical imaging tool that endures a major role in forging a treatment planning strategy, with its primary purpose to assess the extent of local disease in cancer patients, including the evaluation of the spread gross disease to contiguous organs, the assessment of regional nodal involvement in some instances, and, occasionally, the detection of distant metastatic spread.[19]

The use of CT images in radiotherapy treatment planning allows several important advances and results in greater precision in dose distribution, dose optimization, and patient positioning.[20] With technology improvement, more precise methods of target definition are necessary for such precise delivery. While CT has revolutionized the field of radiation therapy, further improvements in imaging are desirable so the dose can be delivered with yet increased accuracy. CT has several limitations such as suboptimal tissue contrast, lack of functional information, and the inability to visualize small groups of cancer cells that are separated from the gross tumor. If these limitations are overcome, the improvement in the target precision and definition can provide better patient outcomes.[21] The primary disadvantage of CT for treatment planning is the low tissue contrast which can result in the tumor definition varying significantly from physician to physician.[22] Other imaging modalities, such as magnetic resonance imaging (MRI) and positron emission tomography (PET), may help in tumor definition due to their improved soft-tissue contrast and functional information.[23,24] In contemporary radiation therapy practice, MRI and PET are often used to complement CT for tumor delineation and normal tissue identification, although only CT is used for dose calculation. The future aim is to increase the usage of these co-register image sets for precise radiation therapy planning.[20]

2.3 Dosimetry and Treatment Planning

Dosimetry of ionizing radiation is a well-established and mature branch of physical sciences with many applications in medicine and biology. Today the term is used to describe either the measurement, quantification of the effects of ionizing radiation or the process of deriving a personalized dose distribution to be delivered to cancer patients in radiotherapy treatment planning.[25]

The focus of treatment planning is to deliver a high dose of radiation to the tumor while sparing the dose received by surrounding healthy tissue, which relies on dosimetry for treatment optimization and avoidance of severe toxicity for patients. Once CT image datasets are loaded and exported, the second phase of treatment planning consists in identifying the gross tumor volume (GTV), clinical tumor volume (CTV), planning tumor volume (PTV) and the OARs - **Figure 2.3.1**.

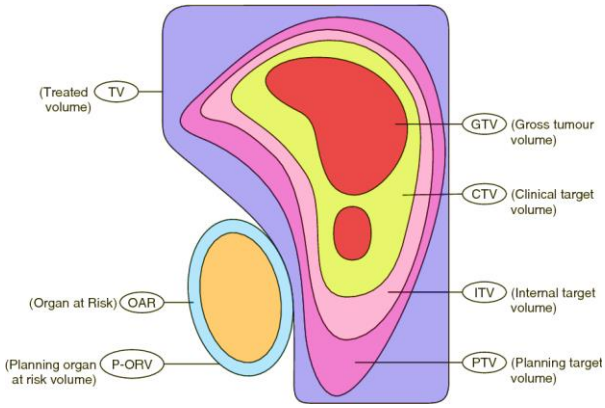

Figure 2.3.1 Definition of target volume. Target volume includes GTV, real and suspect tumor volume defined as CTV, the margin for variations in tumor size or position known as PTV and the volume which receives the dose for cure (treated volume).[26]

The radiation oncologist is responsible for the target definition and organ segmentation through specific contouring tools available in the planning system. Automatic segmentation algorithms can help in outlining organs or regions of bulk density. Depending on the type of lesion, it may be necessary to use multiple images from different sources as explained previously.[27] After delimitation, the radiation therapist/dosimetrist develops a complex plan for each beam line route in the treatment planning system. Most treatment planning systems today use inverse planning, which works backward from the prescribed treatment volume to determine the optimum beam angles and collimation. When appropriate radiation ports are selected, the radiation dose distribution in the patient can be computed, considering tissue heterogeneities in the irradiated volume. Different computed algorithms are used to model the interactions between the radiation beam and the patient's anatomy to determine the spatial distribution of the radiation dose. Newly developed algorithms, such as convolution/superposition and Monte Carlo, provide more accurate dose calculations by using heterogeneity correction.[28] These new algorithms calculate the radiation absorption and scatter of different tissue densities and apply that to the dose calculation, although this is only possible because the tissue density obtained is correlated to the specific Hounsfield units (HU). Variables such as tissue energy penetration must be considered since different organs have different electron densities (e.g., bone or lung vs. muscle).[29]

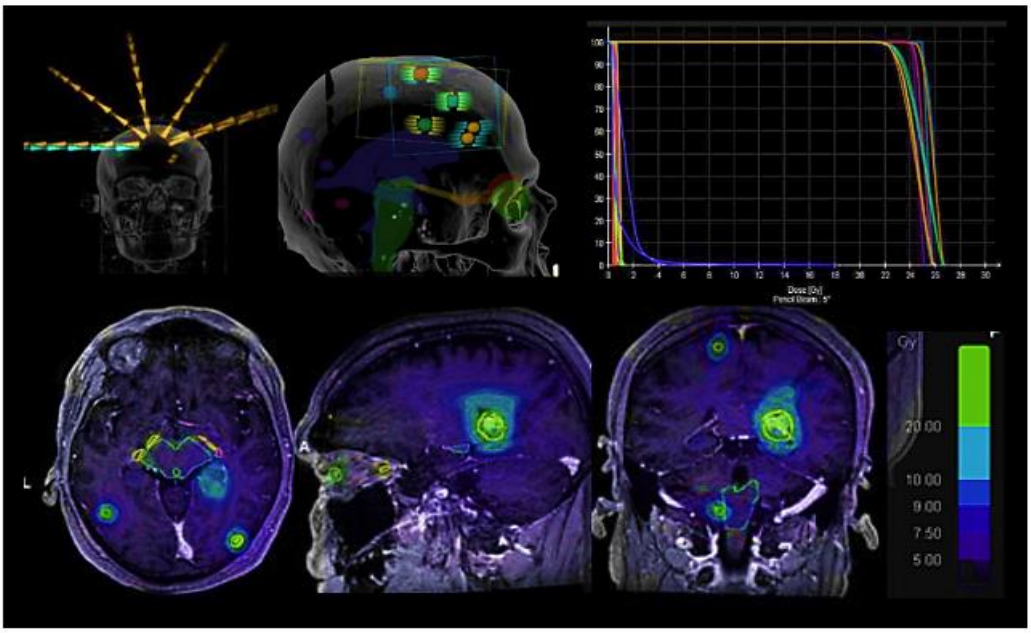

Figure 2.3.2 Example of a treatment plan using single-isocenter multitarget dynamic conformal arc for stereotactic radiosurgery in a patient with 9 brain lesions. The total volume of brain disease was 2.1 cm^3. A GTV to target volume PTV margin of 1 mm was used, with 22 Gy prescribed to each target in a single session. Treatment was delivered with 5 dynamic conformal arcs.[30]

These systems also help navigate beam placement based on avoiding critical structures - constraints, that are more sensitive to radiation in an effort to reduce collateral damage from the therapy. This may include automated, complex programming for multi-leaf collimator (MLC) leaf sequencing to shape the beam around critical structures during dose delivery. These treatment plans (**Figure 2.3.2**) can also be modified to compensate for the reduction in tumor size over the course of treatments.[31]

Despite its limitations, for several reasons CT is currently the only 3D imaging method accepted for treatment planning. Most treatment-planning algorithms were developed specifically for CT as it was the first available 3D imaging modality and CT scanners are more commonly used than MRI or PET. Furthermore, the geometric fidelity of CT is better than MRI in which distortions may occur, and as CT generally has shorter acquisition times than MRI or PET, organ/tumor motion management can be assessed. Most importantly, with CT it is possible to identify the mass attenuation coefficient $\frac{\mu}{\rho}$ (m^2/Kg) or attenuation characteristics for high-energy photons, X- Rays, and gamma rays, as this is critical for accurate dose calculation.

The application of other imaging modalities, such as MRI and PET, can provide additional information to precisely define tumor localization for treatment planning.[32,34] In particular, MRI has better soft-tissue contrast than CT and provides better visual discrimination between tissue that should be treated and what should be not (**Figure 2.3.3**).[35,36] PET allows the identification of areas of metabolic activity and thus allows the radiation oncologist to escalate the radiation dose for the most aggressively growing tumors or regions therein.[37,38]

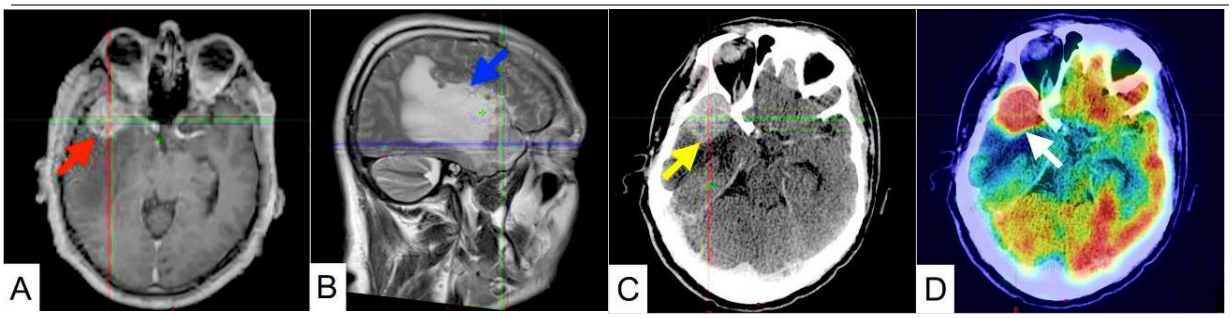

Figure 2.3.3 Pretreatment MRI and positron PET images. (A) T1-weighted contrast-enhanced axial image reveals a well-defined space occupying lesion in the right temporal lobe with intense contrast enhancement (red arrow), effacement of the right lateral ventricle and midline shift. (B) T2-weighted sagittal image shows extensive perilesional oedema extending up to the parietal lobe (blue arrow). (C) Contrast-enhanced axial CT image shows the lesion (yellow arrow). (D) PET axial image fused with contrast enhanced CT showing FDG avidity within the lesion. Maximum standardized uptake value within the lesion was 20.5 (white arrow).[39]

Several novel developments in radiotherapy have introduced new challenges for dosimetry with small and dynamically changing radiation fields being central to many of these applications such as stereotactic body radiotherapy (SBRT) and intensity modulated radiation therapy (IMRT). A rapid transition from conventional three-dimensional conformal radiation therapy (3D-CRT) to volumetric modulated arc therapy (VMAT) treatments and additional new techniques for motion-adaptive radiation therapy are being introduced.[40] There is also an increasing awareness of low doses given to structures not in the target region and the associated risk of secondary cancer induction. Accurate dosimetry is important not only for treatment optimization but also for the generation of data that can inform radiation protection approaches in the future.[39]

2.4 Radiotherapy Treatment

The aim of radiotherapy research is to discover the best approach to provide the best quality treatment for cancer patients. The selection of treatment and therapeutic is chosen following specific clinical guidelines in oncology,[41] depending on the type of cancer, its location, and stage of progression.[12] External beam radiotherapy is an essential therapeutic component for many patients with brain tumors. It can be curative for some patients and prolongs the survival rate for most. Radiation is often chosen as the primary treatment modality for patients with metastatic brain tumors, epidural spinal cord compression, and leptomeningeal metastases. Whereas whole-brain radiation may be administered for certain tumors, such as medulloblastomas or primary CNS lymphomas, involved-field radiation using multiple field techniques has become the standard treatment for most patients with gliomas.

The radiotherapy treatment is established specifically to meet a patient's individual needs, following some necessary phases. Medical consultation is the first phase of the radiation therapy process. In most cases, the oncologist references the patient to a radiation oncologist, who reviews the patient’s medical records, pathology reports and radiology images and performs a physical examination. If, based on this review, treatment by radiation therapy is chosen, the patient will be referred to the next phase, which consists of acquiring the patient body images and planning the treatment specifically to his needs. During image acquisition for radiotherapy planning, the treatment position is defined, and specific immobilization devices are used to minimize the patient motion and magnify patient comfort during the treatment. To accomplish this phase, CT scans and/or MRI are acquired, where occasionally intra venous contrast is used to improve the quality of the information, to define the exact location of the patient tumor for prior treatment delimitation. After image acquisition, all data is exported to the treatment planning software, where the radiation oncologist is responsible

for all organ segmentation in CT images. Thereafter, physicists and dosimetrists are responsible for the treatment configurations and radiation beam selection. The typical standard treatment for cancer patients consists of 25 to 40 radiotherapy fractions depending on the type of tumor and treatment modality. Before starting the irradiation, the patient is positioned on the treatment couch specifically in the treatment position using the immobilization devices pre-defined; this process is reproduced in each day of radiation. Radiation therapists are responsible for patient positioning and for delivering the radiation dose prescribed by the radiation oncologist. Patient internal images are acquired most every day before treatment, using IGRT. These images aim to check if the area of the body being treated has not changed position, and if so, the deviations necessary for patient correction are applied. During the whole treatment session radiation therapists view the patient from outside monitors adjacent to the treatment room and can talk with the patient via intercom. Individual treatment sessions typically do not last long; often, the patient will be in the treatment room for no more than 20 minutes, and much of this time is used for accurate positioning. Upon completion of the whole treatment, a follow-up appointment must be scheduled to monitor the recovery and overall health of the patient. Over the course of radiation therapy, the patient will meet a multidisciplinary team, including radiation oncologists, physicists, dosimetrists, radiation therapists, nurses, and health assistants - **Figure 2.4.1**.

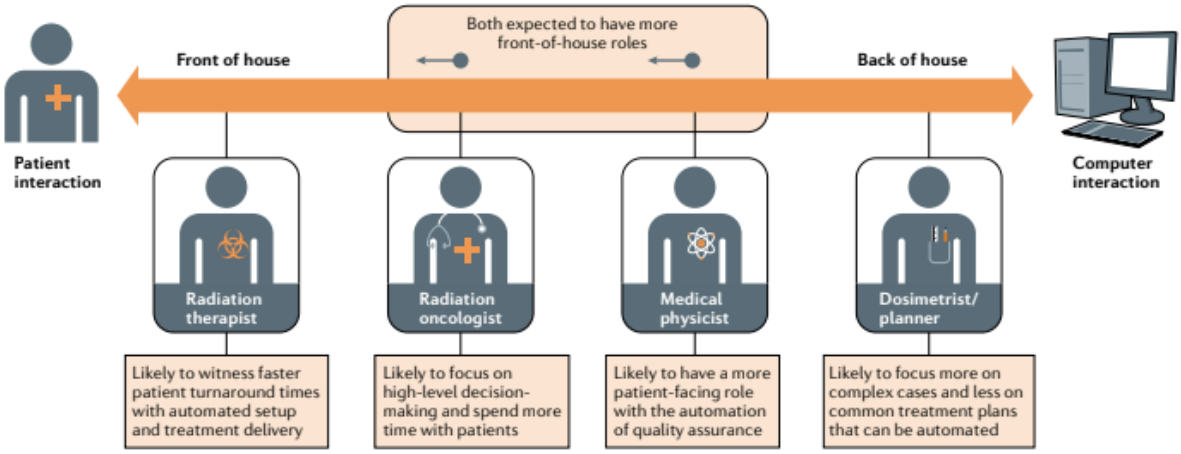

Figure 2.4.1 Radiation therapists, radiation oncologists, medical physicists and dosimetrists are shown along a spectrum according to their overall level of involvement in patient-facing 'front-of-house' tasks versus predominantly computational 'back-of-house' tasks.[42]

Most commonly radiotherapy beams are produced by a linear accelerator (LINAC); a medical treatment device with specific components that function together to accelerate electrons to produce high-energy photons, known as X-Rays. This production is only possible with specific conditions such as having a source of electrons, an appropriate target material, high voltage source and vacuum. Radiotherapy beams are generated in LINACs when the production of radiofrequency waves occurs in the magnetron or klystron depending on if they are low or high-energy linear accelerators. Electrons are produced and subsequently injected into the electron gun by heating a tungsten filament. These charged particles are generated and accelerated through a waveguide that increases their energy to the kiloelectron volt (keV) and megaelectron volt (MeV) range, using oscillating electric fields, reaching velocities near the speed of light. The beam is created when the electrons hit and interact with the tungsten target, with some fraction of the electron energy converted to a spray of photons through the bremsstrahlung process. During its course, the electron beam is redirected with the aid of three magnets that lead to the curvature of the beam – bending magnet, directing it towards the target. By focusing on the tungsten target, electrons lead to megavoltage X-Ray photons and the treatment beam

is produced.[43,44] The bremsstrahlung photons, called X-Rays, move approximately in the same direction as the electrons and have an energy spectrum, ranging from a few 10s of keV up to the maximum energy of the initial electrons. The resulting photon beam then passes through a series of filters and beam-shaping elements that flatten and define the edges of the beam. The photons are then directed towards the patient's tumor isocenter through a series of collimation systems.[45-48] During the treatments, the position used as reference for patient placement is the isocenter. This position corresponds to the location where the different components such as the gantry, collimator and couch rotation axis intercept each other.

2.5 Stereotactic Radiosurgery

With technological development, different radiotherapy techniques emerge. Advances in imaging and RT technology have enabled more precise tumor localization, tracking and dose delivery, leading to a reduction in irradiated brain volume at high radiation doses. Improvements in engineering and computing have enabled technologies such as SRS to be used in routine clinical practice.[49] Radiation techniques have evolved from 3D-CRT to IMRT, VMAT, and stereotactic techniques, including either SRS or SBRT - **Figure 2.5.1**. Currently, there is interest in the use of particle therapy for treating brain tumors because of the ability to concentrate the dose of protons and ions in the target volume while simultaneously sparing surrounding healthy tissues.[50]

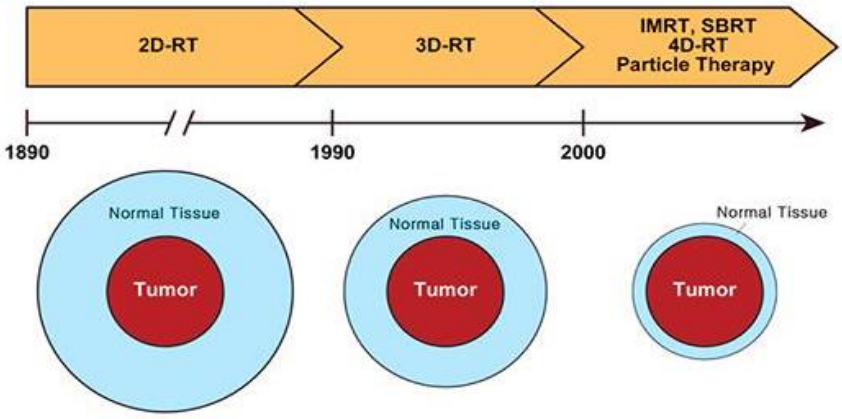

Figure 2.5.1 Evolution of treatment techniques through the years. Modern radiotherapy is characterized by minimizing the volume of normal tissue being unnecessary irradiated.[51]

Frameless SRS has taken on a significant role in the treatment of cranial lesions. The term stereotactic is defined as pertaining to types of brain surgery that use a system of 3D coordinates to locate the site to be operated on. SRS provides an alternative to surgery and whole brain radiotherapy (WBRT) or can accompany these treatments to ensure residual tumor cells are eliminated.[52] This technique exposes a small area of the body to a very high dose of radiation with the highest degree of immobilization, in a single fraction or can be delivered as fractionated stereotactic radiotherapy in two to five fractions.[53] However, no cutting or blade is used in the entire process, but it is still called surgery because the outcome of this treatment is quite similar to ordinary surgeries.[54] As the radiation administered is of a very high dose, it is very important that the beam is highly focused on the tumor so that the peripheral tissues are left unaffected. SRS is frequently employed to treat both malignant and benign brain tumors, at locations where conventional surgical techniques are difficult to assess or unsafe to use, or in other cases when the health status of a patient does not support him to tolerate a

surgical procedure.[55,56] The application of radiosurgery is also restricted to lesions measuring more than 3 cm in diameter. This limitation for SRS is related to the risk of radiation necrosis, late toxicity of radiosurgery. *Korytko et al.*[57] showed that the volume receiving 12Gy (V_{12}) is a predictor of radiation necrosis in intracranial tumors and increases significantly if the volume for V_{12} is greater than 10 cm^3, regardless of the plan conformity. This is an important clinical factor for consideration when designing and adding safety margins to intracranial targets.[58] The main advantage of SRS is the rapid dose fall-off achieved by multiple beam directions and a high degree of conformity index to spare normal tissues, compared to conventional RT, leading to a reduction of the volume of normal brain tissue irradiated at high radiation doses, and minimizing the risk of the long-term consequences of treatment.[59]

This treatment technique represents a further refinement and improvement of conventional radiotherapy, with the advantage of enhanced patient immobilization achieved with the use of either a frame-based or a frameless mask stereotactic system, leading to submillimetric accuracy of patient repositioning. SRS can be delivered using different medical machines, each operating in a completely different manner. They are the radioactive cobalt-60 system Gamma Knife which is designed exclusively to treat intracranial lesions,[60] LINAC which uses multiple beams from different angles centred on the tumor and cyclotrons or proton beams. Each machine has a different source of radiation and could be more or less effective under various circumstances. Some brands sell the equipment together with the software as they are computer-based machines, being a very restrictive market.[53]

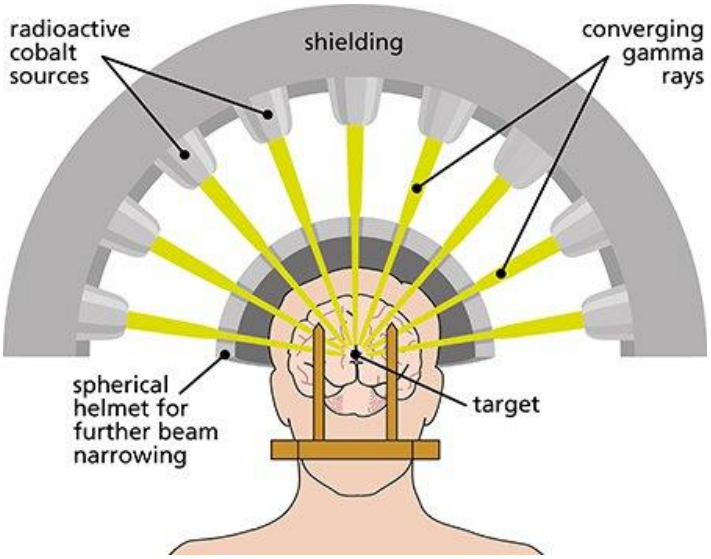

Figure 2.5.2 Gamma Knife stereotactic radiosurgery representation.[61]

Although Gamma Knife units are specialized systems for intracranial radiosurgery - **Figure 2.5.2**, LINAC-based systems are more versatile and can be used to deliver other forms of radiation treatments. LINAC-based SRS is usually performed to treat a diverse group of intracranial lesions, including small arteriovenous malformations, pituitary adenomas, acoustic neurinomas, meningiomas and gliomas. Recently, the use of a single isocenter technique for the simultaneous treatment of multiple brain metastases in a single or few sessions, has been evaluated. Preliminary results are promising, showing an improvement in the efficiency of the delivery while reducing overall treatment time and maintaining a high local control rate.[62] Its role in the management of brain metastases is also evolving, and SRS has been widely adopted as an alternative to whole-brain radiotherapy to treat patients with up to 10 brain metastases, with the aim of reducing the risk of neurocognitive impairment.[63,64]

2.5.1 Patient Immobilization

Due to the high dose delivery, sharp dose gradients and small margins utilized in SRS, accurate patient immobilization is vital to reduce the dose in normal tissue while perpetuating tumor control probability.[65]

The use of a stereotactic head frame affixed to the calvarium in SRS has been extensively studied and has been shown to be associated with excellent target localization during both planning and treatment delivery.[66,67] In this type of immobilization, there is no possibility of removing the frame between the diagnostic and the therapeutic procedures, so they must be closely scheduled. The placement of radiosurgery frames is resource intensive and medically invasive, and the need to maintain and sterilize a stereotactic head frame presents challenges that are obviated using mask-based immobilization. Besides immobilization of the patient, the frame also serves as a fiducial coordinate system for the target since there is no practical intra-fraction motion inside the skull during a treatment. The advantage of rigid frame fixation is its high accuracy in terms of repositioning and intra-fraction motion, benchmarking it as the gold standard in SRS. As such, frame-based SRS depends critically on the maintenance of the spatial relationship of the frame to the skull.[68] However, although this system provides a high degree of accuracy that is necessary when using large and highly conformal doses, there are several disadvantages of frame-based immobilization, including patient discomfort, difficulty performing hypofractionated therapy, and additional effort required to coordinate between personnel on different services. Frame placement through surgical screws involves a risk of bleeding and infection, and patients require premedication.[69] Furthermore, the care of patients wearing head frames creates a resource burden on the day of care, requiring dedicated nursing and physician support. Head frames may also slip, compromising treatment accuracy, and potentially resulting in injury to the patient.[70] The repeated use of a rigid frame system for fractionated treatment is not an optimal solution. As an alternative to frame-based technologies, there is now a variety of frameless immobilization systems that have been advised.[71] A significant development in the delivery of SRS has been the migration from frame-based to frameless radiosurgery, without compromising accuracy in localization or clinical outcomes.

Advances in non-invasive patient immobilization as well as in IGRT, have enabled the use of thermoplastic masks and hypofractionated schemes for single or multiple brain metastases, thus, overcoming the main limitation of invasive head fixation.[72,73] Several studies have shown that image guidance makes setup and repositioning uncertainty with the non-invasive mask immobilization comparable to the invasive stereotactic ring application.[74-76] Nevertheless, this method may have less intra-fractional accuracy due to the non-rigid construction, indirect immobilization of the skull, and unpredictable patient movement. Many studies reported this effect only by means of quantifying pre and post-fractional deviations of the patient's head by either CBCT or ExacTrac.[74,75,77,78]

To ensure accurate patient positioning, different immobilization devices are used in clinical practice. For SRS patients, the conventional immobilization system consists of a full-head thermoplastic mask in combination with a molded cushion head support or an open-face mask with a bite block **Figure 2.5.1.1.** The mask should be capable of limiting intra and inter-fractional motion as well as preserving the patient shape from treatment planning. However, patient setup cannot always be perfectly reproduced for all treatment fractions. This error in positioning can currently be detected only with online image verification of the patient's position. To monitor and maintain the correct positioning of the patient during treatment, various techniques have been employed; volumetric X-Rgay image;[79-83] biplanar X-Ray imaging[84,85] and optical surface imaging.[86-89] These various imaging systems have been reported[90,91] to have accuracy better than 2 mm in translational movements.[92]

For conventional full-head masks, the use of the OSD system is limited by the mask blocking the patient's facial area. The OSD system will mainly display the position of the mask and not the patient. An alternative to closed masks is open-face masks. With open-face masks in combination with an OSD system, the geometrical shifts during positioning and treatment can be monitored and quantified. In addition, open masks are often more comfortable and less claustrophobic. Several studies have presented results for open-face mask solutions, showing good accuracy in patient positioning.[93,94]

Figure 2.5.1.1 (a) Fraxion™ Maskless approach using only bite block; (b) Fraxion™ Frameless approach with bite block and Open-faced Thermoplastic Mask.[95]

2.6 Treatment Verification and Monitoring

2.6.1 Image-Guided Radiation Therapy - IGRT

The evolution of radiotherapy has been ontogenetically linked to medical imaging. Imaging has been used for tumor detection, staging, target volume delineation, treatment planning, delivery verification assessment, and tumor response. Recent advances in imaging technology coupled with improved treatment delivery allow near-simultaneous soft-tissue localization of tumor and repositioning of patients. The integration of various imaging modalities (**Table 2.6.1.1**) for guiding radiation delivery, has improved the assessment of geometric accuracy and uncertainties in contemporary radiotherapy practice ushering in the paradigm of IGRT. As such, a more focused and accepted definition of IGRT is the use of frequent imaging modalities within the radiation treatment room, to ensure correct patient alignment for accurate dose delivery.[96,97] IGRT provides a method whereby deviations of anatomy from the initial plan are determined and this information is used to update dosimetric assumptions, being an effective tool designed to reduce potential systematic and random errors in radiation oncology.[98] Correction strategies may include daily repositioning to register patient position in accordance with the base plan or recalculation of treatment delivery in real-time to reflect the patient's presentation during a given fraction. This philosophy of reevaluating treatment and accounting for the differences between actual patient anatomy on a given day and the snapshot of planned treatment is known as adaptive radiotherapy.[99] The eventual goal is to reevaluate and in certain situations redefine daily positioning for treatment to keep it on the same path as the intended treatment.[100] While IGRT systems are used for final positioning, body tattoos and room lasers are typically used for initial setup, meaning that only three points on the skin surface are the basis for setting up the whole patient.[101]

The two main concerns with IGRT are the resource-intensive nature of delivery and increasing dose exposure from additional imaging acquisition. However, increasing the precision and accuracy of

radiation delivery through IGRT is likely to reduce toxicity with potential for dose escalation and improved tumor control resulting in a favorable therapeutic index.[102]

Table 2.6.1.1 Detailed description of commercially available IGRT systems and their advantages and disadvantages.[103]

Imaging Modality	*Commercial System*	*Mechanism*	*Advantages*	*Disadvantages*
Ultrasound Based	SonArray, Varian Medical Systems B-mode Acquisition and Targeting (BAT), NOMOS Corporation i-Beam, Elekta Oncology	Target localized using in-room ultrasound before treatment.	Volumetric verification of target possible. Simples and inexpensive. No extra dose exposure.	Operator dependent (inter-observer variation). Applicable to superficial or abdominal targets. Cannot be used when the beam is on.
Optical Surface Detection Systems	AligntRT, Vision RT, Catalyst HD, BrainLAB	Two/Tree ceiling mounted video cameras used to provide a 3D-surface image of the patient that is aligned with the reference surface image.	No extra radiation dose. Fast real-time acquisition. Large field of view. Ideal for superficial targets.	No volumetric data. Poor image quality and resolution. No soft tissue data.
MV Planar Imaging	Clinac, Varian Medical Systems Precise and Compact, Elekta Oncology Primus and Oncor, Siemens Medical Systems	Treatment beam is the MV source and images are captured by a flat panel detector behind the patient.	Widely available in-room imaging system. No modification is needed as treatment beam used for imaging. Can be used for dose measurements and quality assurance.	No volumetric data. Poor image quality and resolution. No soft tissues data.
kV Planar Imaging (non-gantry mounted) *kV-kV Ortho* *kV-kV Stereoscopic*	Cyberknife, Accuracy Novalis TX, BrainLAB, ExacTrac	Two kV X-ray sources mounted on ceiling or floor providing orthogonal images.	Good image quality because of kV beam. Lower patient dose than MV imaging. Fast and real time imaging. Corrects translational and rotational errors.	No soft tissue information. Has to depend on bony landmarks or fiducial markers. Need careful calibration for isocentric matching.
kV-CT (Fan beam)	CT-on-Rails-Primatom, Siemens Medical Systems, Varian Medical Systems	Uses an in-room diagnostic CT scanner alongside a linear accelerator with couch displacement between imaging and treatment.	Superior imaging quality with a CT scanner. Provides soft tissue information.	Requires a large room and increased in-room time. Unable to assess intra-fraction motion. Possible positioning error during couch movement.
kV-CBCT (Cone Beam) *MV-CBCT Siemens*	Synergy, Elekta Oncology, Varian Medical Systems, Siemens Medical Systems	Uses an isocentrically gantry mounted kV source and a flat panel detector. A series of kV X-rays are taken by rotating the gantry and reconstructed to a volumetric image.	Clinically well stablished and widely used. Provides good spatial resolution of soft tissue. 4D-CBCT for intra-fraction motion correction is possible.	Requires post-processing of images (slow acquisition). Cannot be used when the treatment beam is on, hence can be used for correcting position error only.
MV-CT (Fan beam)	Helical Tomotherapy	Imaging is done by treatment beam, where ring gantry rotates and the patient couch moves through.	Provides volumetric images for positioning error correction. Can be used for dose verification and dose calculation during treatment.	As an MV beam is used, there is a poor soft tissue contrast compared to kVCT.

The idea of attaching a kV imaging system on a LINAC dates to the 1950s but was only developed in the late 1990s with the addition of kV X-Ray tubes/image receptors orthogonal to the mega-voltage (MV) therapy beam. There are different image-guidance systems available, including kV or MV X-Ray imaging, kV or MV CBCT or MV single slice CT known as tomotherapy.[104,105] kV-CBCT has a major role in setup assessment in clinical practice, becoming the standard image verification system on linear accelerators made by Elekta (Stockholm, Sweden) and Varian Medical Systems.[106]

These systems consist of a retractable X-Ray tube and amorphous silicon detectors and have the capability of 2D and volumetric image acquisition. The kV imaging system can acquire scans throughout a continuous partial or complete gantry rotation around the couch, sharing the same isocenter as the MV treatment beam,[107] acquiring the "average" position of organs with respiratory motion. Geometric accuracy is 1 mm or lesser, with the possibility of 2D image acquisition match with digitally reconstructed radiographs (DRRs) or 3D volumetric acquisition match with X-Ray volumetric images generated from planning CT data sets. Both inter-fraction setup changes and anatomical changes related to organ motion; organ filling (bladder, rectum); tumor reduction and weight changes may be monitored, therefore, before treatment delivery, image verification is crucial in clinical radiotherapy. Patient images are acquired and matched with the CT scan volumetric data set. Through the clipbox visualization is possible to correct the position error associated with the patient structures and apply shifts manually to the LINAC couch. Correcting a setup error means that the patient position must be shifted manually.

Also, scans can be acquired before and after treatment delivery and may give an estimate of intra-fractional changes. For tumors discernible separately from surrounding normal tissue, treatment response may also be monitored, and these scans may be used for dose recalculation or treatment plan adaptation after necessary image processing. kV CBCT gives better contrast resolution compared to MV CBCT but may be limited by artifacts from prostheses and scatter from bulky patient anatomy. The average dose per image in XVI protocols is 1–30 mGy.[108-111]

2.6.2 Surface Guided Radiotherapy – SGRT

SGRT is a rapidly growing non-ionizing image technology that uses stereo vision equipment to monitor patient external surface in 3D, for setup correction and motion management during treatment. The initial purpose of SGRT consisted of replacing lasers and skin marks for patient positioning.[112] Its adoption has been widely used in other clinical applications (e.g., breast, extremities, pelvis, lung and stereotactic radiosurgery),[113] having a major role in radiotherapy gating (treatment delivery only at a certain position of target) and deep inspiration breath hold (DIBH) for left-sided breast cancer with the benefit of minimizing the radiation dose to the heart. There are numerous publications that support its use in the treatment of breast, brain, head and neck cancer, sarcoma, and other conditions.[114,115]

2.6.2.1 Optical Surface Detection System

Monitoring is the process of measuring the location of anatomical structures, and/or landmarks in relationship to each other in a 3D axis. Various technologies have been tested for determining a target location, including mechanical, magnetic, acoustic, inertial, and optical position sensors. Tools such as Catalyst HD™ (from C-RAD, Uppsala, Sweden) among other vendors; AlignRT® (from VisionRT Ltd, London, UK) and BrainLab (Munich, Germany) are optical surface detection systems used in modern clinical practice that are connected directly to the LINAC software, making possible a continuous transmission of information between the two systems. These systems are designed for a maximum level of integration into the treatment process.[116]

Most of these technologies have been tested for medical use in either image-guided surgery or image-guided radiation therapy. The OSD system projects near-violet light onto the patient surface and charge coupled device (CCD) cameras detect the light reflected from the patient. The 3D surface is reconstructed based on the principle of triangulation and the calculated inaccuracy position is displayed in real-time in six dimensions, including translational shifts (vertical, longitudinal, and lateral) and rotational shifts (rot, pitch and roll).[58,117]

The most common active targets are infrared light-emitting diodes (IRLED). To facilitate the setup process, the system uses light of three wavelengths: blue (λ=405 nm), green (λ=528 nm) and red (λ=624 nm). The blue light is the measuring light projected on the patient to determine the skin surface coordinates. The green and red-light projects mismatches of the reference surface versus the live patient surface directly onto the patient skin.[58,117] Various detectors can be used to determine the positions of an optical target; however, CCD cameras are used most often. CCD cameras are simply a collection of light-sensitive cells, or pixels, arranged in either a 1 or 2-dimensional array. When light strikes a CCD cell, electron production is proportional to the intensity of the light incident on the cell. Thus, a 2D CCD array provides a 2D digital "image" of the target, with brighter pixels in the array corresponding to higher light intensity and darker pixels corresponding to lower light intensity. This digital image can then be analyzed to determine the pixel with the highest light intensity. Each CCD camera provides a 2D image of a scene, as viewed from the camera's vantage point. An array of cameras provides several different views of the same scene, each from a different perspective or vantage point. The multiple views of the same scene can be used to reconstruct an accurate 3D location of a patient in the treatment room.[118] However, as mentioned above, the ability to track the patient surface by itself is not sufficient to track the internal target PTV - inside the patient.

The OSD system also provides a real-time monitoring function to detect patient movement during treatment, as opposed to CBCT where the patient position can only be verified at the time when the image is acquired.[118] The translation movement (shift) between the planned position of a set of optical markers and the actual detected marker positions is relatively simple to determine, for instance, by finding the vector displacement difference between the center of the fiducial array in the treatment plan and the detected on the actual patient. The OSD system also has the ability to validate the patient position online for all couch angles, verify couch movements for non-coplanar treatments and monitor patient position during the couch movement. However, determining the rotations (around 3 axes), which when performed, would best align one set of optical marker positions to the other, is a more difficult problem. Several iterative optimization algorithms for determining these rotations have been used successfully, including simulated annealing, and various downhill algorithms such as the downhill simplex, and the Hooke and Jeeves pattern search algorithm.[119,120]

While simple iterative optimization algorithms are sufficient for the solution of the absolute orientation as applied to stereotactic radiosurgery using rigid sets of optical fiducials, non-rigid body monitoring, and/or other image systems (such as ultrasound) used in conjunction with optical

monitoring increases the statistical noise in the optimization and decreases the reliability of these simple algorithms.[3] Several closed-form solutions have been used in addition to iteratively based approaches mentioned above, including singular value decomposition and Horn's algorithm.[121,122]
The challenge lies in the registration of two partial scans of a deformable object; a reference scan and a live scan captured at different points in time. To obtain perfect patient positioning these two scans must match (**Figure 2.6.2.1.1)**. The correspondences are expressed at points distributed evenly over the reference surface so that each point has a corresponding position on the live surface.

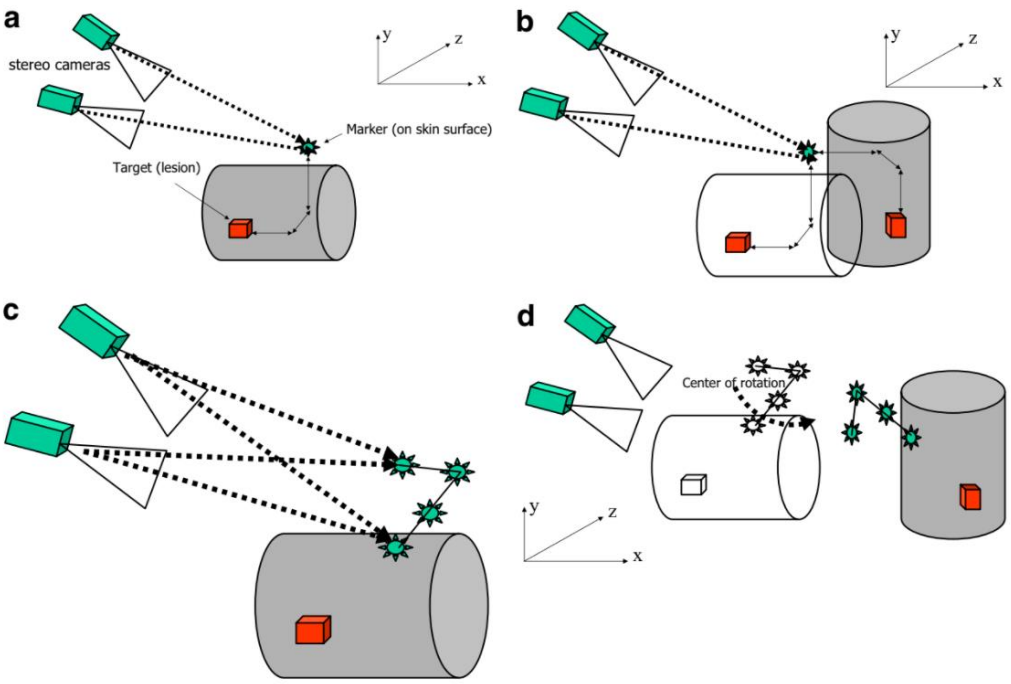

Figure 2.6.2.1.1 (a) The stereo cameras locate the exact (x, y, z) coordinates of a passive or active IR marker in the treatment room. The cameras can detect movements of the marker in the x, y, and z-directions. (b) The marker is in an exact location, but because the patient has been rotated around the marker point, the lesion (target) has moved, undetected by the cameras. (c) An array of markers is used now, fixed to the patient's surface. The collection of points in the array of markers is tracked, not just a single point. (d) Using an array of markers allows rotational movement to be detected, in this example, a rotation about the z-axis.[118]

Geometric accuracy is within 1-2 mm, with its application being commonly used in situations where the external surface acts as a reliable source for internal position or organ motion. Positioning based on soft tissue on the surface does not always correlate well with the internal treatment volume in the abdomen and pelvis. As such, it is always recommended to perform IGRT to assess internal setup deviations. The combination of IGRT and SGRT would be ideal.[113,115]

2.7 Quality Assurance in Radiotherapy

Quality assurance (QA) programs are essential to assess all steps in the chain between the first patient contact to the last treatment session and englobes a conjunction of specific procedures that ensures a consistent and safe fulfillment of the dose prescription to the target volume, with minimal dose to normal tissues and minimal exposure to personnel.[123] The sequential process is shown in **Figure 2.7.1** and each step in the integrated process of RT needs quality control (QC) and QA to prevent errors and assure patients will receive the prescribed treatment correctly. The importance of QA in RT has long been recognized in the profession and as such, it is common practice to have defined regular quality control programs in treatment facilities. Because of the complexity of radiosurgery treatments, the QA program must include a treatment procedure checklist that reflects the treatment step sequence and should be written in sufficient detail to minimize the risk of misadministration or injury.[124] Comprehensive guidelines have been recommended by various international organizations, such as the European Society for Therapeutic Radiology and Oncology and the American Association of Physicists in Medicine (AAPM).[125]

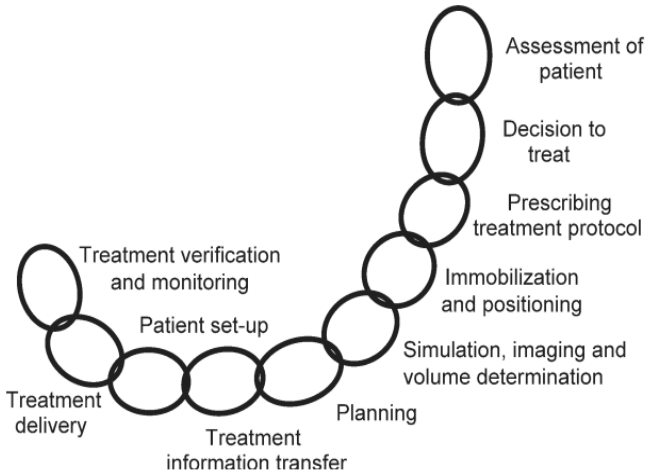

Figure 2.7.1 Sequential process of planning and delivering radiotherapy to patients.[126]

The current paradigm of quality management in RT focuses on measuring the functional performance of RT equipment by measurable parameters with tolerances set at strict with achievable values.[126] A large number of parameters having some inaccuracy contribute to the overall uncertainty in the 3-dimensional dose and distribution delivered to a patient. Most QA documents specify acceptable tolerance levels for individual parameters without considering the cumulative effect of the uncertainty in the dose delivered to a specified volume in a patient. The reason is that such uncertainty propagation is very difficult to assess and is considered by many to be scientifically unsound because of the combined effect of systematic and random uncertainties.[127] Otherwise, detailed recommendations about individual equipment parameters and dosimetric procedures do not guarantee technical quality unless the cumulative effect at the patient level is addressed. Analysis of individual parameters should not be the main focus of a QA program, but rather serious attempts should be made to understand the cumulative effect of all procedures at the patient level. One would begin by defining an acceptable overall uncertainty, resulting from all radiotherapy tests performed. This uncertainty is the result of many procedures that have both random and systematic uncertainties associated with them. The concern is to define these various uncertainties and combine them in a meaningful way.[12]

2.8 SRS Guidelines

Specific guidelines are an essential tool envisioned to assist practitioners in providing appropriate radiation oncology care for patients. Robotic, non-isocentric, frameless SRS is a treatment consisting of dozens of non-isocentric beams with distinctive QA procedures and continuous target tracking that result in comparable dose conformity and reduction in an intra-fraction systematic error. Imaging, planning, and treatment typically are performed in close temporal proximity. Treatment delivery should be accurate to approximately 1 mm, which leaves little room for error in the overall process.[121]

The mechanical precision and electronic complexity of the treatment delivery unit require implementation of and adherence to an ongoing QA program, through multiple checking, preferably by different individuals. This program assures that the SRS treatment unit is in compliance with the recommendations of the treatment unit manufacturer, with the specified clinical tolerances recommended by the American College of Radiology, AAPM, and American Society for Radiation Oncology and with applicable regulatory requirements. It is recognized that various test procedures, with equal validity, may be used to ascertain that the treatment-delivery unit is functioning properly and safely. The test results should be documented, signed by the person doing the testing, and archived. Important elements of the treatment-delivery unit QA program are as follows:

1. Radiation-beam alignment testing to assure the beam can be correctly aimed at the targeted tissues.
2. Calculation of radiation dose per unit time (or per monitor unit) based on physical measurements for the treatment field size at the location of the target.

SRS is an image-based treatment. Imaging, whether by CT, MRI, or other applicable modalities should assure the creation of a spatially accurate anatomic patient model for use in the treatment-planning process. The chosen image sets should allow the optimal definition of the target(s) and critical structure(s) and the chosen imaging modality must be thoroughly investigated before use in the SRS treatment-planning process. Some imaging considerations are the following: partial volume averaging, pixel size, slice thickness, the distance between slices, image reformatting for the treatment-planning system, spatial distortion and image warping, motion artifacts, magnetic susceptibility artifacts, and others. Both high 3D spatial accuracy and tissue-contrast definition are very important imaging features if one is to utilize SRS to its fullest positional accuracy. The medical images used in SRS are used for focalizing target boundaries and generating target coordinates at which the treatment beams are to be aimed. They are used for creating an anatomic patient model (virtual patient) for treatment planning, and they contain the morphology required for the treatment plan evaluation and dose calculation.[121]

SRS treatment-planning systems are very complex. Data from medical imaging devices are used in conjunction with specific algorithms to produce anatomically detailed patient models illustrating the dose distribution with a high degree of precision.[121] A relevant prerequisite for the treatment with small photon beams is adequate small field dosimetry, which is now comprehensively covered in International Commission on Radiation Units and Measurements Report (ICRU) 91[129] and is based on the International Atomic Energy Agency technical report series 483.[130] Concerning stereotactic treatments, accurate dose calculation is also a significant requirement and the ICRU Report 91 recommends that the dose calculation should be performed with a type-B algorithm

whenever heterogeneous tissue densities are present (e. g., in the lung[131]). Type-B algorithms explicitly consider changes in lateral electron transport, while type-A do not, making them more inaccurate in inhomogeneities. Another prerequisite for stereotactic treatments is the mandatory use of a stereotactic frame or image-guided beam delivery. This is also described in the ICRU Report 91 and follows previously published guidelines.[132–135] When the SRS technique is used, the inverse treatment-planning methodology is necessary to provide computer-selected weights for a very large number of independent treatment beams. As such, it significantly complicates the treatment-planning process and requires QA steps that are different than the information provided in some earlier reports on treatment-planning QA (AAPM TG-53 report).[136] The QA program for SRS involves elements that may be considered to be both dosimetric and nondosimetric, furthermore, it is recognized that various testing methods may be used, with equal validity, to assure that a system feature or component is performing correctly.

Once the individual components of the SRS planning and treatment technique are commissioned, it is recommended that the QA program include an "operational test" of the SRS system for geometric accuracy before clinical treatment begins, or whenever a plan modification is implemented for a fractionated treatment schedule. This testing should mimic the patient treatment and should use all of the same equipment used for treating the patient. For instance, to obtain quantitative results, phantoms can be used.[124,128]

Regarding dose prescription, ICRU Report 91 recommends that constraints should be included for the target volumes as well as the OAR's and planning organ at risk volumes (PRV's). Traditionally, in stereotactic treatments, a dose is prescribed to the target covering the isodose line. New compared to this practice in ICRU Report 91, is the volumetric approach, in which the absorbed dose is prescribed to the isodose surface which should cover the optimal percentage of the PTV while optimally restricting the dose to the PRV. The term "optimal" is then strongly dependent on the actual treatment situation. For SRS of a single brain metastasis away from any OAR this might mean that close to 100% of the PTV should be covered by the prescription isodose while for lung SBRT only 95% PTV coverage might be safely reached or for spinal SBRT only 80–85% of the PTV can be covered by the prescribed isodose due to the constraints on the spinal cord. The ICRU Report 91 recommends that reporting for stereotactic treatments should contain the following information:

- Clinical decisions (e. g. reason for dose prescription and fractionation according to an organ at risk-adapted prescription approach, preceding surgical interventions; previous or simultaneous systemic treatment);
- Delineated volumes;
- Prescription and planning aims;
- Description of treatment planning system (i. e. algorithm, voxel size, calculation dose grid and uncertainty for Monte Carlo based systems);
- Dose documentation to target volumes and organs at risk:

  I. Calculated dose–volume histograms;

  II. PTV median dose ($D_{50\%}$) as well as PTV $D_{near\text{-}min}$ and PTV $D_{near\text{-}max}$;

  III. Optionally the median dose ($D_{50\%}$) for existing GTV/CTV and internal target volume (ITV) contours (for lung SBRT documentation of these values is required);

  IV. For OAR at least three values should be reported mean dose, $D_{near\text{-}max}$ and another relevant $V_{D\%}$ value;

V. Dose homogeneity (if available mean dose to PTV and standard deviation of mean dose to PTV);

VI. Dose conformity CI is given by the volume encompassed by the isodose hypersurface with the prescribed isodose volume (PIV), the volume of PTV and the volume of the target receiving the prescribed dose or more (PTV_{PIV}). As an example, Paddick's CI is given by:

$$CI = \frac{PTV \times PIV}{PTV_{PIV}^2} \qquad (2.8.1)$$

- For radiosurgery of the brain also the dose-gradient GI given by the volume encompassed by the isodose hypersurface with half the prescribed dose (PIV_{half}) and the volume encompassed by the isodose hypersurface with the prescribed dose (PIV):

$$GI = \frac{PIV_{half}}{PIV} \qquad (2.8.2)$$

- Documentation of stereotactic frame settings or image guidance;
- Plan verification and patient-specific quality assurance;
- Number of treated fractions:
- Follow-up schedule.[135]

The near-minimum and near-maximum doses to the PTV ($D_{near\text{-}min}$ and $D_{near\text{-}max}$) were introduced in ICRU Report 83 as the $D_{98\%}$ and $D_{2\%}$. However, for very small volumes of <2 cm^3, which are often present in stereotactic treatments, the PTV $D_{98\%}$ and $D_{2\%}$ indices are hardly meaningful: therefore, in accordance with previous reports [13] the ICRU Report 91 recommends using $D_{near\text{-}min}$= $D_{V\text{-}35mm3}$ and $D_{near\text{-}max}$= D_{35mm^3} for volumes <2 cm^3. Nevertheless, the value of 35mm^3 as a minimal meaningful 3D cube might evolve with time depending on the calculation grid size and calculation accuracy in a single voxel and the ICRU Report 91 near minimum and near maximum dose description for tumors of extremely small size (e. g., PTV of < 100 mm^3) is still debated.[135]

2.9 SGRT and Frameless Approach for CNS Tumors

It has been proved that SGRT can be safely used in H&N and CNS treatment sites by using advanced open-face immobilization masks, with the aim to provide submillimeter accuracy and precision during treatment delivery. The ability of OSD systems to non-radiographically collect a live surface image, determine positional correction vectors to match the image to a predefined reference image, and monitor sub-millimeter movements, have made it a successful component of SRS where small targets and small margins are present. A recent publication has documented a benefit for various disease sites including left breast cancer, brain cancer, and lung cancer. The benefits come from two perspectives mainly: setup and monitoring. Quicker patient setup can potentially reduce the imaging dose while active patient monitoring can potentially enhance localization and treatment delivery accuracy.[137]

Laura I Cerviño et al.[138] evaluate the clinical experience with a frameless and maskless technique for stereotactic radiosurgery using minimal patient immobilization and real-time patient motion monitoring during treatment. The study considered the first 23 patients treated with this

technique. Head positioning was achieved with a patient-specific head mold made from expandable foam that conforms to the patient's head. The face of the patients was left open for maximal comfort and so that motion of a region of interest consisting of the forehead, nose, eyes, and temporal bones can be monitored during treatment using an OSD system - Vision RT. The initial setup of the patient was performed with the surface imaging system using the surface of the patient obtained from the treatment planning CT scan. The initial setup was confirmed and finalized with CBCT prior to treatment. The shifts for the final setup based on the CBCT and the duration of all the steps in the treatment process were recorded. Patients were monitored during treatment with surface imaging, and a beam hold-off was initiated when the patient's motion exceeded a prespecified tolerance. The average total setup time including surface imaging and CBCT was 26 minutes, while the portion corresponding to surface imaging was 14 minutes. The average treatment time from when the patient was placed on the treatment table until the last treatment beam was 40 minutes. Eight (35%) patients needed repositioning during the treatment. The average shifts identified from CBCT after initial setup with surface imaging were 1,8 mm in the anterior-posterior direction, and less than 1 mm in the lateral and superior-inferior directions. The longest treatment times (including beam hold-offs) happened for patients who fell asleep on the treatment table and were moving involuntarily. The frameless and maskless treatment using minimal immobilization and surface imaging has proven to be reasonably fast for routine clinical use.[138]

Zhao et al.[139] reported on a pilot trial to investigate the feasibility and setup accuracy of the minimal face and neck mask immobilization with OSD guidance. They enrolled 20 patients undergoing standard of care IMRT treatment to the head and neck area and employed both optical guidance as well as daily CBCT to determine any resulting setup errors. Surveys were administered to assess patient comfort and total treatment time and resulting shifts were recorded. Another component of the study reported by *Zhao et al.* was to compare two shoulder restriction methods to determine which one provided better patient setup. They concluded that approximately 5–10% of the fractions had shifts greater than 5 mm and about 0–3% had shifts greater than 7 mm. The average total treatment time was determined to be about 20 min, which was in line with the time slot allocated for head and neck IMRT treatments. They also reported that patients gave high comfort scores to the open immobilization masks and that moldable cushions provided better patient setup than shoulder stirrups.

Gopan and Wu.[140] examined the accuracy of surface imaging for rigid and non-rigid setups in head and neck cancer radiotherapy by comparing internal 3D image pixel values for CT registration and surface spatial information for Align RT registration. They concluded that while Align RT system could be used for verifying and correcting daily rigid setup for head and neck radiotherapy further investigations were needed to improve the accuracy for non-rigid realignment.

Li et al.[141] developed a new enlarged precut open-face thermoplastic mask with eyes, nose, and mouth shown and the mask can achieve clinically acceptable levels of 1±5 mm for both immobilization and surface imaging.[141]

Webo Ei et al.[142] investigated the improvement of patient setup accuracy and reduction of setup time for SGRT compared to a conventional setup. A total of 60 H&N cancer patients were retrospectively included. Patients were categorized into three groups: oral cavity, oropharynx and nasopharynx/sinonasal sites with 20 patients in each group. They were further separated into two (2) subgroups, depending on whether they were set up with the aid of SGRT. The Align RT system was used to perform SGRT. Positioning was confirmed by daily kV-kV imaging in conjunction with weekly CBCT scans. Translational and rotational couch shifts along with patient setup times were recorded. Imaging setup time, which was defined as the elapsed time from the acquisition of the first image set to the end of the last image set, was recorded. Average translational shifts were larger in the non-SGRT group. Vertical shifts showed the most significant reduction in the SGRT group for both the oropharynx and the oral cavity groups. Pitch corrections were significantly higher in the SGRT

group for oropharynx patients and higher pitch corrections were also observed in the SGRT groups of oral cavity and nasopharynx/sinonasal patients. The average setup time when SGRT guidance was employed was shorter for all three treatment sites although this did not reach statistical significance. The largest time reduction between the SGRT and non-SGRT groups was seen in the nasopharynx/sinonasal group. This study suggests that the use of SGRT decreases the magnitude of translational couch shifts during patient setup. However, the rotational corrections needed were generally higher in the SGRT group. When SGRT was employed, a definite reduction in patient setup time was observed for nasopharynx/sinonasal and hypopharynx cancer patients.[142]

The above-mentioned studies established that employing SGRT resulted in a high level of accuracy for the fractionated treatment of head and neck cancers. These studies also showed that patient anxiety and claustrophobia levels were in general lower when an open mask used for SGRT replaced the conventional closed mask traditionally used for head and neck treatments. At least two of these studies also concluded that when SGRT was employed the treatment times were similar to those for non-SGRT fractionated IMRT head and neck radiotherapy treatments.

3. Materials and Methods

To introduce the work developed and the tests performed in the Radiotherapy Department at Hospital CUF Descobertas, this chapter starts with a flowchart description of the overall project. The flowchart presented in **Figure 3.1** gives an overview of all events before presenting a more detailed explanation of each phase. A brief description of the equipment and software used during the investigation will be presented in the next chapter.

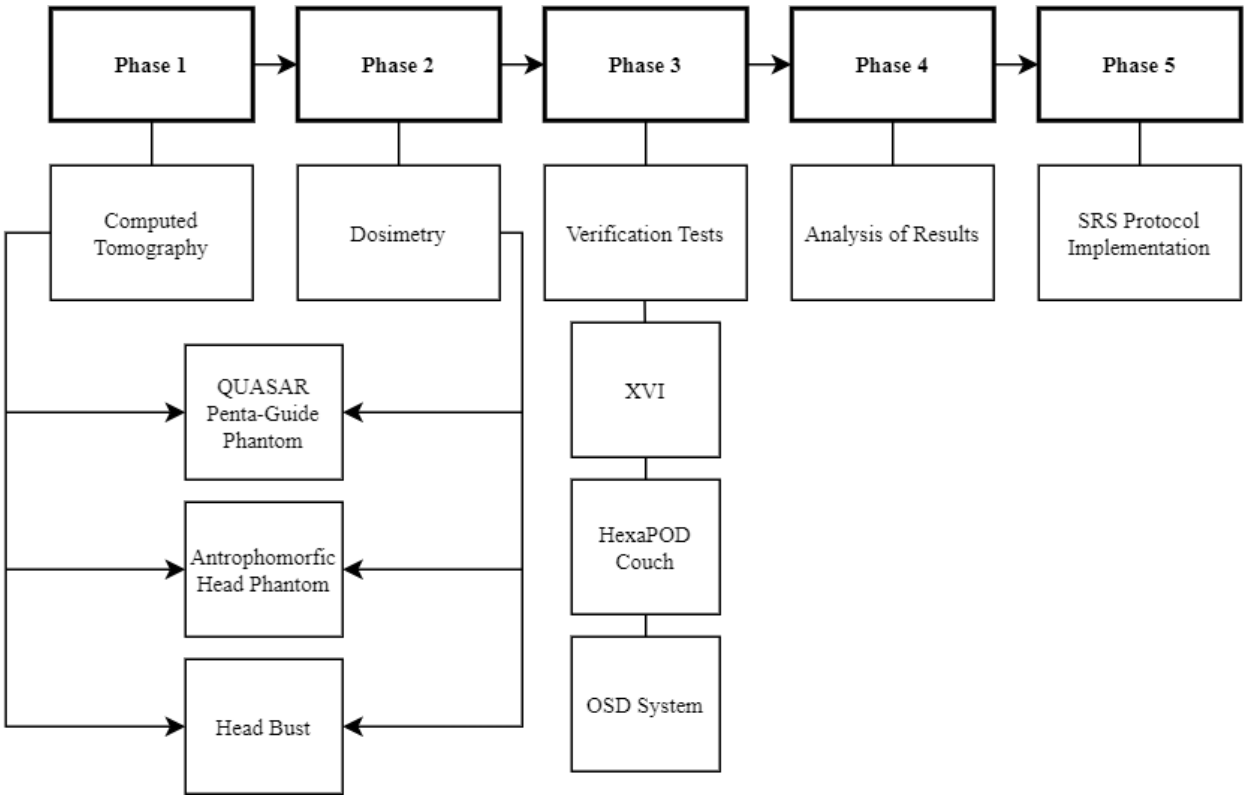

Figure 3.1 Investigation Project flowchart.

3.1 Equipment and Software

3.1.1 Discovery RT CT Scanner

The Discovery RT CT Scanner (from GE Healthcare, EUA) is a new advanced radiation therapy planning computed tomography system. Discovery RT is a CT simulator that offers a unique set of features that enables flexible patient positioning, software to address challenges presented by patient motion and metal, precise treatment planning and an efficient workflow, all combining to deliver uncompromised radiation therapy planning for oncology patients. CT Simulation is used to duplicate the radiation-treatment machine in terms of its geometric, mechanical, and optical properties by creating a three-dimensional image data set. This data is then used by the clinicians to localize the tumor and plan treatment without physically having the patient present. Discovery RT boasts an 80 cm bore with an 80 cm field-of-view, enabled by Max Field of View (MaxFOV), a new feature of this system. GE Healthcare's Smart Deviceless 4D technology delivers workflow efficiency and patient comfort in 4D motion assessment. Smart Deviceless 4D provides and displays images of all phases of a breathing cycle, which helps to simplify the motion assessment workflow.[143]

Figure 3.1.1.1 GE Discovery RT CT Scanner.

3.1.2 Linear Accelerator Elekta Versa HD™

Linear Accelerator Elekta Versa HD™ (from Elekta, Sweden) is equipped with the Agility MLC to deliver accurate, precise, and efficient radiosurgery to patients with multiple brain lesions. The combined use of these technologies with image guidance and patient positioning (enabled by XVI and HexaPOD™ couch) allows high-definition dynamic radiosurgery.[144] The Versa HD is a digital LINAC capable of delivering 6 MV, 6 MV FFF, 10 MV, 10 MV FFF, and 15 MV photon beams, as well as electron beams of 4, 6, 8, 9, 12, and 15 MeV. The maximum field size is 40 × 40 cm^2, defined by a pair of sculpted diaphragms mounted orthogonal to the MLC. The MLCs replace the jaws in the orthogonal direction and there are no backup jaws or diaphragms. The 80-pair interdigitating MLCs have a projected leaf width of 5 mm at the isocenter overall leaves. The tungsten MLCs in the Agility collimator are 9 cm thick and have a leaf speed of 3.5 cm/s. The carriage can travel up to 3 cm/s giving a maximum MLC speed of 6.5 cm/s. MLCs have a small tongue-and-groove interleaf gap, less than 0.1 mm, and are defocused from the source to minimize the interleaf leakage. The Agility collimator has a primary collimator speed of 9 cm/s and an isocenter clearance of 45 cm^2.

MOSAIQ is a comprehensive and integrated information system by Elekta Care Management that manages all aspects of the radiation oncology program. It uses a common database for radiation and chemotherapy records, being a single point of access for patient data. With MOSAIQ Radiation Oncology, all patient information is collected and accessible, from diagnosis through treatment and follow-up, so that clinicians can deliver the best possible care for every patient.

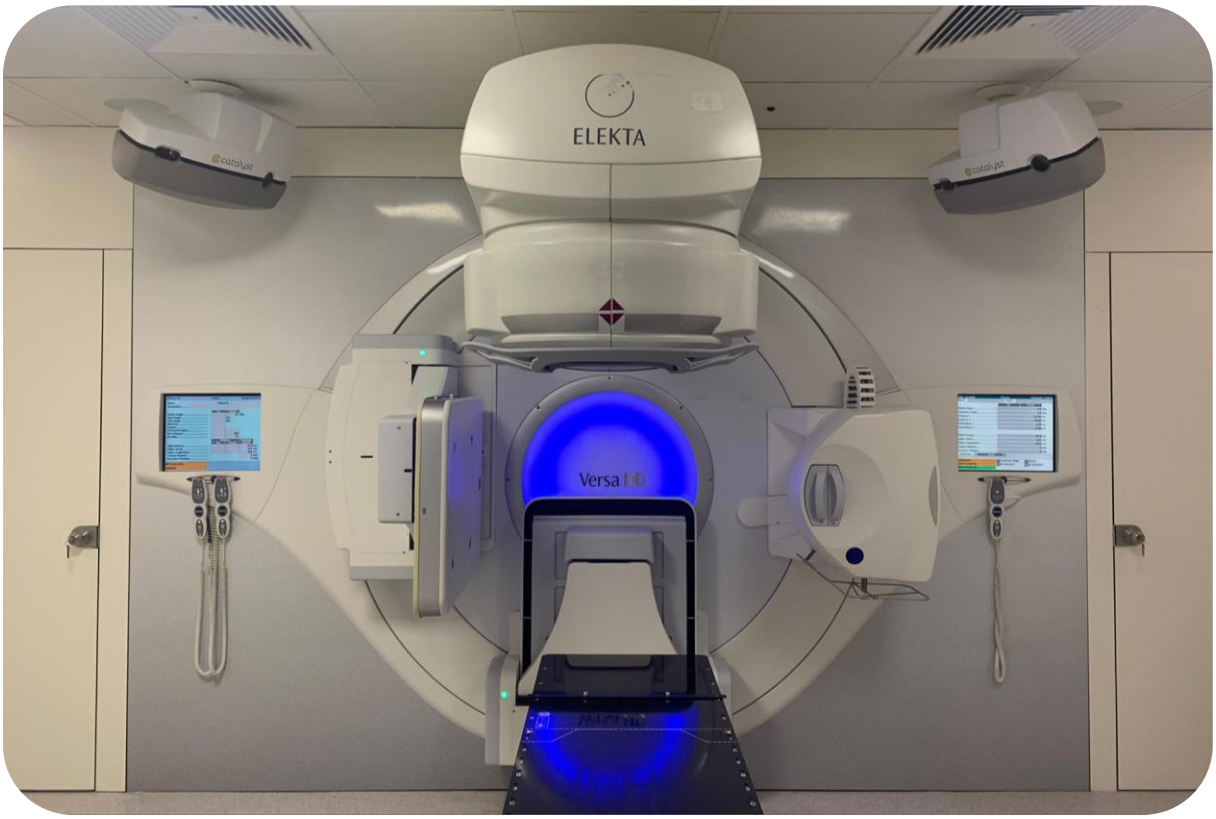

Figure 3.1.2.1 Linear Accelerator Elekta Versa HD™.

3.1.3 HexaPOD™ evo RT Couch

HexaPOD™ evo RT iGUIDE**,** (from Elekta, Sweden) is a robotic patient positioning couch system with 6-DOF. It allows the clinical user to remotely correct for misalignments of the patient not only along the traditional translational axes, but also for roll, pitch and yaw (rotational X, Y, Z). The 6-DOF given by the robotic couch allows the user to reposition the patient of any misalignments detected by state-of-the-art image guidance systems, thereby closing the gap in the 6-DOF-chain of IGRT localization and tumor isocenter targeting in any direction within sub-millimeter accuracy.[145]

The iGUIDE Tracking System along with the iGUIDE software (version 2.2.3) controls the robotic couchtop and validates the table position. The high-precision camera tracks the markers on the reference frame in real-time, making it possible to calculate the position of the robotic couch and patient. The iGUIDE software is adapted to the XVI coordinate system.

Figure 3.1.3.1 HexaPOD™ evo RT System. (1) iGUIDE Tracking System (2) HexaPOD™ evo RT Couch and (3) iGUIDE Reference Frame.[145]

3.1.4 Elekta Versa kV-CBCT (XVI)

The Elekta X-Ray Volume Imaging system XVI (from Elekta, Sweden) is an electronic imaging device that provides real-time 2D, 3D, and 4D image guidance before, during and after treatment delivery, and is intended to support the confirmation of patient positioning, monitoring, and management of internal motion, and decision making in response to the target position, size, shape, and displacement resulting from organ deformation and anatomical movement in relation to surrounding critical structures. XVI facilitates precise and accurate dose placement, and patient set-up correction, through visualization of internal anatomy including target, registration critical structures, and soft tissue with or without the use of implanted markers.[146]

The XVI software (version 5.0.2) runs on the control cabinet. The control system uses the Microsoft® Windows® operating system. The XVI control system controls the kV generator, acquires images, and reconstructs volume images from the acquired image sets. In the VolumeView™ mode, XVI acquires a sequence of 2D projection images while the digital accelerator gantry rotates. XVI uses the acquired images to reconstruct a 3D anatomical volume, which can be used for with imported CT reference data.

3.1.5 Catalyst HD™

Catalyst HD™ (from C-RAD AB, Sweden), is a real-time surface image-guided solution with submillimetric accuracy for online patient tracking before and during treatment delivery. With the three cameras – **Figure 3.1.5.1** - it is possible for a large patient surface coverage (1300x800x700mm) with optimal 360-degree coverage; fully support non-coplanar delivery and patented color map projected on the patient body during patient setup.[147] The Catalyst HD™ system includes three application modules, cPosition for fast and accurate patient positioning, cMotion for motion detection during the treatment delivery procedure and cRespiration for respiratory-gated treatment. All laser components that are part of the Catalyst HD™ system are classified as Class 2 lasers according to IEC 60825-1, and they comply with Food and Drug Administration. performance standards for laser products except for deviations pursuant to Laser Notice N0. 50, dated June 24, 2007. Class 2 lasers emit visible radiation in the wavelength range from 400 nm to 700 nm where eye protection is normally afforded by aversion responses including the blink reflex.[147]

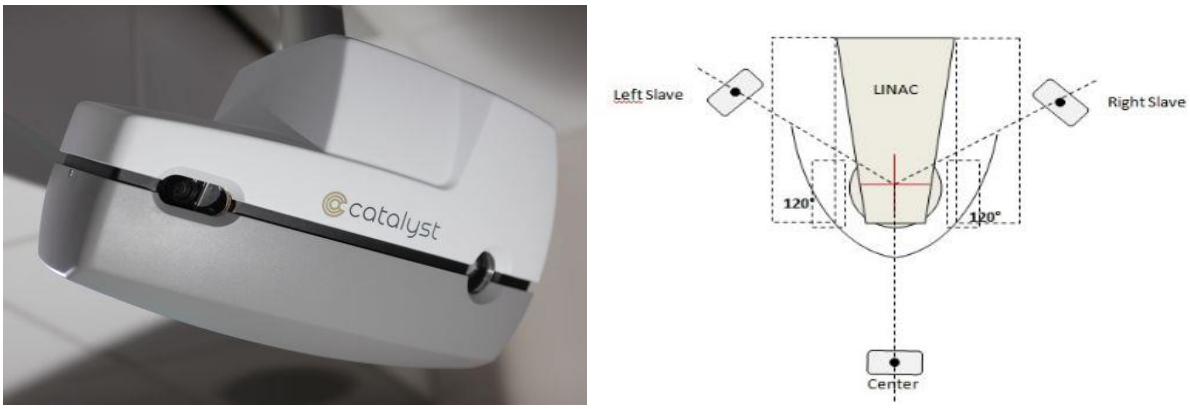

Figure 3.1.5.1 (A) Catalyst HD™ Lateral camera; (B) Camera arrangement with 120 º from each slave and center.[147]

The c4D software (version 5.3.2) provides the user information about the patient surface image during the Catalyst HD^{TM} scan. It comprises a non-rigid algorithm to calculate the isocenter shift due to patient setup or movement. This algorithm utilizes a non-rigid registration of the object to handle object motions during the scan. The isocenter shift is then calculated in real-time and the patient surface image is displayed on the screen.[147]

3.1.6 Elekta Fraxion™

Fraxion™ (from Elekta, Sweden)**,** is a patient-specific cranial frameless immobilization device that allows accuracy in treatment delivery. It consists of a patient control unit (PCU), and a Fraxion frame with a headrest and front piece. It also includes a unique vacuum mouthpiece and head vacuum cushion which fits into two holes on the bottom of the headrest to achieve accurate and comfortable patient immobilization, and when combined with partial or full head thermoplastic masks, ensures patient immobilization and positioning accuracy. The PCU provides the necessary vacuum for securing the mouthpiece to the patient's maxilla, thus securely immobilizing the patient. In addition, the PCU is used to form the vacuum cushion.[148]
It has several options for immobilization:

- Unique vacuum mouthpiece;
- Thermoplastic mask immobilization;
- Thermoplastic mask and mouthpiece combination.

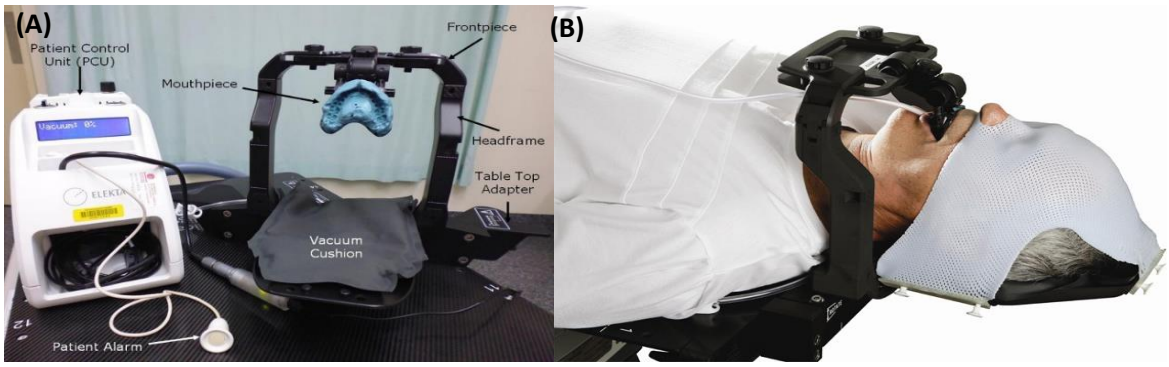

Figure 3.1.6.1 Fraxion™ system for patient-specific cranial immobilization. (A) Components of the Elekta Fraxion™ stabilization system. PCU, headframe and front piece with mouthpiece and inflated vacuum headrest (image courtesy of Princess Alexandra Hospital Radiation Oncology Department). (B) Elekta Fraxion™ system in place for patient setup.[149]

3.1.7 QUASAR™ Penta-Guide Phantom

The QUASAR™ Penta-Guide Phantom is recognized globally as the preferred tool for the commissioning and daily testing of IGRT systems. The QUASAR™ Penta-Guide Phantom ensures the accuracy of LINAC-mounted On-Board Imaging (OBI) guidance systems, including kV, MV, and XVI using CBCT. Its simple and innovative design facilitates intuitive verification of spatial alignment and isocenter coincidence on IGRT and SGRT systems. The addition of an optional Penta-Guide Tilt-Plate provides intuitive verification of 6-DOF couch adjustments. Combined with the analysis software, Penta-Guide provides detailed image quality metrics that evaluate the performance of your CBCT imaging systems.[150]

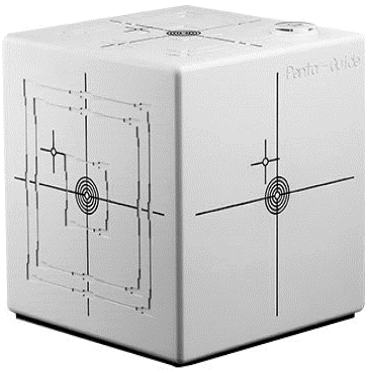

Figure 3.1.7.1 QUASAR™ Penta-Guide phantom used for Routine QA.[150]

Phantom specifications:

- Cube, 16 cm, acrylic, 5 kg;
- 4 x 4, 10 x 10, and 12 x 12 cm^2 light field alignment;
- Laser alignment lines;
- Built-in bubble level;
- Free software available for download;
- Internal imaging and registration markers designed to minimize CT artifacts;
- User's Guide and cardboard container for storage and handling are included.[157]

3.1.8 Phantom Model HZ-023

The Phantom Model HZ-023 is a Daily Check device specially designed to perform the Catalyst HD™ daily check.[147]

Figure 3.1.8.1 Phantom Model HZ-023.[147]

3.1.9 Head Bust

A hairdresser's head bust was used to perform one of the tests, to evaluate the detection performance of the OSD system. The advantage of its use is the fact that the bust has an identical shape of a human head and its color mimics the color of a lighter skin. Later, its applicability could not fulfill the pre-requisites to perform the other tests due to its hollowness, since there was no reference point that could be used for image verification. Afterwards, an anthropomorphic head phantom was built from scratch to continue with the testing.

Figure 3.1.9.1 Head Bust.

3.1.10 Anthropomorphic Home-Made Phantom

Anthropomorphic phantoms are objects that simulate patients, made of materials with similar tissue characteristics to normal biological organisms. Due to their availability and likeness to real patients, anthropomorphic phantoms can be used for a variety of tasks. Rather than image multiple patients, they can be used for trials to assess the optimal use of radiation such as in new protocols or image reconstruction techniques. Since the head bust could not be used to perform further testing due to its hollowness and no reference point, an anthropomorphic home-made phantom was built manually to mimic the shape of a human head – **Figure 3.1.10.1**

The home-made phantom construction process began with the choice of specific materials in order to mimic the structure and density of the human head in the best possible way. Paraffin was used for the general structure and shape of the head; small objects with air (tubes) to mimic the respiratory airways; radiopaque materials (screws) to create small landmarks; modeling clay to mimic brain density; plaster and compresses to create the human scalp. The neck; ears; nose and eyes were molded from clay. The overall weight of the home-made phantom was 4 kg. After its construction, a CT scan was performed to verify whether the various densities of the materials corresponded in a similar way to the internal anatomical structures. After evaluation, there was a lot of artifacts in the images due to the radiopaque materials placed inside. Subsequently, the phantom was opened, and the excess material was removed. The advantage of using this home-made phantom is the fact that can be used to test the OSD system and perform kv-imaging verification.

Figure 3.1.10.1 Anthropomorphic Home-Made Phantom mimicking the human head.

3.2 Methodology

As previously mentioned, the principal objective of this thesis is to test the viability regarding the implementation of a maskless immobilization approach with only a vacuum mouthpiece suction system for head fixation in patients with CNS tumors who will undergo SRS treatment under the guidance of an OSD system coupled with 6-DOF robotic couch for submillimetric position correction. The combination of all these systems concomitantly has not been validated in the literature since most SRS treatments are performed with full closed or open-face thermoplastic masks, without OSD system monitorization. As such, system validation is necessary to assess the system precision at extreme configurations, such as maximum isocentric couch rotations, maskless approach, OSD system camera pod occlusions, together with 6-DOF couch movements. To validate the implementation of an OSD system concomitantly to the use of a frameless immobilization device, five verification tests were performed in the Radiotherapy Department of Hospital CUF Descobertas, with all data being registered.

Each test was thought and planned according to the results that were intended to be obtained, considering each equipment used. The tests were carried out in an experimental manner, where specific table rotations and gantry angulations were chosen to test the most extreme configurations. There is evidence in the literature of tests identical to those performed, regarding the 4th test, but no specific guidelines were followed. All quality controls performed were followed according to equipment manuals. For the performance of the tests, specific equipment and software was used, as described in the previous chapter. **Table 3.2.1** summarizes the tests performed in the Radiotherapy Department.

Table 3.2.1 Summary of the performed tests in the Radiotherapy Department at Hospital CUF Descobertas

Test Nr.	Test Name	Equipment	Software	Phantom	Gantry Angulation	Couch Rotation	Description/Aim
1	CW and CC XVI-CBCT Systematic Error Assessment	XVI vs LINAC	MOSAIQ XVI	HeadPhantom	CW e CC	No	Assessment of the positional errors regarding the isocenter matching alignment between the kilo-voltage cone beam computed tomography (kV-CBCT) imaging system and Linear Accelerator (LINAC). 6 clockwise (CW) and 6 counterclockwise (CC) acquisitions were performed to test the viability of acquiring CW CBCT or CCW CBCT during SRS treatments.
2	HexaPOD Couch and XVI Mechanical Error Assessment during Couch Rotations	HexaPOD Couch vs XVI	MOSAIQ XVI iGuide	PentaGuide	No	0°, 15°, 30°, 45°, 60°, 75°, 90°, 270°, 285°, 300°, 315°, 330°, 345°	Assessment of the 6-DOF HexaPOD couch and kV-CBCT mechanical error regarding the isocenter calibration. The position error calculated by XVI after image acquisition should be identical to the positional error calculated by the 6-DOF robotic couch inside the treatment room. The difference between the two systems – mechanical error, should be accountable since the couch isocenter is calibrated according to the isocenter of the XVI.
3	OSD System Performance in Coplanar Angles	OSD System vs HexaPOD Couch	MOSAIQ c4D	Bust	0°, 45°, 90°, 135°, 180°, 225°, 270°, 315°	No	It comprises the gantry rotation with HexaPOD couch always at 0º to test the performance of the OSD system cameras on detecting the bust surface. Assess in which gantry angulations exists camera occlusions due to the XVI Ampoule, XVI panel detector and gantry head.
4	OSD System Performance with Couch Rotations	OSD System vs HexaPOD Couch	MOSAIQ iGuide c4D	HeadPhantom	No	30°, 60°, 90°, 270°, 300°, 330°	It comprises the gantry at 0º and rotation of the 6-DOF robotic couch. All values that appear in OSD system when the couch is rotated must be the inverse of the 6-DOF robotic couch actual value and should maintain a tendency throughout the couch rotation.
5	Positional Error Agreement between OSD System and HexaPOD Couch at Non-Coplanar Angles	OSD System vs HexaPOD Couch	MOSAIQ iGuide c4D	HeadPhantom	30°, 45°, 315°, 330°	30°, 60°, 90°, 270°, 300°, 330°	Rotate the Gantry and the 6-DOF robotic couch to verify if the HexaPOD Couch Positional Error Values and the OSD System Calculated Couch Correction values are the same. Check the non-coplanar angles where the two system differ the most.

3.2.1 Submillimeter Computed Tomography Acquisition and Dosimetry of QUASAR™ Penta Guide phantom, Anthropomorphic Head Phantom and Head Bust

Prior to all tests, a CT scan was performed on QUASAR™ Penta Guide phantom - **Figure 3.2.1.1**, head bust - **Figure 3.2.1.1** and anthropomorphic head phantom **Figure 3.2.1.3**. The anthropomorphic head phantom was built specifically to assess the accuracy and limitations of the OSD system regarding the continuous detection of its surface, without signal inconsistencies at different gantry angles and couch rotations, especially at non-coplanar angles. Both phantoms were positioned on the CT table, each at the time, and then aligned with the three lasers present in the room. CT data images were acquired during this phase and must serve two key purposes: create a reference image, with high geometric fidelity and accuracy, that will be used afterward in the matching process during image acquisition; and to provide a map of the electron density information to be used in dosimetry. CT scan protocols have pre-determined parameters such as reconstruction algorithm, slice width, tube current, the field of view (FOV) and other parameters to produce high-quality images to match the imaging task. The following parameters were used for all CT acquisitions.

Table 3.2.1.1 CT acquisition parameters.

Acquisition Parameters	Helical Thickness (mm)	FOV (cm)	Pitch	Speed (mm/rot)	Scan Type	kV	mA
Values	0,625	23,6	0.938:1	9,37	Cine	120	215

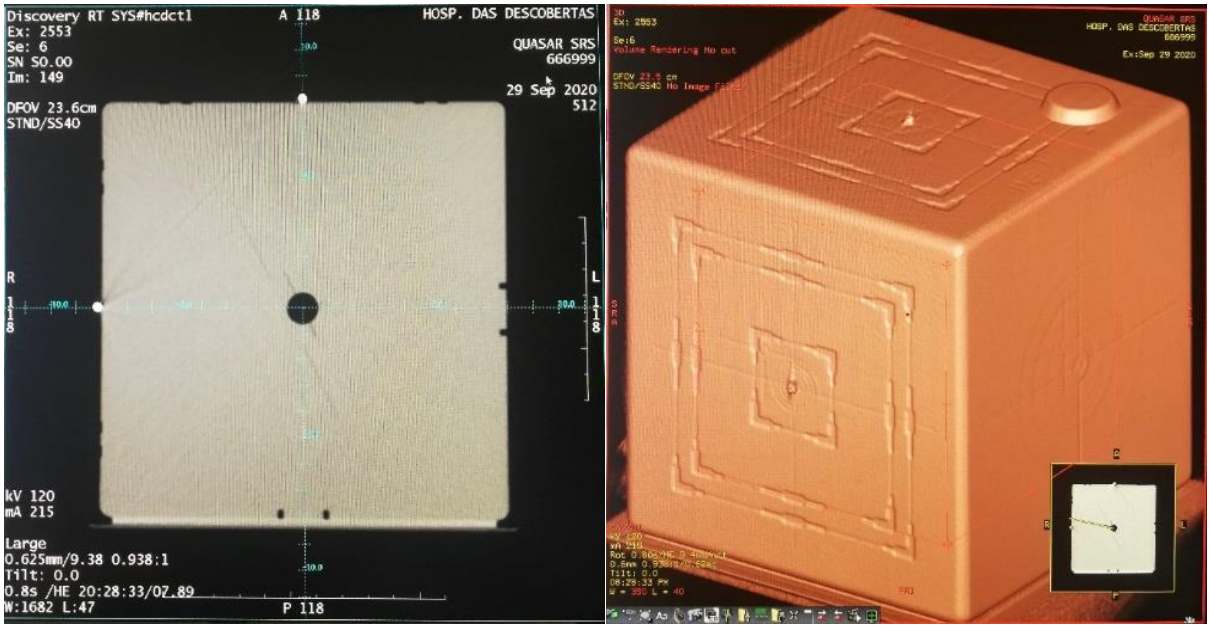

Figure 3.2.1.1 (A) QUASAR™ axial view; (B) 3D External Reconstruction of QUASAR™.

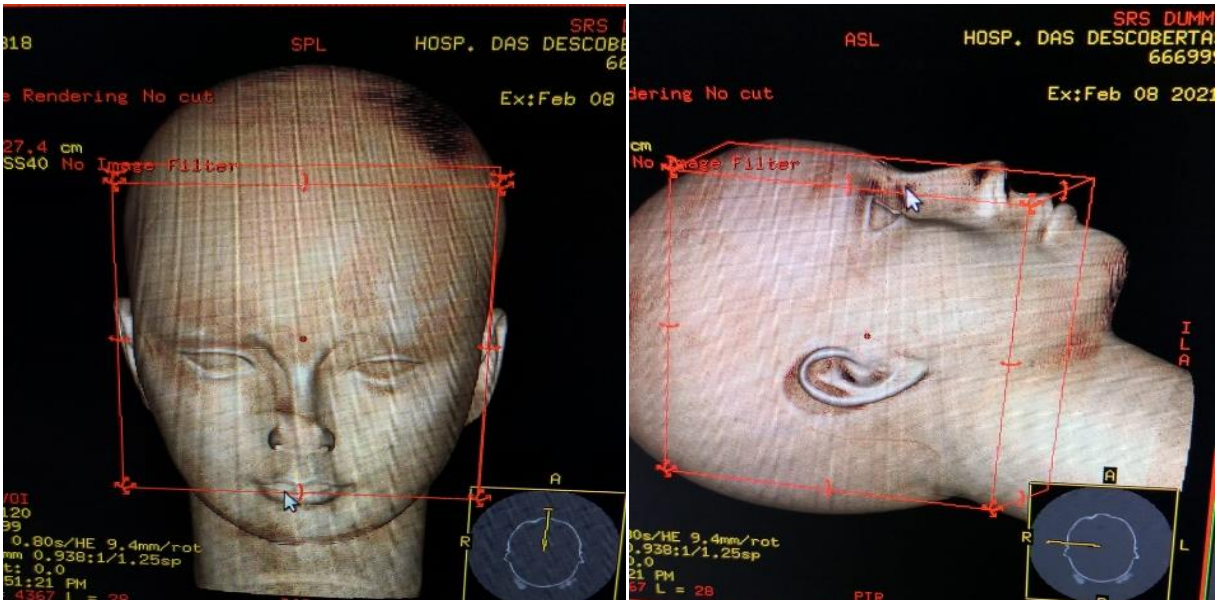

Figure 3.2.1.2 (A) 3D External Reconstruction of Head Bust in frontal view; (B) 3D External Reconstruction of Head Bust in lateral view.

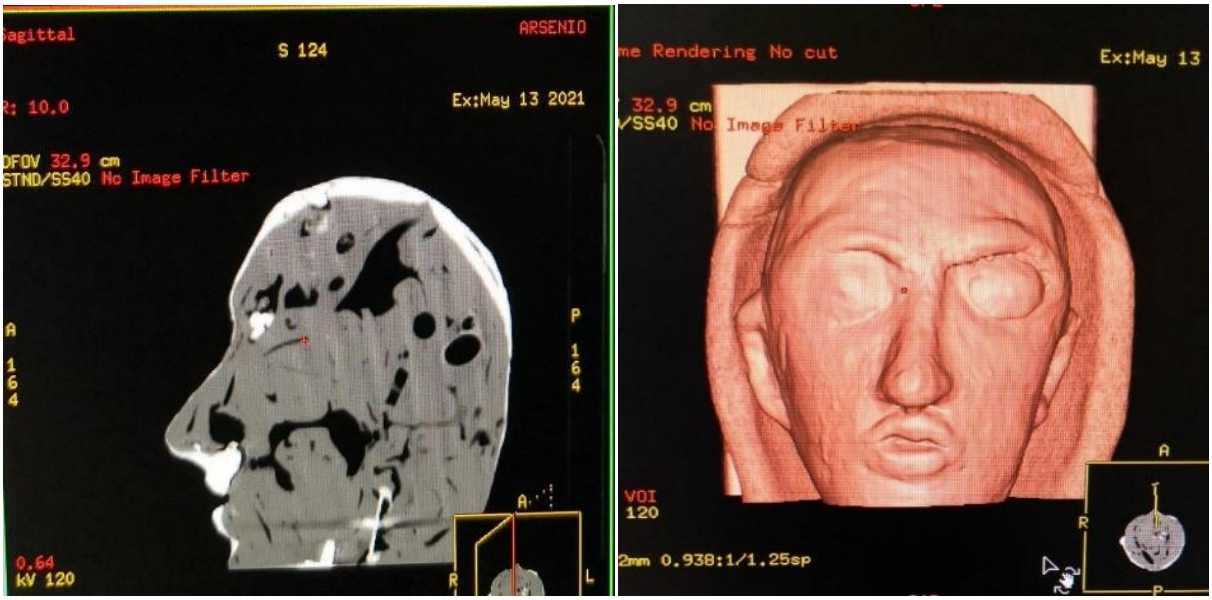

Figure 3.2.1.3 (A) Anthropomorphic Head Phantom sagittal view; (B) 3D External Reconstruction of Anthropomorphic Head Phantom.

Data was imported to Monaco treatment planning system (TPS) after acquisition, where the external contour was delimited and isocenter defined. Setup beam fields were also programmed for the specific gantry angulations and couch rotations seen in **Table 3.2.1**.

3.2.2 Systematic Error Assessment between CW and CC CBCT Acquisition

Quality assurance programs of CBCT should be created to ensure that quality image requirements are met; verification data collection standards are regularly assessed and maintained; errors and uncertainties are reduced and minimize the risk of accidents and incidents. Each component of the verification process – from the acquisition of planning data to the subjectivity in decision-making by individuals – may have a certain level of error or uncertainty within it. Ideally, these should be measured so that the overall accuracy of the verification process is known. This can be taken into consideration when assessing the validity of the image match data, which is an important measure when determining planning margins.[151]

For IGRT systems based on CBCT integrated into a linear accelerator, the reproducibility of isocenter alignment between CT image and X-Ray volumetric image with the kilovoltage (kV) beam is critical to minimize matching errors. The 1st test conducted was to assess the systematic error associated to the Elekta Versa kV CBCT – XVI - regarding the system's precision in isocenter matching, which consisted of CBCT acquisitions for CW and CC gantry directions, with 200º rotations to perform CBCT with small field of view of an anthropomorphic head phantom with 0º couch rotation **Figure 3.2.2.2**. The scanning parameters are presented in **Table 3.2.1.1**. While performing CBCT, the automatic registration match method "Grey Value – Translation + Rotation (T+R)" was used to verify the isocenter position in all translational directions (lateral 'x', longitudinal 'y', and vertical 'z') and rotation (pitch, roll and yaw). After each acquisition, the calculated position error in translation (mm) and rotation (º) was registered, and no couch correction was applied derived from the positioning errors in phantom-matching. **Figure 3.2.2.1** represents the steps performed in the 1st test.

Table 3.2.2.1 Scanning Parameters of the 1st test.

Acquisition Parameters	Automatic Registration Method	Nº Frames	Filter	Gantry Speed (rot/min)	Collimator Cassette	kV	mA
Values	Grey Value (T+R)	330	F1	360º	S20	120	528

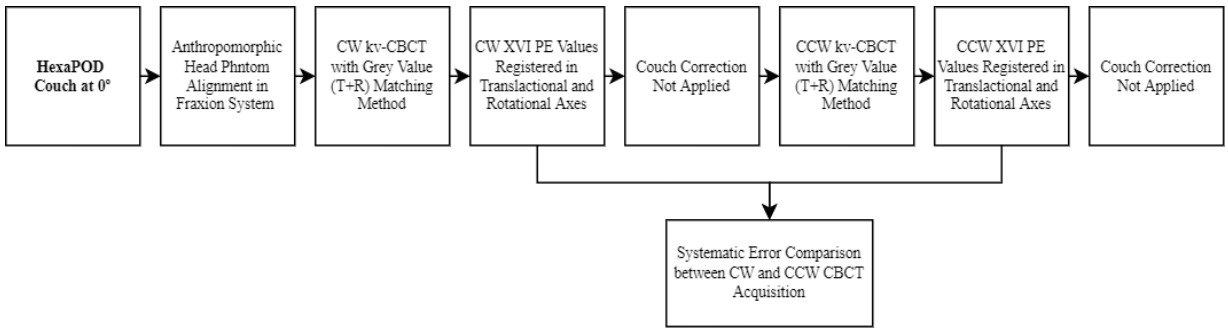

Figure 3.2.2.1 Steps performed in the 1st test.

Figure 3.2.2.2 Anthropomorphic head phantom alignment with cushion head set on Fraxion™ system.

3.2.3 Mechanical Error Assessment between HexaPOD Couch and XVI during Couch Rotations

The HexaPOD couch system is designed for sub-millimeter exact patient positioning for radiotherapy treatments. This system uses relative table movements (RTMs) to move to a treatment target that does not match external markings. XVI and HexaPOD couch are two connected systems, where HexaPOD couch uses positional error values sent from XVI to position the treatment target so that it is exactly oriented at the isocenter as defined by the treatment planning system. As such, when a patient is aligned, the position and orientation of the treatment target can only be approximated. To get the exact position, the imaging system scans the volume around the isocenter and then reconstructs it. The positional offsets between the reconstructed volume and the volume used for planning are calculated, generating the image registration positional error values. The PE values are transferred to the iGUIDE software (automatically or manually, depending on the system configuration) which translates the PE values into movement commands for the robotic couch. The radiation therapist then performs an automatic remote table move in 6-DOF so that the treatment target is oriented as required at the isocenter.

The 2nd test was performed with the Penta Guide phantom to assess the mechanical error existent between the two systems. When manually couch rotation is performed inside the treatment room, the HexaPOD couch iGuide system software calculates automatically the positional errors detected after couch rotation. Theoretically, the PE values calculated by HexaPOD should be in agreement with the ones calculated by XVI after image acquisition and matching. It must be considered that, for each manual couch rotation performed, the positional error considered necessary to be corrected to achieve the isocenter position by the HexaPOD couch iGuide system varies. Since it’s not possible to acquire CBCT images with couch rotations - due to the risk of gantry collision, to confirm the iGuide system PE Values calculated, the only way to test the feasibility of the system was to perform the 2nd verification test mentioned in the methodology. The 2nd test consisted in manually rotating the couch from 0º to a certain rotation, registering the PE values in translation and rotation axes calculated by iGuide software, applying manual translational corrections with the HexaPOD couch remote control, rotating the couch to the starting position at 0º and confirm with the PE values obtained by matching with the kv-CBCT image. If the radiation isocenter is correctly calibrated between the two systems, the same PE should be presented.

The process mentioned was repeated inside the treatment room at 15 º; 30 º; 45 º; 60 º; 75 º; 90 º; 270 º; 285 º; 300 º; 315 º;330 º; 345 º. The HexaPOD couch PEs were registered for each rotation, in all translation and rotation axes. After applying manual correction, the couch was set to its initial position at 0º, CBCT was acquired, and the position error calculated by XVI was registered and compared. **Figure 3.2.3.1** represents the steps performed in the 2nd test.

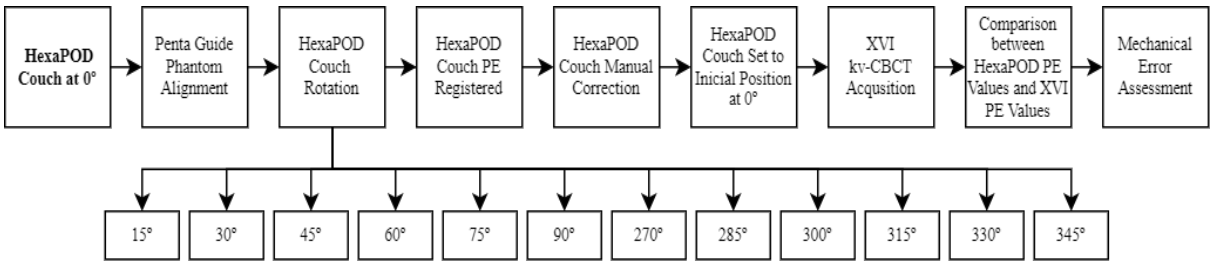

Figure 3.2.3.1 Steps performed in the 2nd test.

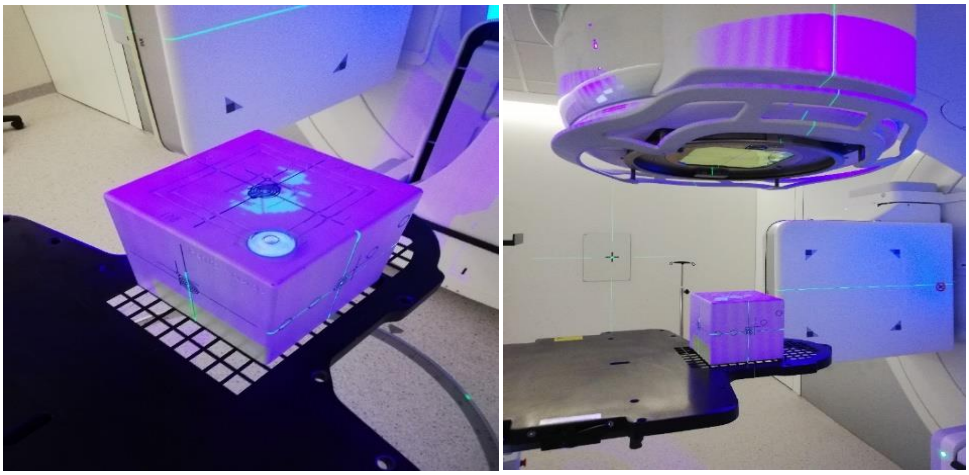

Figure 3.2.3.2 QUASAR™ Penta Guide phantom alignment.

3.2.4 OSD System Routine QA for SRS Treatment

The OSD system used in this experiment requires a Routine Quality Assurance (QA) to be performed prior to SRT/SRS treatments or verification tests. The calibration is valid for four hours, thereafter SRT/SRS treatments cannot proceed, and a new Routine QA must be performed. The Routine QA requires a daily check phantom provided by the vendors and a QUASAR™ Penta Guide Phantom. The purpose of the QA procedure is to align the Catalyst HD™ system to the radiation isocenter by aligning the routine QA phantom using verification imaging (MV/kV). The results are saved in the "Routine QA History" and can be viewed in the Advanced mode. The routine QA is performed in two steps. The first step consists in aligning the three Catalyst HD™ cameras to the same coordinate system. The procedure for this step is the same as for a standard daily check using the daily check device and the room lasers. In the second step the final adjustment of the Catalyst HD™ coordinate system is performed. This is accomplished by aligning the routine QA phantom using a reference image of the phantom and verification imaging (MV/kV). The frequency of the performed QA procedure is defined by the user. The QA of the LINAC verification imaging systems is recommended to be performed before the routine QA of the Catalyst HD™ system. If a patient synchronization event occurs during routine QA, that in a normal workflow would have send the user to c4D Welcome screen, c4D stays in the current routine QA workflow and an information dialog is displayed to the user.[147]

Preparation:
It is recommended to use a CT image of the routine QA phantom as a reference data set. In order to create such a reference data set, the phantom is scanned with a conventional CT scanner using a slice thickness of high resolution, 1 or 1,5 mm. The CT data set is then sent to the treatment planning system, where the isocenter is carefully located and marked at the geometrical centre of the cube. A QA plan is then created in the record and verify system and the reference image set including the structure and beam data is sent there. It is crucial to have the isocenter marked correctly in the reference data set.[147]

QA Procedures:[147]

1. Restart c4D by selecting the "Exit" button in the Welcome screen. If you are an advanced user select "Exit" in Advanced mode.
2. Log on to the system as an administrator user by entering a user name and a password. Select "OK" and switch to Clinical mode.
3. From the Welcome screen select the symbol for "Routine QA".
4. Firstly, perform the steps for a standard Daily Check procedure.
   4.1. Align the side marks on device model HZ-023 to the room laser.

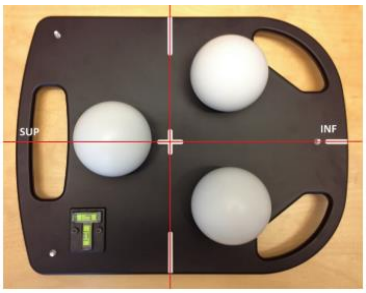

Figure 3.2.4.1 HZ-023 Phantom model aligned accordingly to sagittal and axial room lasers.

   4.2. Align the lines at the centre of the spheres to the vertical room laser as in the figure below:

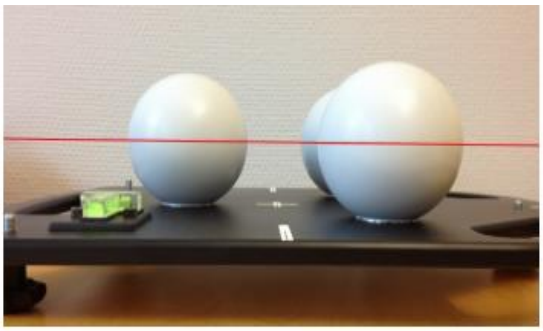

Figure 3.2.4.2 HZ-023 Phantom model aligned accordingly to coronal room lasers.

4.3. Select “Check” or press the button “Scan” on the remote control to start the daily check.

4.4. Initially a test is performed to ensure the scanner's linearity. A progress bar indicates the progress of the operation.

4.5. The device is then scanned. The scan is automatically repeated five times to ensure the highest possible accuracy. A progress bar indicates the progress of the scanning and algorithm calculation. The information displayed is:

- Current deviation - the system drift since the previous daily check or routine QA if a routine QA has been performed.
- Total deviation - the total drift since the last isocenter adjustment.
- Result:
  - Daily Check OK - the deviations are within the tolerance.
  - Daily Check Outside Tolerance! - highlighted in red, if the deviations are outside the tolerance.
  - Object not recognized! - highlighted in red, if the object is not recognized. Make sure that you have the correct object and that the whole object is visible in the scanned image.
- Accepted Deviation - the tolerance values for the different deviations.
- Last Daily Check - date and time for the last Daily Check.

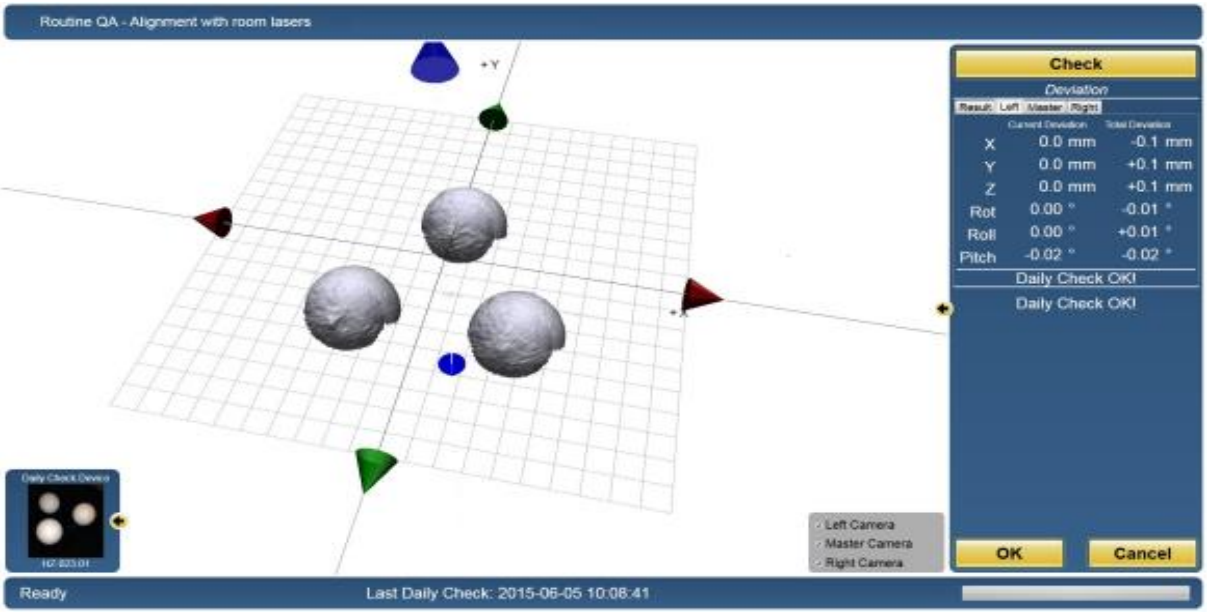

Figure 3.2.4.3 Routine QA - Alignment with room lasers.

5. Select "OK" to save Daily Check the result.

6. The next step is the radiation isocenter alignment.

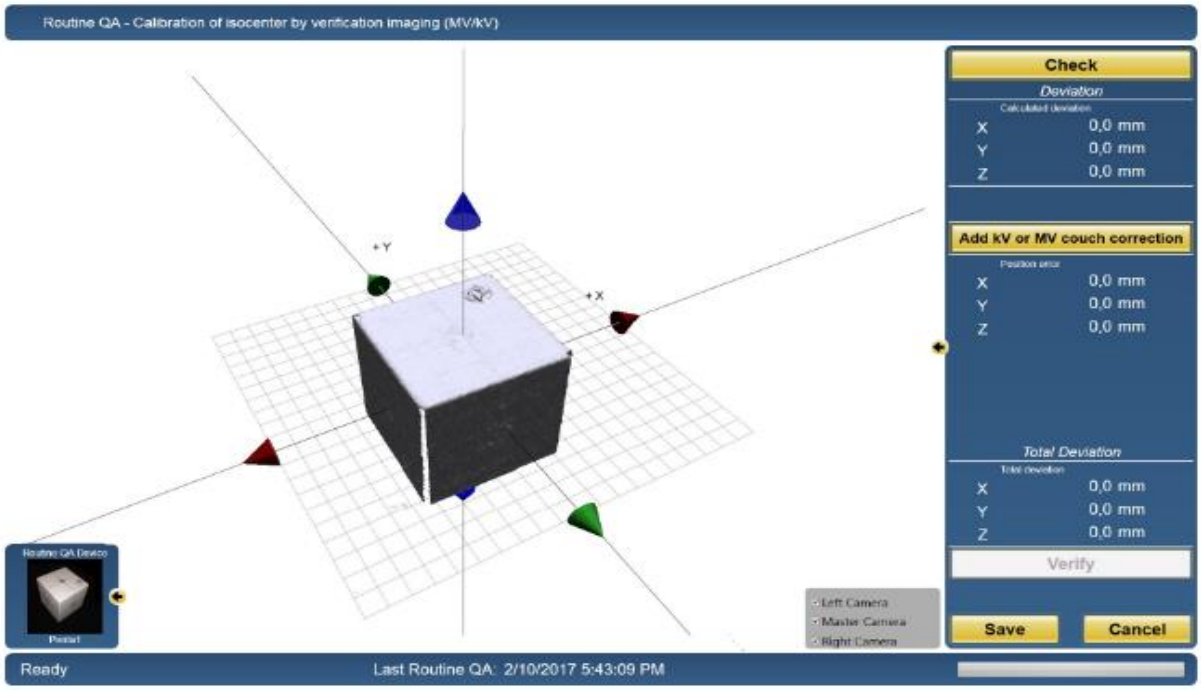

Figure 3.2.4.4 Routine QA – Calibration of Isocenter by Verification Imaging (MV/kV)

7. Align the routine QA phantom to the radiation isocenter by using verification imaging (MV, CBCT or kV). Adjust the couch according to the result.

Figure 3.2.4.5 QUASAR™ Phantom aligned inside by the room lasers.

8. Press "Check" when phantom is in the final position.

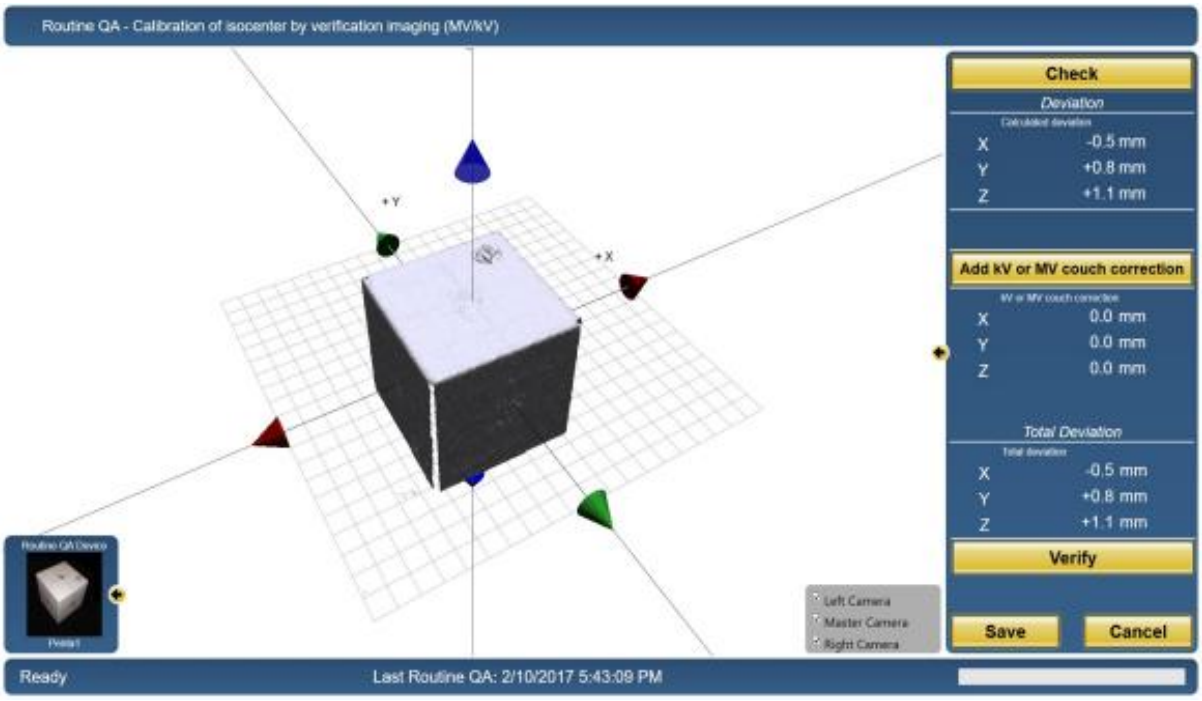

Figure 3.2.4.6 Routine QA – Calibration of Isocenter by Verification Imaging (MV/kV) with respective deviation.

9. The deviation between the alignment to the room lasers and the alignment to the isocenter is presented.

10. Depending on the accuracy of the couch it could be a small difference between the optimal position according to verification imaging and the final position of the phantom after the couch adjustment. The difference is typically within 0.5 mm, depending on the accuracy of the couch. If this is the case, you have the possibility to correct this setup error. To do this follow the steps below:

a. Acquire new verification images (MV, CBCT or kV) and match the images. Do not adjust the couch.
b. Select "Add kV or MV couch correction"
c. Enter the residual couch correction according to the verification imaging system and press "OK".
d. The total deviation is the difference between the calculated deviation and the residual couch correction.

11. Press "Verify" to visually see the resulting correction. The Catalyst HD™ system is compensating the acquired images according to the final result.

12. Select "Save" to use the compensation. To cancel the alignment according to the verification imaging press "Cancel". Only the Daily Check procedure using the room lasers will then be used.

After routine QA, the phantoms used to perform the tests must be selected manually or via synchronization to proceed to the next step - “pre Setup”, where the phantom will be configured for the position module. Specifically for SRS patients, the image scanned must be with high image resolution. To define the pre-setup for the SRS workflow a window is displayed. On the screen, it can be seen the information about the phantom’s identification, name and site.

Figure 3.2.4.7 Catalyst HD™ Pre-Setup Window.

Before each SRS treatment, it is important to check that the settings are optimal for the patient. This is done by pressing the “Settings”-button. The setting view is presented.

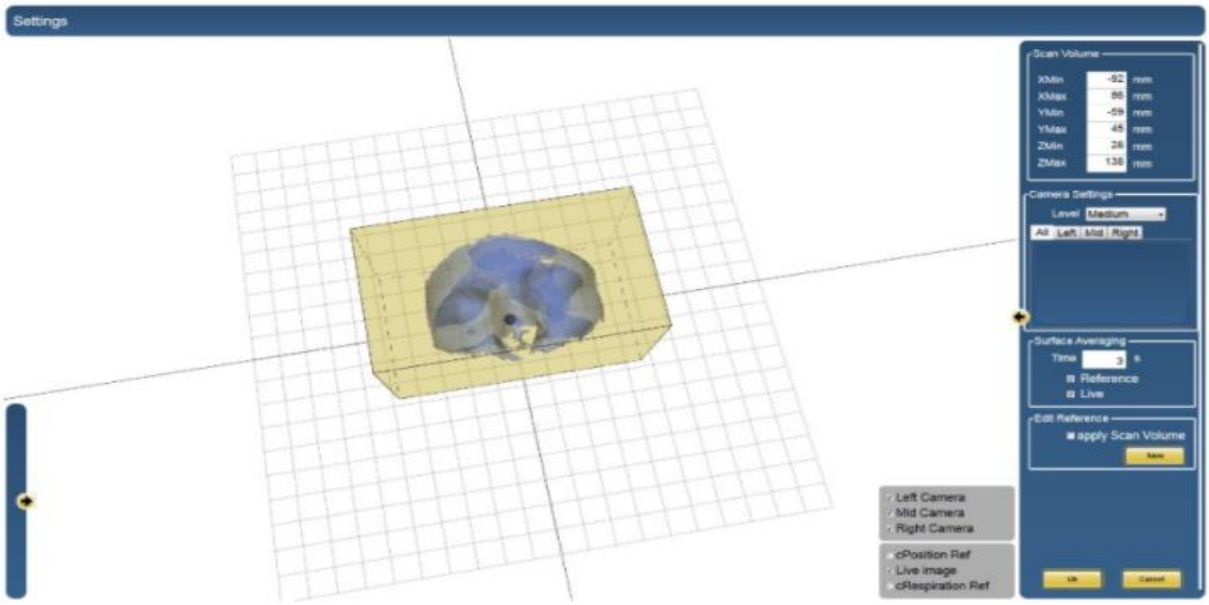

Figure 3.2.4.8 Pre-setup Camera Settings.

For SRS treatments with an open mask setup, the color of the mask and the patient’s skin shall significantly differ. To detect the movements of the patient the camera settings shall be optimized to the skin of the patient.

Specific for SRS treatments:

- Scan volume - adjust the scan volume to only include the opening of the mask.
- Edit Reference - If a CT image has been imported as a Position reference use the "Edit reference" function to crop the Position reference to include a surface as similar as possible to the opening of the mask.
- Camera settings - For treatments involving non-coplanar fields it is important that the camera settings are equivalent for the three cameras. Always use the predefined levels if possible.

If the exposure time setting is very high, the update rate of the 3D surface images will be slower. The cameras Left/Mid and Right were selected one at a time and inspected the surface and image view (for overexposing and underexposing indication). If required, the camera settings must be adjusted one at a time. For the mid camera, it is sometimes required to rotate the couch to set the camera settings. Make sure that the surface is not overexposed, see examples below.

- Optimal settings - no or very small red (overexposed) and blue (underexposed) areas in the relevant section of the camera image.

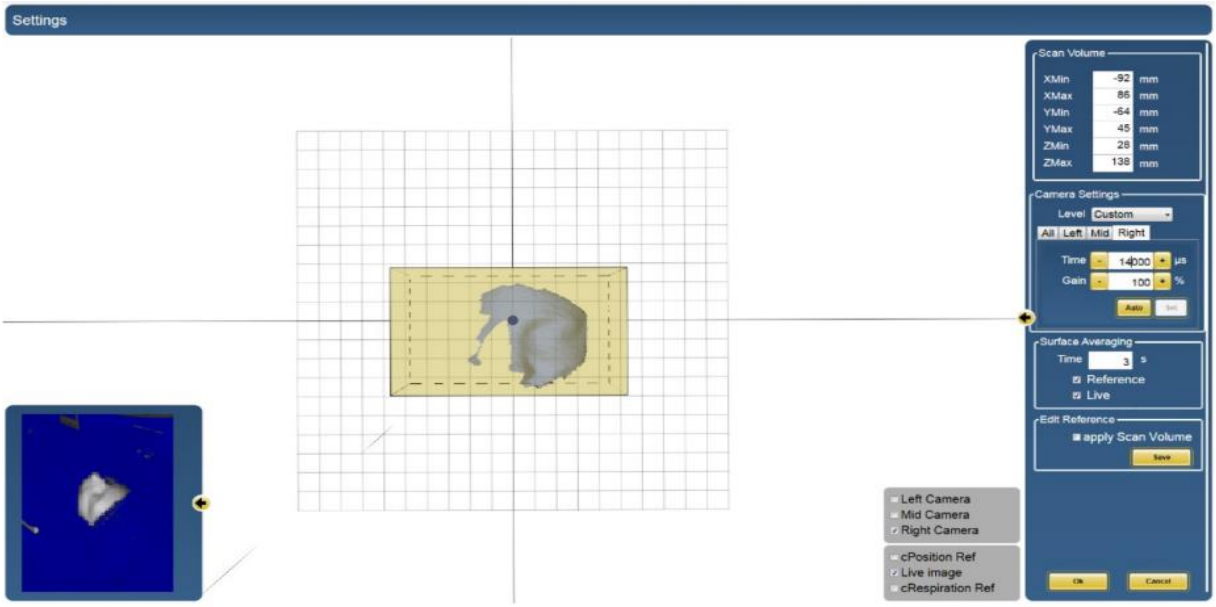

Figure 3.2.4.9 Pre-setup with Optimal Camera Settings.

- Overexposed - Red areas in the camera image (overexposed). If this is the case you should decrease the time and/or gain. Start by decreasing the time.

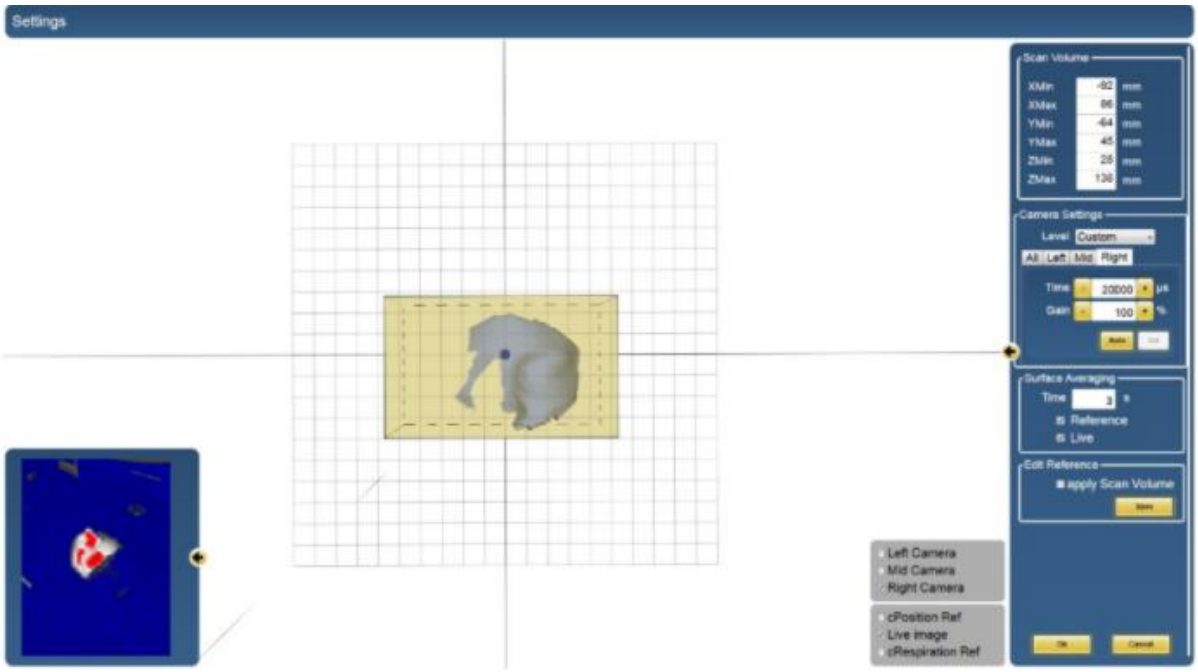

Figure 3.2.4.10 Pre-setup with Overexposed Camera Settings.

- Underexposed - Blue or dark areas in the camera image (underexposed). If this is the case, you should increase the time and/or gain. Start by increasing the time.

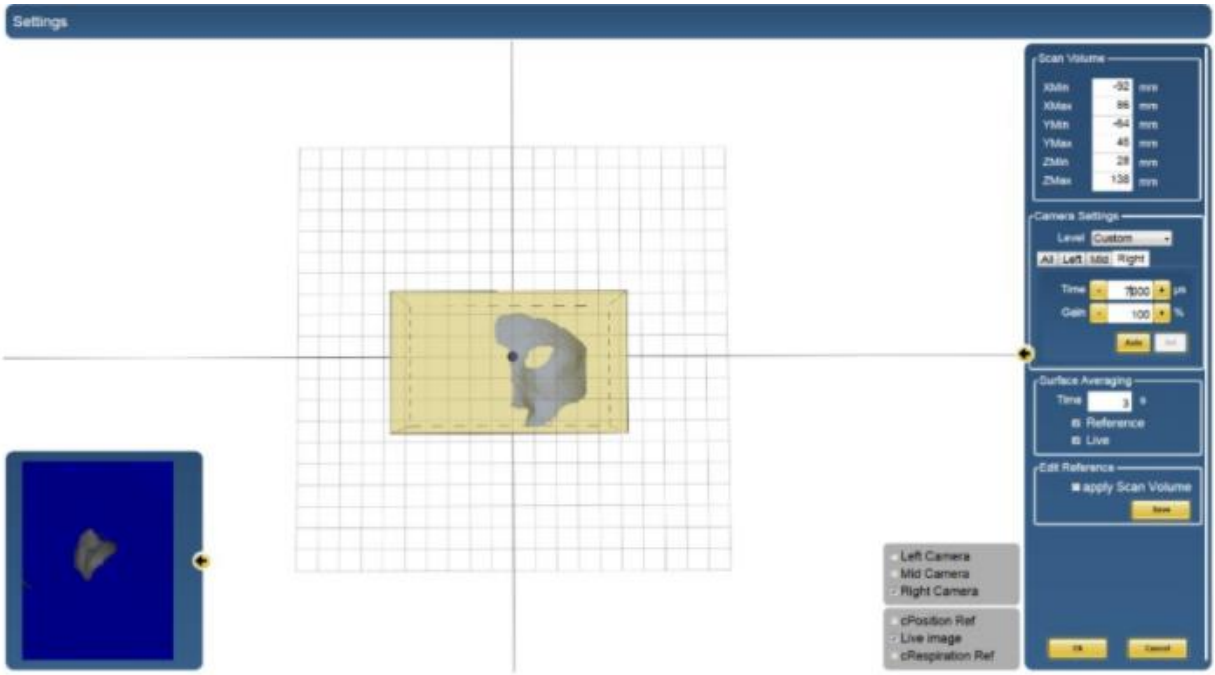

Figure 3.2.4.11 Pre-setup with Underexposed Camera Settings.

3.2.5 Optical Surface Detection Test at Coplanar Angles

Before performing any test on the OSD system, a routine QA for SRS was performed at least 4 hours prior to the use of the equipment. In specific gantry angulations, camera occlusions and consequent signal interruptions are expected during the optical surface acquisition since two of the OSD system camera pods are located on the ceiling laterally to the treatment couch, and the other one is located on the ceiling centrally at the end of the treatment couch. As a result of gantry rotations during treatments, the gantry head; XVI R-Ray tube and XVI panel detector can occlude one or two of the lateral camera pods, resulting in a smaller area monitored and potentially leading to inaccurate detection reading. The use of the central camera together with the lateral cameras, eliminates this problem, and for every gantry angle there are at least two camera pods (central plus one lateral) available for surface acquisition, allowing accurate monitoring in all situations. The 3rd test was conducted with the head bust to test the performance of the OSD system cameras on detecting the bust surface in angulations where were occlusion of the cameras **Figure 3.2.5.1**, **Figure 3.2.5.2**. This test consisted in rotating the gantry manually inside the treatment room at specific angulations; 0º; 45º; 90º; 135º; 180º; 225º; 270º; 315º respectively, always with 0º HexaPOD couch rotation. Each camera pod used a near-violet light onto the head bust and a CCD camera to detect the light reflected from it. The 3D surface was reconstructed based on the principle of triangulation and the calculated position errors were displayed by the c4D software in real-time with 6-DOF, including translational shifts (vertical, longitudinal and lateral) and rotational shifts (pitch, roll and yaw).[56,152] Translational vector displacements were calculated from the PEs obtained. **Figure 3.2.5.3** demonstrates the parameters used to define camera occlusion.

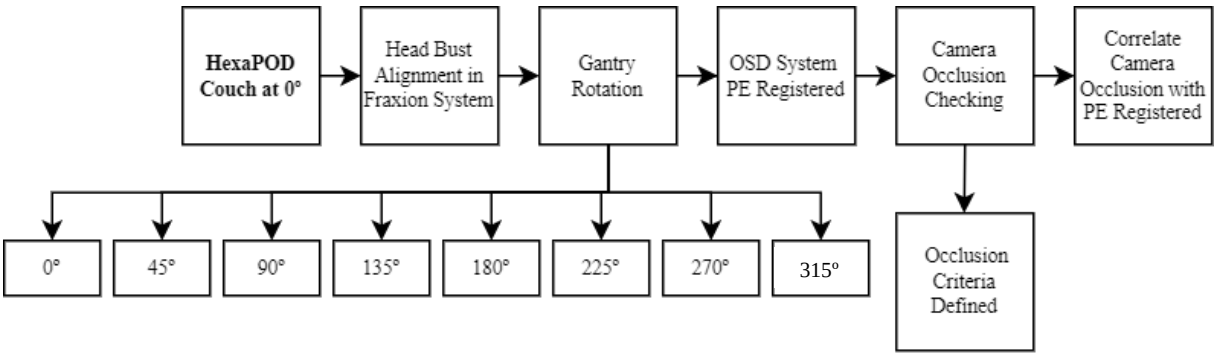

Figure 3.2.5.1 Steps performed in the 3rd test.

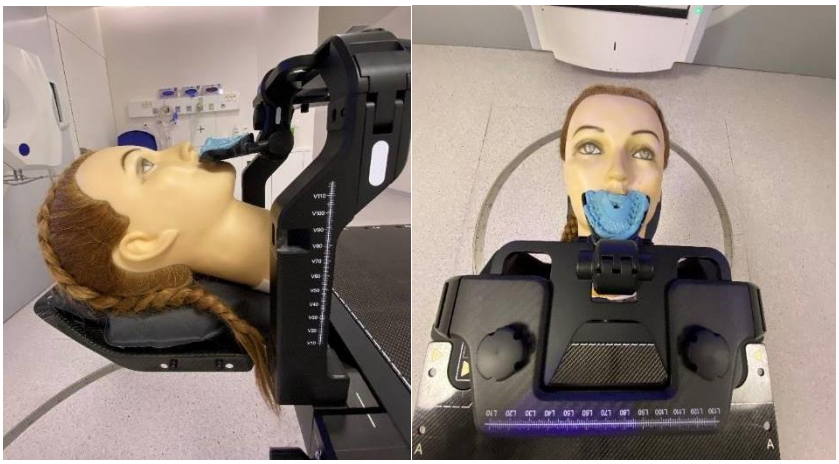

Figure 3.2.5.2 Head bust alignment with Fraxion™ system.

Figure 3.2.5.3 Gantry at 315º to assess camera occlusions.

Table 3.2.5 Parameters defined to establish camera occlusion. Color Black represents the occlusion of the camera regarding one of the three occluders: XVI Detector; XVI X-Ray Tube and Gantry Head. Color Red means there is no camera visibility due to occlusion. Green means there is no camera occlusion.

	XVI Detector	X-Ray Tube	Gantry Head	Visibility
Lateral Left Camera				
Lateral Right Camera				
Frontal Camera				

3.2.6 Optical Surface Detecting Test with Couch Rotations

The 4th test was conducted with the anthropomorphic head phantom to test the performance of the OSD system cameras on detecting the phantom surface at different couch rotations. The HexaPOD couch was rotated manually inside the treatment room at 0º; 30º; 60º; 90º; 270º; 300º; 330º respectively, always with 0º gantry angulation. The test was repeated 3 times for each couch rotation to obtain more statistically significant results. The purpose of this test was different from the previous, one since no camera occlusions are performed due to the 0º gantry angulation. Nevertheless, when couch rotations are performed, the coordinate axis automatically rotates, and the OSD system should detect the specific rotation implied. The OSD system and HexaPOD couch PE values were registered in the translation and rotation axis for each couch rotation.

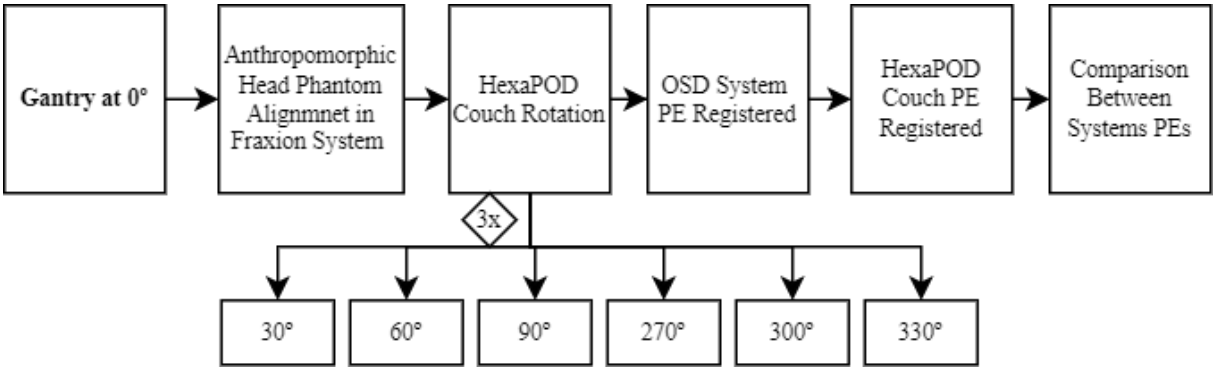

Figure 3.2.6.1 Steps performed in the 4th test.

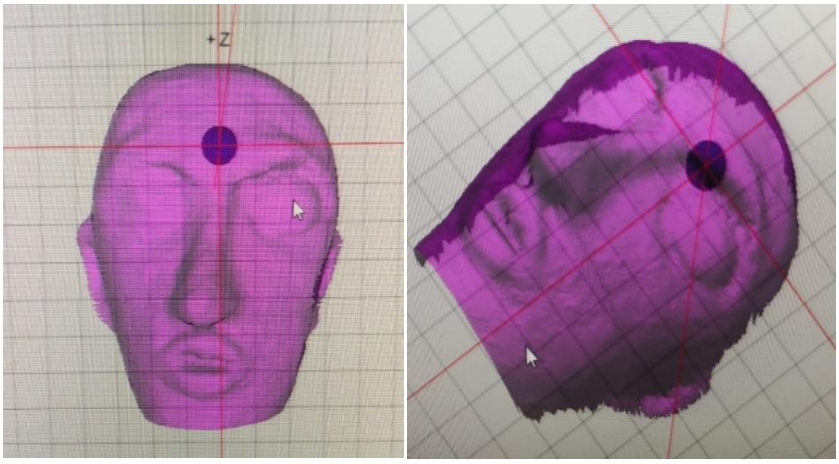

Figure 3.2.6.2 Spatial orientation of the external surface of Anthropomorphic Head Phantom in the c4d software.

3.2.7 Positional Error Agreement between OSD System and HexaPOD Couch at Non-Coplanar Angles

Quality control guideline TG142[153] recommends that the coincidence of treatment isocenter, mechanical isocenter as well as imaging isocenter, should be verified annually. Presently, treatment platforms have become more complex with multiple imaging modalities for localization throughout treatment. Therefore, is critical to quantify the targeting accuracy of the systems involved throughout the entire SRS treatment. The 5th test consisted in comparing the PE values of the OSD system and HexaPOD couch in a non-coplanar angle approach. The agreement between the imaging system and the mechanical correction system PEs was assessed. The non-coplanar angle test was conducted with the anthropomorphic head phantom and consisted in rotating both the gantry and couch manually inside the treatment room. **Figure 3.2.7.1** shows a schematic of the test performed.

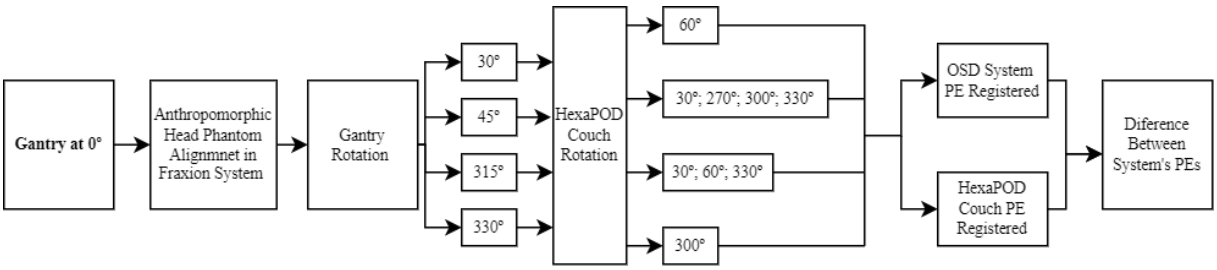

Figure 3.2.7.1 Steps performed in the 5th test.

4. Results

4.1 1st Test - CW and CC XVI-CBCT Systematic Error Assessment

The first test was performed to check the uncertainty regarding the isocenter matching alignment of the XVI. An enhanced method of determining if the CBCT isocenter alignment is calibrated is to make multiple acquisitions of a phantom in CW and CC rotation, comparing and analyzing the positional errors obtained. For this test, the anthropomorphic head phantom was used. The phantom was precisely aligned through the lasers inside the treatment room. A first CBCT scan was acquired for position verification, and all position errors were corrected in translation and rotation axes. After the first correction, six CW and six CC CBCT acquisitions were conducted without any correction applied. The position errors in translational and rotation directions are registered in **Table 4.1.1.**

Table 4.1.1 XVI Position Error in Translation (mm) and Rotation (°).

		Prior Correction	CW						CC					
Acquisition		**1st**	**1st**	**2nd**	**3rd**	**4th**	**5yh**	**6th**	**1st**	**2nd**	**3rd**	**4th**	**5th**	**6th**
Translation (mm)	x	0,5	0,0	0,0	0,0	0,0	0,0	0,0	0,0	0,0	0,0	0,0	0,0	0,0
	y	0,8	-0,3	-0,3	-0,3	-0,3	-0,3	-0,3	-0,3	-0,3	-0,3	-0,3	-0,3	-0,3
	z	1,3	0,0	0,0	0,0	0,0	0,0	0,0	0,0	0,0	0,0	0,0	0,0	0,0
Rotation (°)	Pitch	0,3	0,0	0,0	0,0	0,0	0,0	0,0	0,0	0,0	0,0	0,0	0,0	0,0
	Roll	-0,4	0,1	0,1	0,1	0,1	0,1	0,1	0,3	0,3	0,3	0,3	0,3	0,3
	Yaw	-0,2	0,0	0,0	0,0	0,0	0,0	0,0	0,1	0,0	0,0	0,0	0,0	0,0

A total of 12 CBCT scans were acquired using the automatic registration match method "Grey Value (T+R)" to verify the isocenter position in all translational and rotational directions. The mean and standard deviation ($\mu \pm \sigma$) of the position error regarding the CW acquisition in lateral, longitudinal and vertical translation axis are respectively 0,0±0,0 mm; -0,3±0,0 mm; 0,0±0,0 mm and in rotation axis pitch, roll and yaw are 0,0°±0,0°; 0,1°±0,0° and 0,0°±0,0°. The mean and standard deviation of the position error regarding CC acquisition in lateral, longitudinal and vertical translation axis are respectively 0,0±0,0 mm; -0,3±0,0 mm; 0,0±0,0 mm and in rotation axis pitch, roll and yaw are 0,0°±0,0°; 0,3°±0,0°, and 0,017°±0,041° respectively. **Figure 4.1.1**, **Figure 4.1.2** and **Figure 4.1.3** represent the comparison of position error values in all translation axis (mm) between CW and CC acquisition.

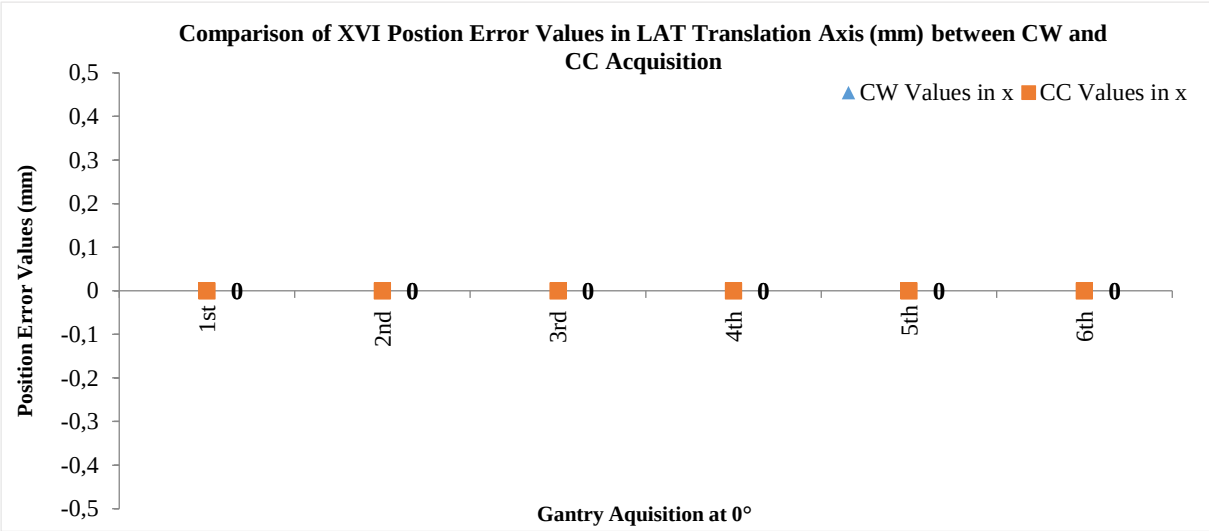

Figure 4.1.1 Comparison of XVI Position Error Values in LAT Translation Axis (mm) between CW and CC Acquisition.

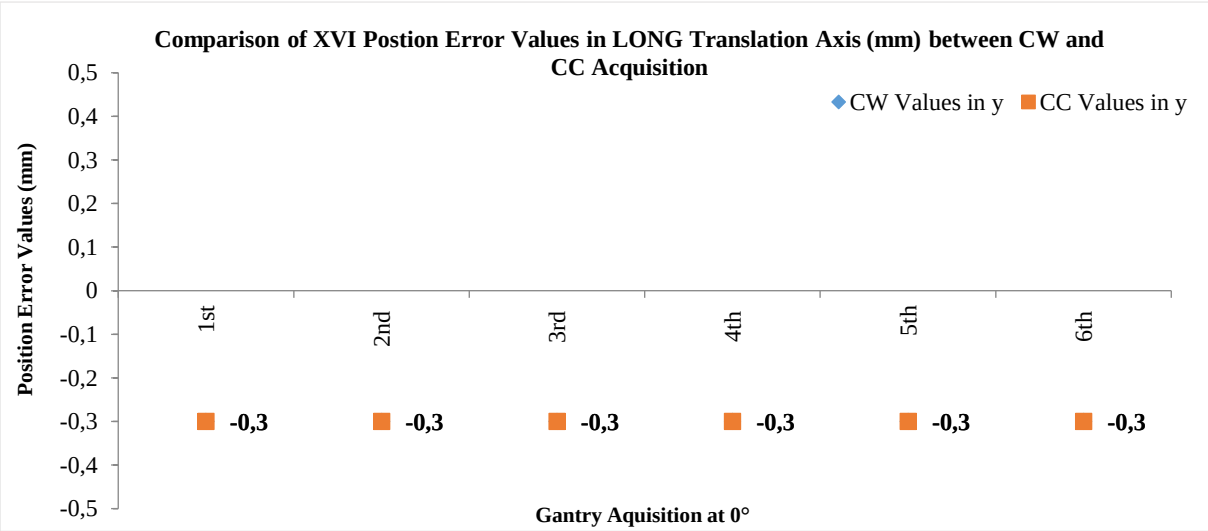

Figure 4.1.2 Comparison of XVI Position Error Values in LONG Translation Axis (mm) between CW and CC Acquisition.

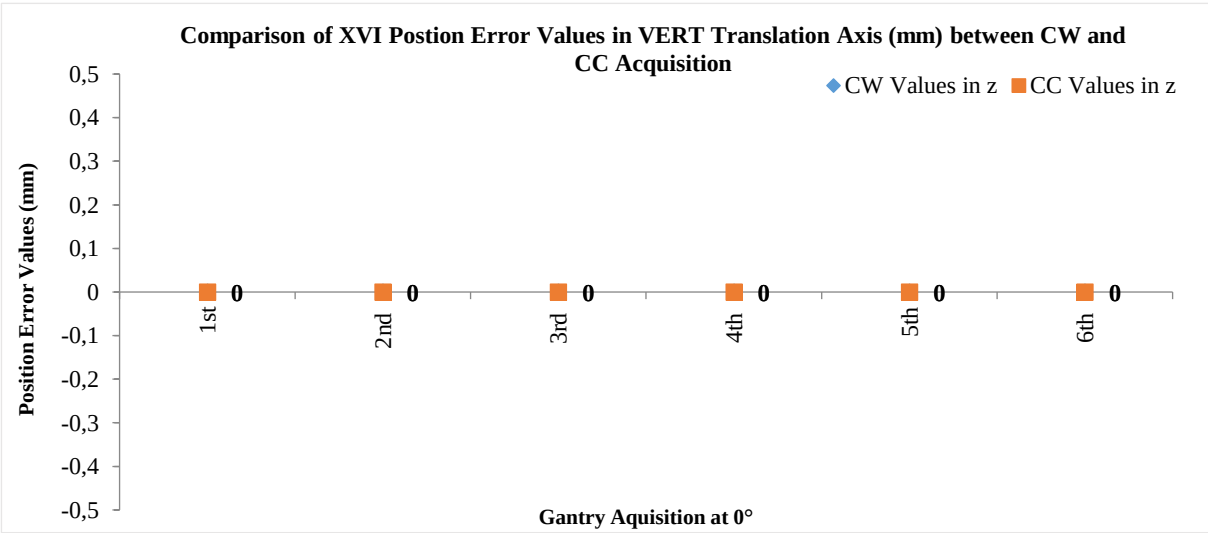

Figure 4.1.3 Comparison of XVI Position Error Values in VERT Translation Axis (mm) between CW and CC Acquisition.

Figure 4.1.4 and **Figure 4.1.5** shows the comparison between CW and CC XVI systematic error in translation (mm) and rotation (°) axes regarding the anthropomorphic head phantom.

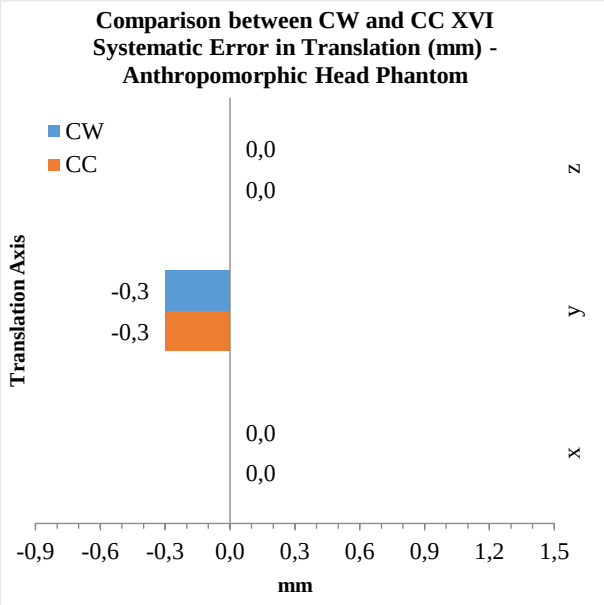

Figure 4.1.4 Comparison between CW and CC XVI Systematic Error in Translation (mm).

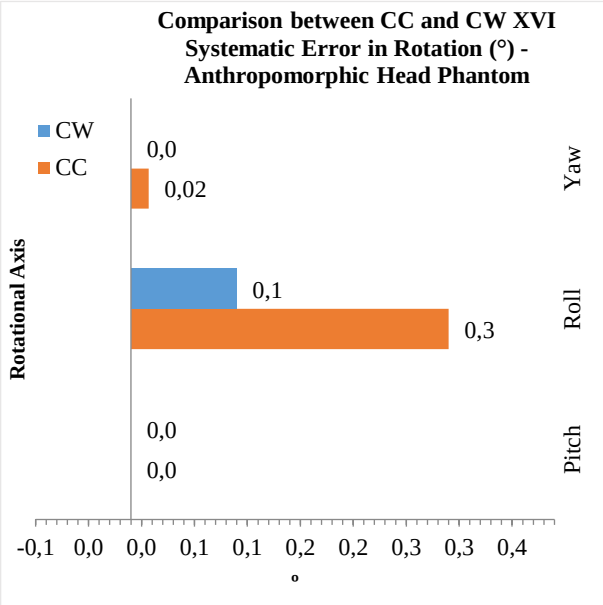

Figure 4.1.5 Comparison between CW and CC XVI Systematic Error in Rotation (°).

The results obtained show that the XVI has a systematic error occurring in the translational axis with the same magnitude and direction independently of the type of acquisition CW or CC, corresponding to -0,3 mm deviation in longitudinal. Regarding the rotational axis, the XVI showed a systematic error of 0,1° in roll in all CW acquisitions, a systematic error of 0,3° in roll in all CC acquisitions and 0,02° in yaw on the CC acquisition.

4.2 2nd Test - HexaPOD Couch and XVI Mechanical Error Assessment during Couch Rotations

With the continuous progress of image-guided technology, the accuracy of position verification and correction during radiosurgery is also enhanced. The successful development and application of the HexaPOD – 6-DOF treatment couch in clinical practice is to improve the accuracy of patient position correction in 6-DOF, which has been developed for high-precision corrections of translational and rotational setup errors. The isocenter of the HexaPOD couch system is calibrated according to the isocenter of the XVI system. As far as PE correction is concerned, the iGUIDE software is adapted to the XVI coordinate system. Since the existence of deviations between isocenters will increase the PE, a test with QUASAR™ phantom was performed to assess if the couch positional error was in congruence with the XVI position error. For that purpose, the HexaPOD couch was rotated manually inside the treatment room with different couch rotations, 0°; 15°; 30°; 45°; 60°; 75°; 90°; 270°; 285°; 300°; 315°; 330° and 345° respectively. Between each couch rotation, a CBCT scan was conducted with HexaPOD couch at 0°. The couch Actual Values and couch Set Values were registered for each couch rotation from the iGUIDE software and are presented in **Figure 4.2.1**, **Figure 4.2.2** and **Figure 4.2.3**.

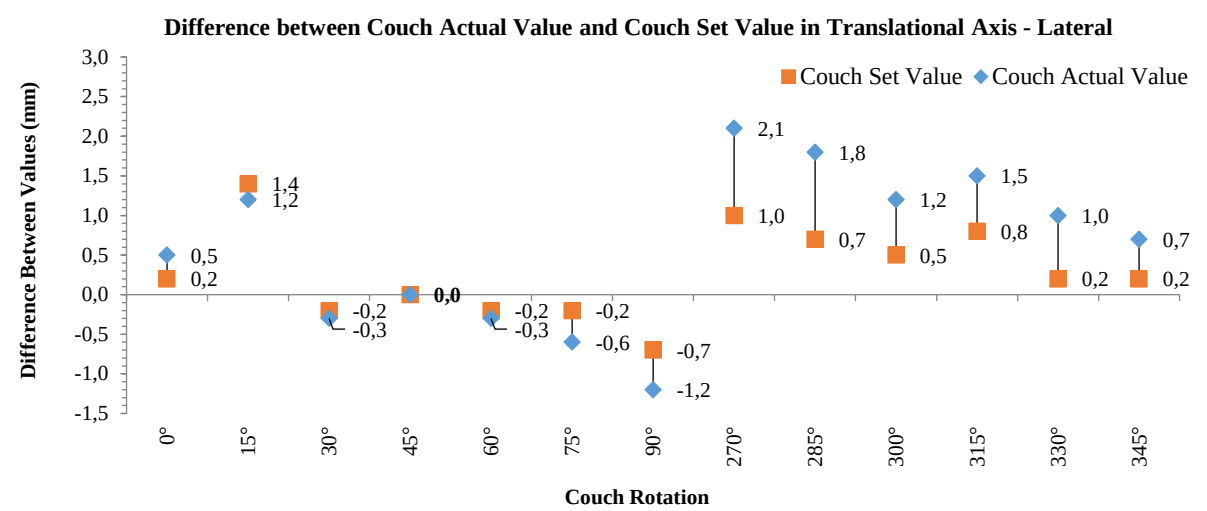

Figure 4.2.1 Difference between Couch Actual Value and Couch Set Value in Translational Axis - LAT.

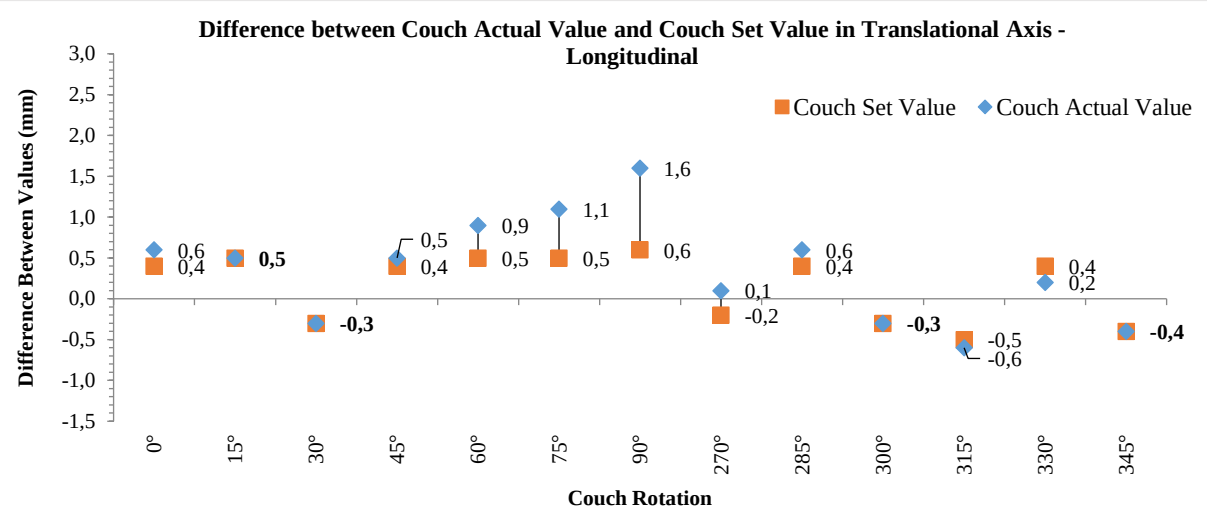

Figure 4.2.2 Difference between Couch Actual Value and Couch Set Value in Translational Axis - LONG.

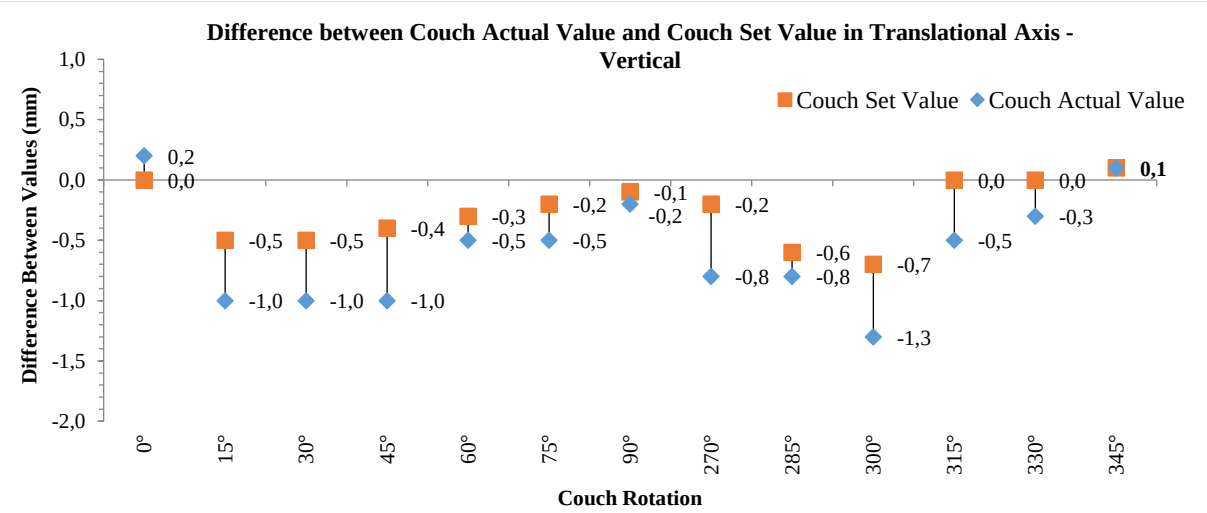

Figure 4.2.3 Difference between Couch Actual Value and Couch Set Value in Translational Axis - VERT.

The couch Set Value is the target set coordinates. Through each couch rotation, iGUIDE software automatically calculates the couch's Actual Value which corresponds to the position of the couch in the coordinate system at an exact moment. Since CBCT acquisitions are not possible with couch rotations due to the risk of gantry collision, the feasible way to confirm if the suggested correction from iGuide software at different couch rotations corresponds to the given XVI PE, is to rotate the couch manually inside the treatment room to the certain angulation and then correct manually the couch to the Set Value. The difference between the couch's Actual Value and the Set Value is the correction applied manually inside the treatment room. The correction applied should be identical to the PE calculated by XVI, after CBCT acquisition at 0º couch rotation. The mechanical error will comprise the difference between the correction manually applied and values calculated by XVI. A total of 13 CBCT scans were acquired between each couch rotation using the automatic registration match method "Grey Value (T+R)". The same acquisition parameters were used as mentioned in the previous test. All translational and rotational XVI PE were registered. **Figure 4.2.4**, **Figure 4.2.5** and **Figure 4.2.6** represent graphically the comparison between the calculated HexaPOD Expected Positional Error at 0º with XVI PE after image acquisition, in all translation axes. The same PE is expected if the iGUIDE software is correctly calibrated with the XVI coordinate system.

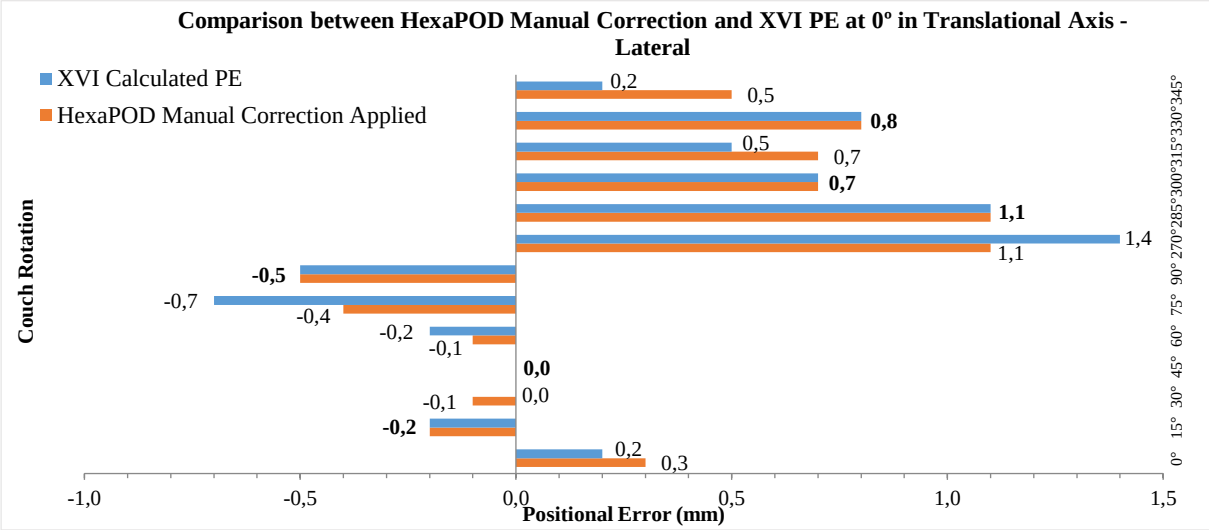

Figure 4.2.4 Comparison between HexaPOD Manual Correction and XVI PE at 0º in Translational Axis – Lateral.

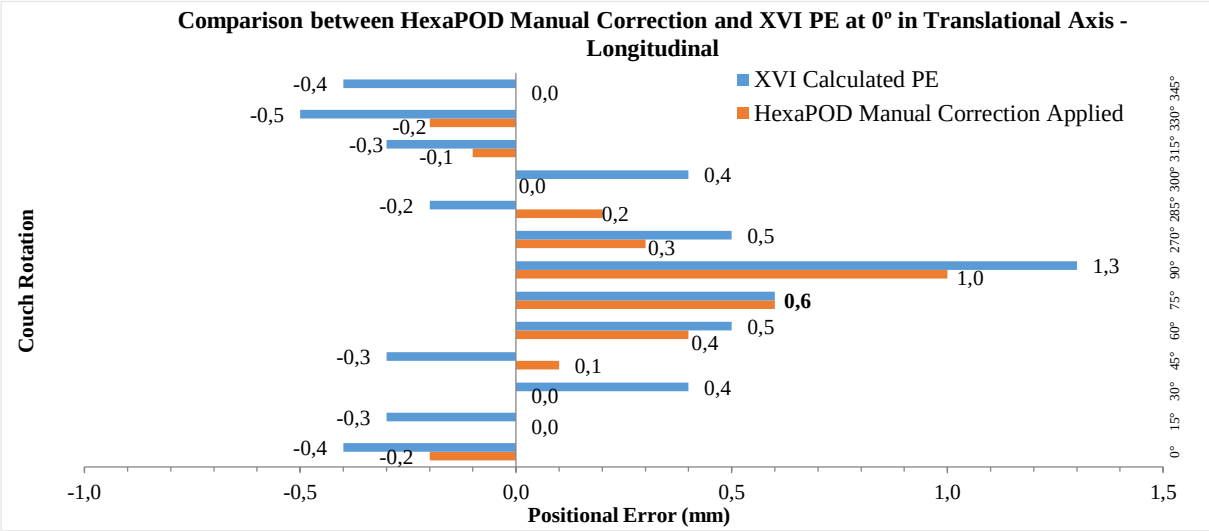

Figure 4.2.5 Comparison between HexaPOD Manual Correction and XVI PE at 0º in Translational Axis – Longitudinal.

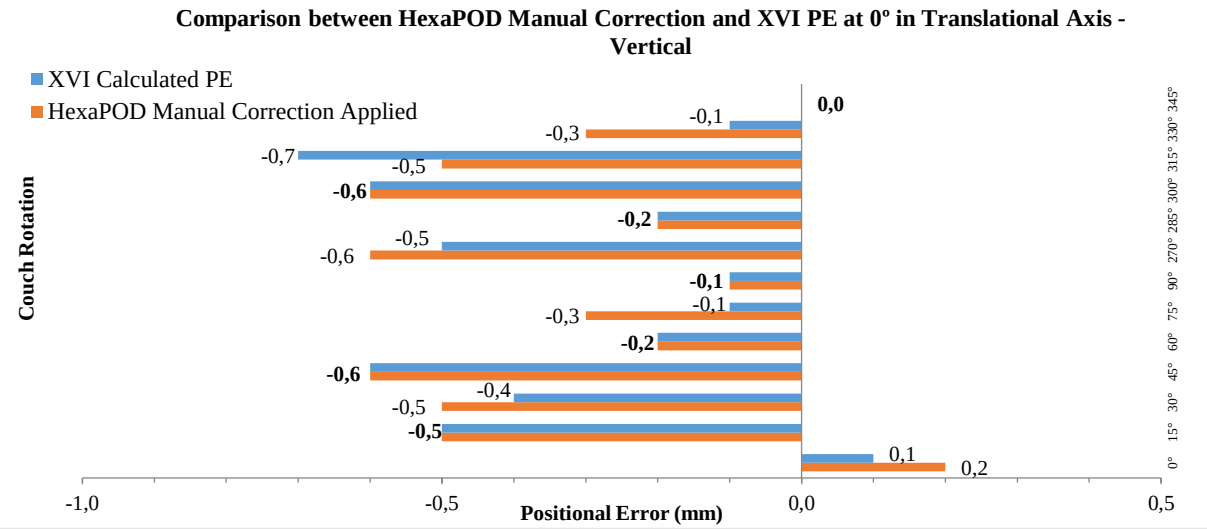

Figure 4.2.6 Comparison between HexaPOD Manual Correction and XVI PE at 0º in Translational Axis – Vertical.

Since the manual correction applied to the HexaPOD inside the treatment room for each couch rotation should be identical to the PE calculated by XVI after CBCT acquisition at 0º couch rotation, **Figure 4.2.7** represents the mechanical error between the HexaPOD and the XVI for the couch rotations performed. The mechanical error corresponds to the difference between the two system's PEs.

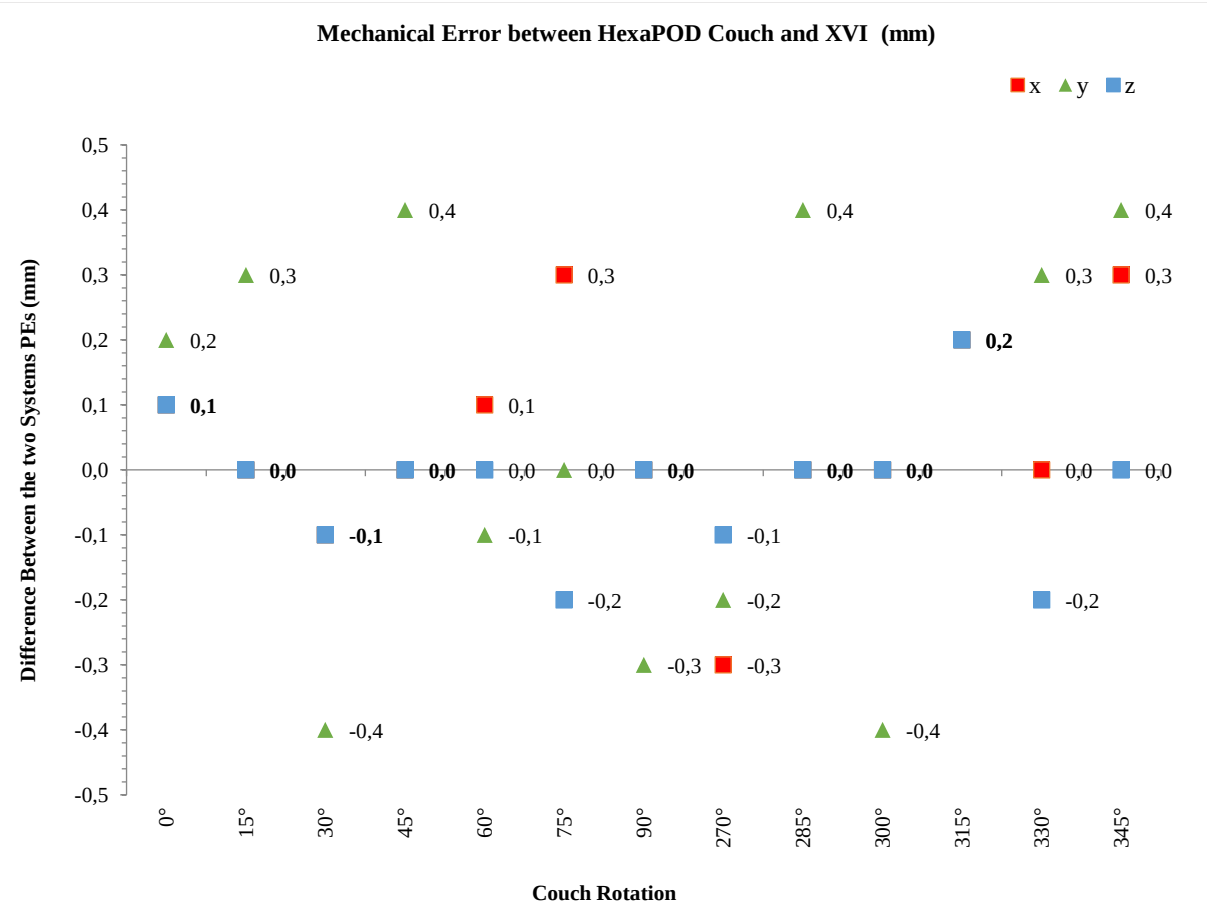

Figure 4.2.7 Mechanical Error Between HexaPOD Couch and XVI (mm).

Figure 4.2.7 shows that the major PE difference between the two systems occurred in the longitudinal axis with a mean and SD of 0,06±0,3 mm, with a maximum PE difference of ±0,4 mm between the two systems at couch rotations 30°; 45°; 285°; 300° and 345° respectively. The mean and SD of the PE differences on lateral axis are 0,05±0,3 mm, with a maximum PE difference of ±0,3 mm between the two systems at couch rotation 75°; 270°; 345° and no differences at 15°; 45°; 90°; 285°; 300° and 330° respectively. The vertical axis shows a small difference between the two systems, with a mean and SD of 0,02±0,1 mm. Couch rotation 15°; 45°; 60°, 90°; 285°; 300° and 345° show no differences between the two system's PEs. The maximum difference occurs at 75° and 330° with -0,2 mm. The lower dispersion of values in **Figure 4.2.7**, the higher congruence in isocenter alignment between the two systems, the smaller the mechanical error.

4.3 3rd Test - OSD System Performance in Coplanar Angles

To evaluate the OSD system performance in detecting the head bust surface during coplanar angles, one technical performance test was conducted. The coplanar angle test consisted of the rotation of the gantry at different angulations of 0°, 45°; 90°; 135°, 180°; 225°; 270º and 315° respectively with 0° couch rotation, to understand if the OSD system PEs varied in magnitude regarding the gantry angulation, since in some gantry angles, the LINAC occlude one of the lateral camera pods, resulting in a smaller surface image and potentially leading to inaccurate monitoring.

- **Coplanar Angle Test**

Inside the treatment room, the gantry was rotated manually for each gantry angulation referred, and the OSD system PEs were registered from c4D software in translational and rotational axes. The difference between Couch Absolute (CA) which is the isocenter position – target, and Couch Relative (CR) which is the actual head bust coordinates in an exact moment, corresponds to the PE and subsequent necessary displacement to achieve the optimal head bust position. The translational module vector displacement (VD) was calculated for each gantry angulation and corresponds to the necessary distance to range from the CR position to the CA position (isocenter) regarding the coordinate system. Camera visibility was also assessed during the rotation of the gantry. **Table 4.3.1** shows the results obtained.

Table 4.3.1 Assessment of camera visibility during coplanar angle test and respective calculated shift displacements for each gantry angulation at couch rotation 0°. Green color means no occlusion of camera pod; red color means occlusion of camera pod.

			Gantry Angulation (°)															
			0 °		**45 °**		**90 °**		**135 °**		**180 °**		**225 °**		**270 °**		**315 °**	
			PE	**VD**	**PE**	**VD**	**PE**	**VD**	**PE**	**VD**	**PE**	**VD**	**PE**	**VD**	**PE**	**VD**	**PE**	**VD**
Axes	Translation (mm)	Lat	0,2		-0,4		0,2		-0,1		0,0		0,0		0,1		-0,1	
		Long	0,1	**0,3**	0,0	**0,4**	0,2	**0,3**	0,0	**0,1**	0,1	**0,1**	0,1	**0,1**	0,1	**0,2**	0,3	**0,3**
		Vert	-0,2		-0,1		0,1		-0,1		0,0		0,0		-0,1		0,0	
	Rotation (°)	Pitch	0,0		-0,1		0,1		-0,1		0,0		0,0		0,1		0,1	
		Roll	-0,1		0,3		0,0		0,0		0,0		0,0		0,0		0,1	
		Yaw	-0,1		-0,1		-0,1		0,2		-0,1		-0,1		0,0		-0,1	
	Camera Visibility	Lateral Right																
		Frontal																
		Lateral Left																

In specific gantry angles, the gantry; XVI detector or XVI X-Ray Tube can occlude one or two camera pods, resulting in a smaller surface image detected and potentially lead to inaccurate monitoring if only one of the lateral pods are used. The PEs confirm to be larger in anterior oblique angles, corresponding to a translational vector displacement of 0,4 mm in the anterior left oblique (45º) and 0,3 mm in the anterior right oblique (315º). The camera accuracy in detecting the phantom surface seems to be directly related to the occlusion of the lateral right camera pod and lateral left camera pod, being noticed that in angles where gantry and XVI occludes one/two of the pods, larger vector displacements are seen to correct the head bust set up position. During the test, both lateral right and left pod were occluded five times each during the gantry rotations. Overall, the use of the central pod together with one of the lateral pods eliminates this problem, and for every gantry angulation there are at least two camera pods (central plus one lateral) available for surface acquisition, allowing for accurate monitoring in all situations. **Figure 4.3.1** demonstrates geometrically the variation of OSD system PEs (mm) in all translational axes per gantry angulation (°).

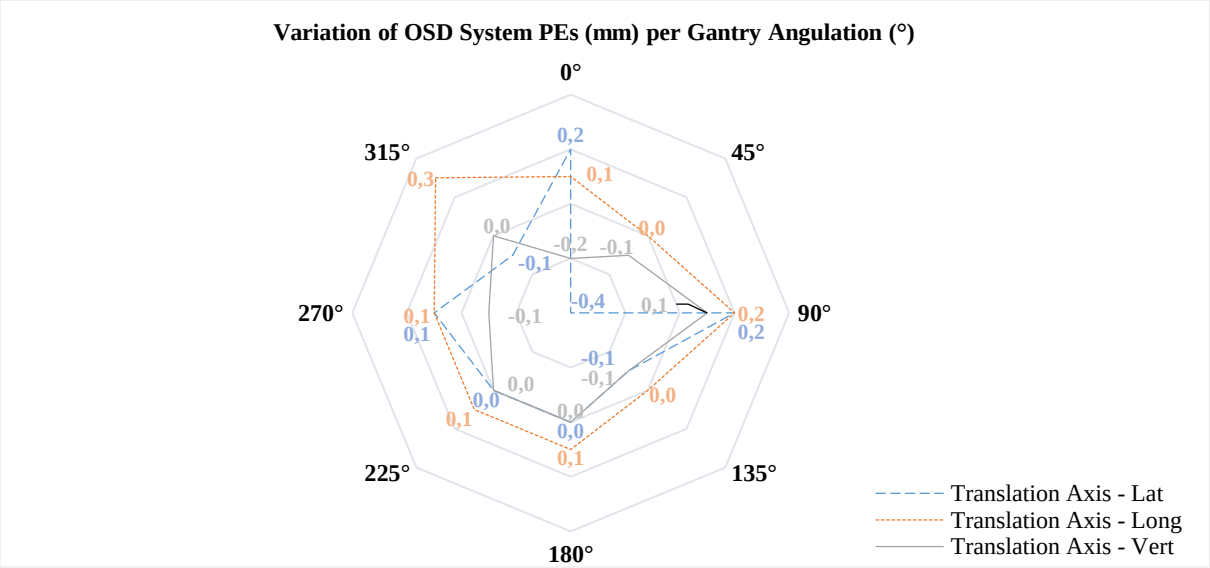

Figure 4.3.1 Variation of OSD System PEs (mm) per Gantry Angulation (º).

The translational VD was calculated for each gantry angulation based on the square root of the quadratic difference between CA, which is the isocenter position, and CR, which is the actual phantom coordinates. **Figure 4.3.2** demonstrates geometrically the calculated translational vector displacement (mm) per gantry angulation (°).

Overall, the translational vector displacement for each gantry angulation ranged from 0,1 mm to 0,4 mm, with larger offsets in the anterior oblique angles where most occlusions occurred.

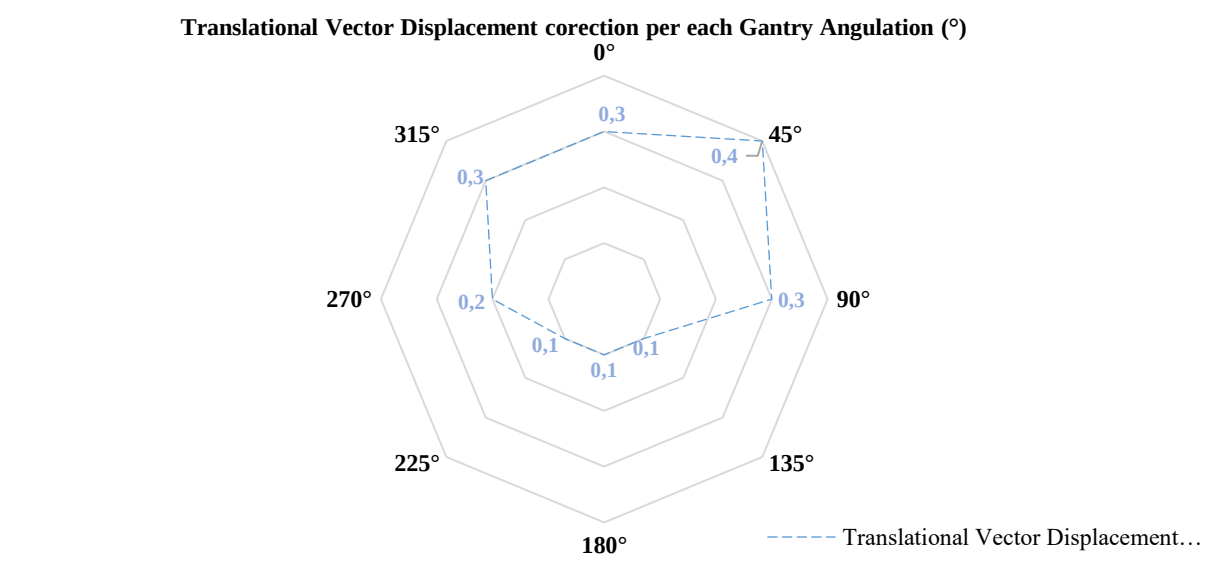

Figure 4.3.2 Translational Vector Displacement correction per each Gantry Angulation (º).

4.4 4th Test - OSD System Performance with Couch Rotations

The 4th test consisted in the rotation of the couch at 0°, 30°; 60°; 90°, 270°; 300° and 330° with gantry angulation at 0° respectively. The fields with the couch rotations were loaded to the MOSAIQ system. The OSD mode was changed from patient positioning mode to the real-time monitoring mode and the couch was rotated to the given couch angles. When the couch was in the correct position, the OSD system PEs were registered. This test focused on two points, the first was to assess if the OSD system PEs varied in magnitude regarding the couch rotation; the second was to test the OSD system performance in detecting the anthropomorphic head phantom surface without inconsistencies during couch rotations. All the values were registered from c4D software**. Figure 4.4.1** demonstrates geometrically the variation of OSD system PEs (mm) in translational axes for each couch rotation (°).

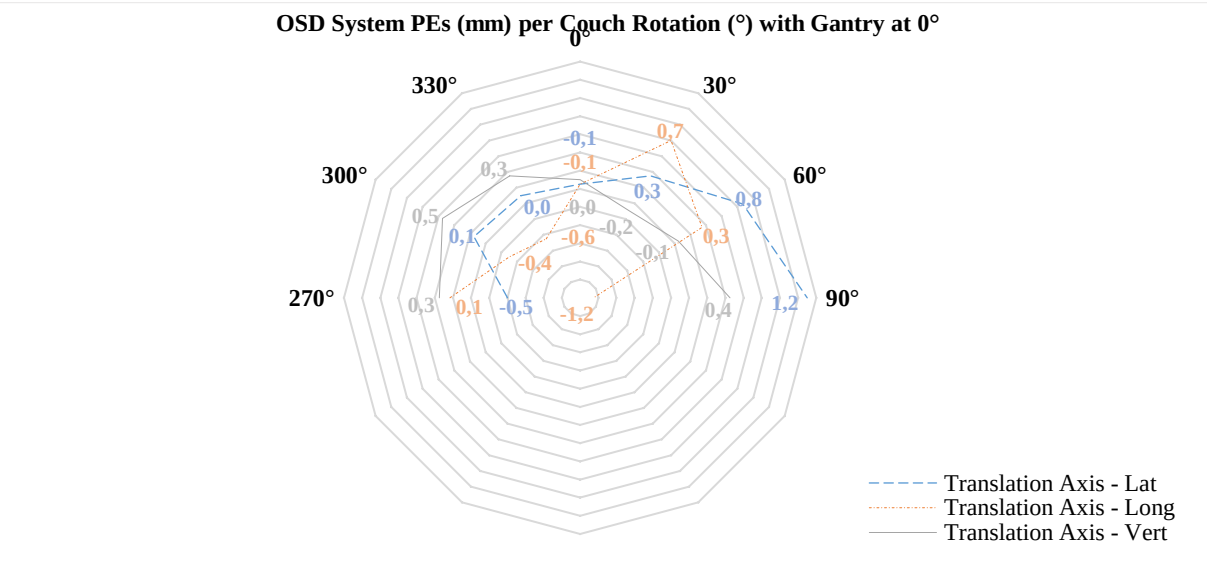

Figure 4.4.1 OSD System PEs (mm) per Couch Rotation (º) with Gantry at 0º.

With the geometric analysis of **Figure 4.4.1**, it is possible to detect in all translational axes a larger magnitude of PEs in the right couch rotations 30°, 60° and 90° respectively. The overall mean and SD shifts for each translational axis in lateral, longitudinal and vertical was 0,3±0,6 mm; -0,2±0,6 mm and 0,1±0,2 mm respectively. The maximum OSD system PE value in the lateral axis was detected at 90° corresponding to an 1,2 mm shift displacement; in the longitudinal axis was detected at 90° corresponding to an -1,2 mm shift displacement and in vertical axis was at 300° corresponding to an 0,5 mm shift displacement. The translational vector displacement was calculated for each couch rotation based on the difference between CA, which is the isocenter position, and CR, which is the actual phantom coordinates. **Figure 4.4.2** demonstrates geometrically the calculated translational vector displacement (mm) per couch rotation (°).

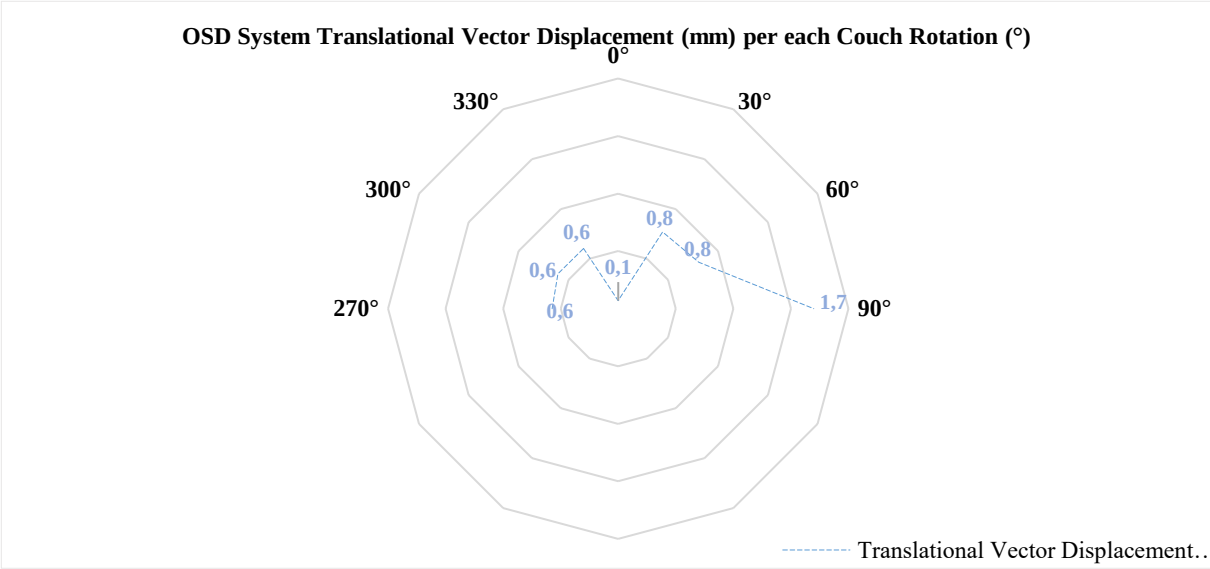

Figure 4.4.2 OSD System Translational Vector Displacement (mm) per each Couch Rotation (º).

Overall, the translational vector displacement regarding couch rotation ranges from 0,1 mm at 0º to 1,7 mm at 90º.

4.5 5th Test - Positional Error Agreement between OSD System and HexaPOD Couch at Non-Coplanar Angles

Non-coplanar SRS treatments requires perfect alignment between treatment beam axis, couch axis, and OSD system isocenter such that the axes remain constant while any of these components change position. HexaPOD and the OSD system are two independent systems that can work in compliance. As the OSD system operates as a tracking monitoring tool before and during treatment regarding patient positioning, it calculates its isocenter shifts in relation to the couch. The HexaPOD couch aims to improve the accuracy of patient position correction in 6-DOF and calculates its isocenter shifts in relation to the isocenter. That's the reason why OSD system isocenter shifts are inversely calculated by c4D software due to its geometric displacement in the treatment room. Since

their independence is known, to conduct a feasible comparison with the HexaPOD couch, the calculated isocenter shifts by the OSD system must be converted inversely in all translational and rotational axes to assess the discrepancy regarding their radiation isocenter alignment. The final test was conducted to assess if the isocenter shifts at different gantry angulations – anterior oblique angles - and couch rotations calculated by HexaPOD iGUIDE software were in agreement with the isocenter shifts calculated by the OSD system c4D software, and to calculate the overall OSD system uncertainty regarding the isocenter alignment. For that purpose, non-coplanar angles were chosen to conduct the test with a specific conjunction of gantry angulations and couch rotations. The anthropomorphic head phantom was used. The gantry and the couch were rotated manually inside the treatment room according to the angulations and rotations presented in **Table 4.5.1**.

Table 4.5.1 Gantry Angulations and Couch Rotations performed during the 5th test.

Gantry Angulation (º)	**30**	**45**				**315**			**330**
Couch Rotation (º)	60	30	270	300	330	60	90	330	300

The HexaPOD couch Set Value represents the actual coordinates regarding the phantom isocenter position. The couch Actual Value is the isocenter shift necessary to be corrected to achieve the isocenter position. The couch Actual Value from HexaPOD and the inverse of the isocenter shift calculated by the OSD system were registered in **Table 4.5.2** and **Table 4.5.3**.

Table 4.5.2 HexaPOD Calculated Isocenter Shifts at Different Gantry Angulations and Couch Rotations.

		HexaPOD Calculated Isocenter Shifts										
	Gantry	**30°**	**45°**				**315°**			**330°**	**Mean**	**SD**
	Couch	**60°**	**30°**	**270°**	**300°**	**330°**	**60°**	**90°**	**330°**	**300°**		
mm	x	-0,4	0,1	1,8	1,1	0,8	-0,5	-0,9	0,8	1,1	**0,4**	**0,9**
	y	0,6	0,3	0,8	0,2	-0,2	0,6	1,2	-0,2	0,0	**0,4**	**0,5**
	z	-0,2	-0,4	0,1	-0,1	-0,3	-0,2	-0,2	-0,3	-0,2	**-0,2**	**0,1**
º	P	-0,4	-0,2	0,5	0,4	0,2	-0,4	-0,4	0,3	0,4	**0,0**	**0,4**
	R	0,2	0,1	0,4	0,2	0	0,2	0,4	0	0,2	**0,2**	**0,1**
	Y	60	30	270	300	330	60	90	330	300	**-**	**-**

The isocenter shifts calculated by HexaPOD couch seem to be reproducible for each couch rotation independently of the gantry angulation. The couch within this study showed larger offsets for bigger couch rotations in the lateral axis. The largest offset occurred at gantry angulation 45º with 270º couch rotation, with 1,8 mm in the lateral direction. The smaller offset occurred in the smaller couch rotations, 30º and 60º respectively. The largest shifts were seen in the lateral and longitudinal directions corresponding to a median displacement and SD of 0,4±0,9 mm and 0,4±0,5 mm respectively. The vertical direction shows the smaller offsets since the couch rotation is performed around the vertical axis.

Table 4.5.3 Inverted Catalyst HD Calculated Isocenter Shifts.

	Inverted OSD Calculated Isocenter Shifts											
	Gantry	**30°**	**45°**				**315°**			**330°**	**Mean**	**SD**
	Couch	**60°**	**30°**	**270°**	**300°**	**330°**	**60°**	**90°**	**330°**	**300°**		
mm	x	-0,7	-0,4	0,1	-1,0	-0,6	-1,5	-1,6	0,1	-0,1	**-0,6**	**0,6**
	y	0,1	0,1	0,8	0,6	0,5	0,0	0,9	0,6	0,6	**0,5**	**0,3**
	z	-0,1	-0,1	-0,5	-0,4	-0,3	0,2	-0,1	-0,2	-0,2	**-0,2**	**0,2**
°	P	0,3	-0,5	0,7	-0,2	0,2	0,5	0,75	0,3	0,1	**0,2**	**0,4**
	R	0,2	0,3	0,4	0,6	0,7	-0,5	-0,1	0,5	0,6	**0,3**	**0,4**
	Y	-0,3	-0,2	-0,2	-0,4	-0,7	-0,3	-0,45	-0,1	-0,3	**-0,3**	**0,2**

The largest offset occurred at 315° gantry angulation with 90º couch rotation with -1,6 mm in the lateral direction. The smaller offsets occurred at 45º gantry angulation with 30º couch rotation. The shifts with bigger magnitude were seen in the lateral and longitudinal directions corresponding to a median displacement and SD of -0,6±0,6 mm and 0,5±0,3 mm respectively.

Table 4.5.4 Module of the Difference Between the OSD System and the HexaPOD Couch Correction Values.

	Module of the Difference Between the OSD System and the HexaPOD Couch Isocenter Shifts											
	Gantry	**30°**	**45°**				**315°**			**330°**	**Mean**	**SD**
	Couch	**60°**	**30°**	**270°**	**300°**	**330°**	**60°**	**90°**	**330°**	**300°**		
mm	x	0,3	0,5	1,7	2,1	1,4	0,7	0,1	0,8	1,2	**1,0**	**0,6**
	y	0,6	0,3	0,0	0,4	0,7	0,4	0,6	0,8	0,4	**0,5**	**0,2**
	z	0,2	0,3	0,6	0,3	0,1	0,1	0,4	0,2	0,0	**0,2**	**0,2**
°	P	0,1	0,3	1,2	0,2	0,4	0,1	0,1	0,6	0,5	**0,4**	**0,4**
	R	0,4	0,4	0,8	0,8	0,7	0,5	0,2	0,5	0,8	**0,5**	**0,2**
	Y	0,25	0,2	0,2	0,2	0,7	0,8	0,3	0,1	0,3	**0,3**	**0,2**

Figure 4.5.1, **Figure 4.5.2**, **Figure 4.5.3** and **Figure 4.5.4** shows the module of the difference betweenthe HexaPOD couch and the OSD system isocenter shift calculation in all translational axes (mm) for each couch rotation (º) with gantry angulation at 30º, 45º, 315º; 330º respectively.

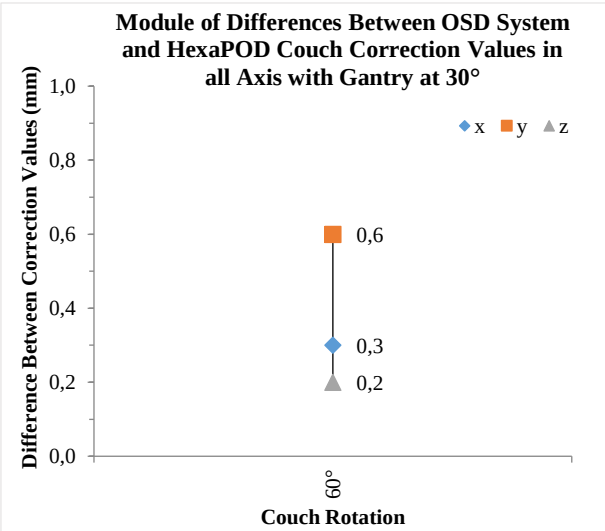

Figure 4.5.1 Module of Difference Between OSD System and HexaPOD Couch Correction Values in all Axis with Gantry at 30º.

At the 30º gantry angulation with 60º couch rotation, the major difference between the calculated isocenter shifts occurred in the longitudinal axis corresponding to a discrepancy of 0,6 mm, and 0,3 mm in lateral and the small shift in the vertical axis, 0,2 mm respectively.

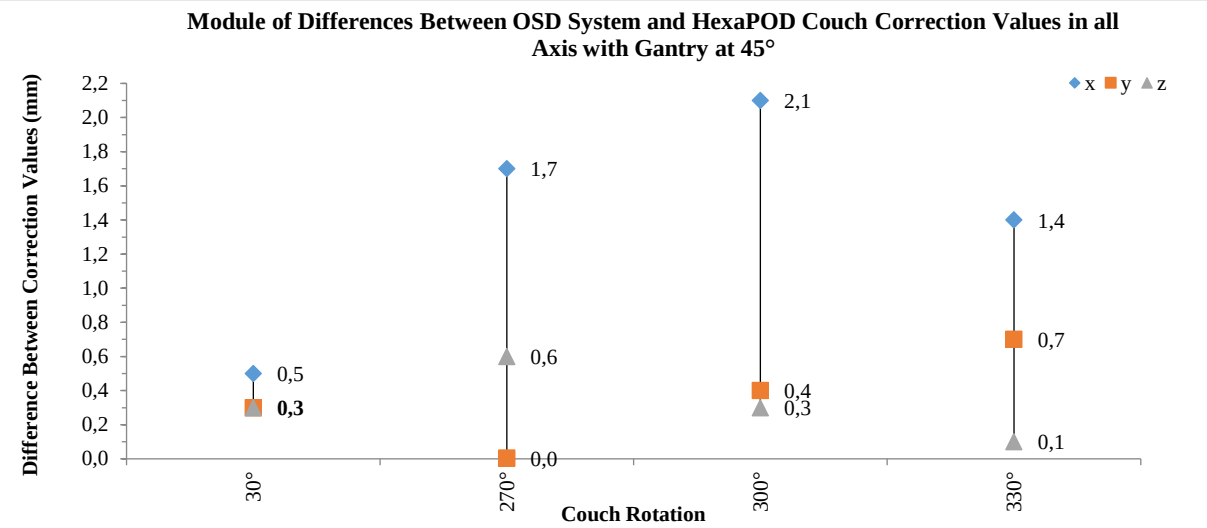

Figure 4.5.2 Module of Differences Between OSD System and HexaPOD Couch Correction Values in all Axis with Gantry at 45°.

For the 45º gantry angulation, the major difference between the calculated isocenter shifts occurred in the lateral axis at 270º; 300º and 330º couch rotations, corresponding to a discrepancy of 1,7 mm; 2,1 mm and 1,4 mm respectively between the HexaPOD couch and the OSD system due to the occlusion of one of the lateral camera pods. Overall, in all couch rotations, the agreement between the two systems was inferior to 1 mm in longitudinal and vertical axes.

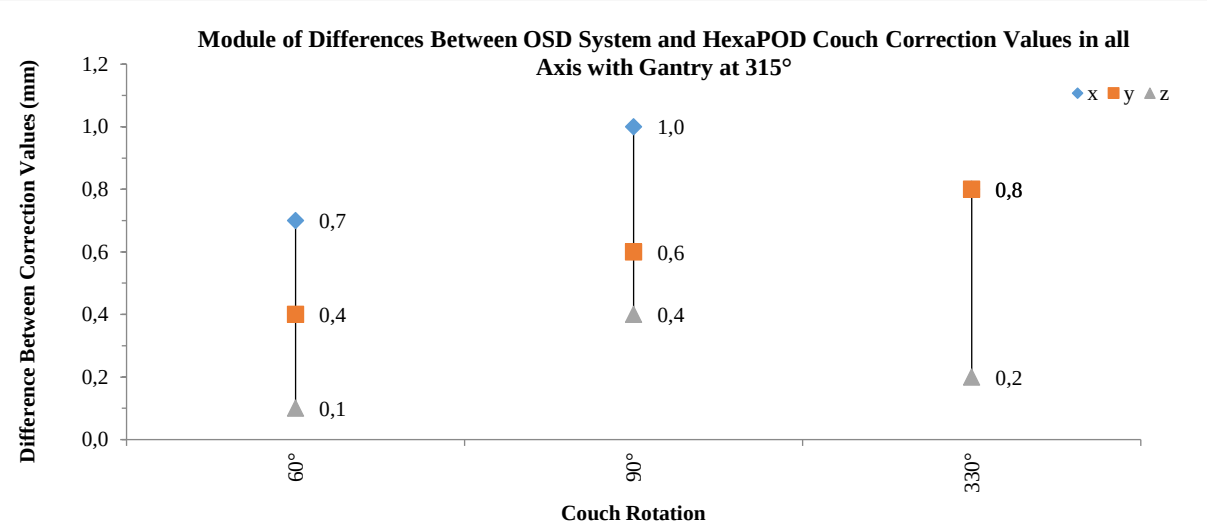

Figure 4.5.3 Module of Differences Between OSD System and HexaPOD Couch Correction Values in all Axis with Gantry at 315°.

For the 315º gantry angulation, the major difference between the calculated isocenter shifts occurred in the lateral axis at 90º couch rotation, corresponding to a discrepancy of 1 mm in lateral axis between the HexaPOD couch and the OSD system. In the overall couch rotations, the agreement between the two systems was within 1 mm in all translational axes.

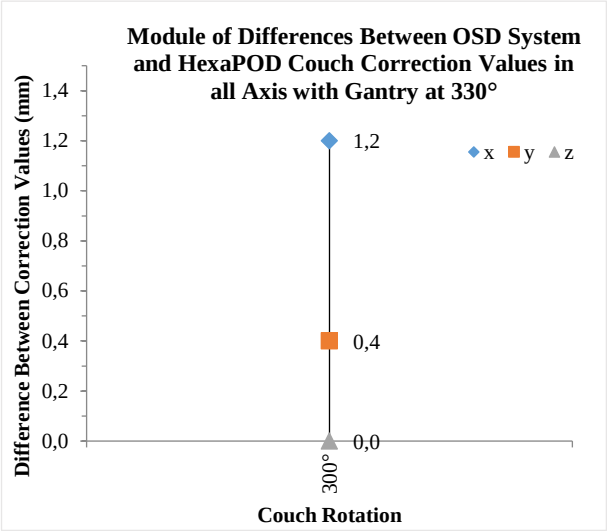

Figure 4.5.4 Module of Differences Between OSD System and HexaPOD Couch Correction Values in all Axis with Gantry at 330°.

At the 330º gantry angulation with 300º couch rotation, the major difference between the calculated isocenter shifts occurred in the lateral axis corresponding to a discrepancy of 1,2 mm between the HexaPOD couch and the OSD system due to the occlusion of one of the lateral camera pods. The longitudinal axis had a 0,4 mm discrepancy. Overall, the mean difference between the two systems is 1±0,6 mm in the lateral axis, 0,5±0,2 mm in the longitudinal axis and 0,2±0,2 mm in the vertical axis, which is consistent with a maximum mean of 1 mm difference between the two systems isocenter shifts.

5. Discussion

Most external beam radiotherapy treatments consider desirable and usually achievable an accuracy of ±3 mm. With stereotactic radiosurgery, however, like LINAC based SRS treatments of patients with multiple brain metastasis, somewhat higher accuracy is desired, and with modern techniques, submillimeter accuracy is achievable but requires careful verification. Regarding the technical capability to accurately align the delivery system to the isocenter, current mechanical engineering standards meet this requirement easily. When using frameless, image-guided SRS (using thermoplastic immobilization masks, CBCT online match procedures, robotic couch...), it is necessary to match the imaging isocenter to the mechanical isocenter, which is an achievable goal for standard QA according to AAPM TG142[147] (1 mm/0,5°).

The 1st test was performed to check the uncertainty regarding the isocenter matching alignment of the XVI. A total of 12 CBCT anthropomorphic head phantom scans (6 in CW and 6 in CC) were acquired using the automatic registration match method "Grey Value (T+R)" to verify the isocenter position in all translational and rotational directions, with no corrections being applied. The results obtained show that the XVI has a systematic error occurring always with the same variation and magnitude independently of the type of acquisition - CW or CC, corresponding to an -0,3 mm deviation in the longitudinal translational axis. Regarding the rotational axis, the XVI showed a systematic error of 0,1° in roll in all CW acquisitions, and 0,3° in roll in all CC acquisitions. The results demonstrate that there are no significant differences in performing the CBCT acquisition whether CW or CC rotation in this study. These errors can occur due to some fluctuation and instability of the system or can be related to the accuracy of the registration algorithm "Grey Value (T+R)" since this algorithm uses all the grey value pixels in the registration volume – clipbox, to calculate the translations and rotations. It does a registration on the greyscale intensity values of the voxels in the registration volume to perform a correlation ratio procedure for automatic registration.

Barber et al.[154] reported deviations of several millimeters between automatic registration algorithms in patient data. Smaller deviations are observed in the present study, which are an indicator that the uncertainty observed in image registration is induced by algorithm similarity metric matter rather than the imaging system. While these results are favorable to use the automatic image registration methods, phantom results alone for image uncertainty do not incorporate the many other uncertainties and errors in the treatment chain: MV-kV beam coincidence, anatomical deformation, mobile anatomy, motion blur effects, and contrast agents. These uncertainties will also have an impact on the final accuracy of the automatic image registration in the clinical workflow. The results presented in this study provide a "best-case" baseline scenario for consideration of the algorithm alone, providing guidance on these factors assuming other influencing factors are held constant. The uncertainty of the registration algorithm "Grey Value (T+R)" is found to be acceptable for clinical use, within the normal range of acquisition settings.

The successful development and application of 6-DOF HexaPOD treatment couch in clinical practice is to improve the accuracy of patient position correction in six degrees of freedom. Since its isocenter is calibrated according to the isocenter of the XVI, the existence of deviations between the two systems should be accountable. The 2nd test was conducted to assess the mechanical error regarding HexaPOD Couch and XVI. The mechanical error corresponds to the difference between the two systems PEs. It was assessed if the HexaPOD couch positional error at different couch rotations was in congruence with XVI position error after CBCT acquisition. The major PE difference between the two systems occurred at the longitudinal axis, corresponding to a difference of ±0,4 mm at couch

rotation at 30°; 45°; 285°; 300° and 345° respectively. Considering that the longitudinal axis is the one that endures greater deviations, these deviations may result from the drift associated to the table in the longitudinal direction. This outcome corroborates the literature regarding HexaPOD couch precision being under 0,5±1 mm for a 95% CI.[147] Furthermore, the results are within the tolerance of 1 mm suggested by the AAPM TG142, for the coincidence of radiation and mechanical isocenter.[153]

Before performing any test on the OSD system, a routine QA for SRS has to be performed at least 4 hours prior to the use of the equipment. Regarding the 3rd test, the OSD system performance in coplanar angles – with 0º couch rotation – in some gantry angulations the LINAC demonstrated to occlude one or two camera pods, due to the XVI detector, XVI X-Ray tube or gantry, resulting in a decreasing surface image reading and potentially leading to inaccurate monitoring if only one of the lateral camera pods is used. The Couch Relative values – the necessary isocenter shifts – confirm to be larger in anterior oblique angles, corresponding to a translational vector displacement of 0,4 mm in anterior left oblique 45º, and 0,3 mm in anterior right oblique 315º. The camera accuracy in detecting the phantom surface seems to be directly related to the occlusion of the lateral right camera pod, central camera pod and lateral left camera pod. The use of the HexaPOD frame and the Fraxion system frame to simulate the vacuum mouthpiece array, did not comprise any camera pod readings during this study. On contrary, in angles where the gantry; XVI detector or XVI X-Ray tube occluded one/two of the pods, larger vector displacements were seen for position correction due to signal inconsistency. The lateral right camera pod was the one with more occlusions during the gantry rotations performed. In general, the use of the central camera pod together with the lateral camera pods eliminates this problem, and for every gantry angulation there are at least two camera pods (central plus one lateral) available for surface acquisition, allowing for accurate monitoring in all situations. The suggested procedure to solve this problem is to retract the XVI detector and XVI X-Ray tube before SRS treatments for a more precise and continuous patient surface monitoring. Overall, for each gantry angulation performed, the OSD system calculated isocenter vector displacement were within 0,5 mm in translation axis.

The 4th test consisted in only rotating the couch with gantry angulation at 0° respectively. This test focused on two points, the first was to assess if the OSD system PEs varied in magnitude regarding the couch rotation; the second was to test the OSD system performance on detecting the anthropomorphic head phantom surface without inconsistencies during couch rotations. A larger magnitude of PEs was observed in the right couch rotations at 30°, 60° and 90° respectively. These results may suggest that the table has bigger drifts occurring when the rotation is conducted in the right direction. The maximum OSD system PE value in the lateral axis was detected at 90° couch rotation corresponding to an 1,2 mm shift displacement; in the longitudinal axis was detected also at 90° couch rotation corresponding to an -1,1 mm shift displacement and in the vertical axis was at 300° couch rotation corresponding to an 0,4 mm shift displacement. Overall, the translational vector displacement regarding couch rotation ranges from 0,1 mm at 0º to 1,7 mm at 90º. This last value is considered an outlier and can be explained due to the mechanical error of the table which can be triggered from a drift when the table reaches out the maximum rotation in the right direction.

Ans Swnnen et al[155] also evaluated the accuracy of a commercial optical surface tracking OSD system - Catalyst HD™ - on a TruebeamSTx with a 6-DOF couch to demonstrate how it can be implemented to monitor patient positioning during non-coplanar single isocenter stereotactic treatments of brain metastases. To check whether the Catalyst HD was able to accurately visualize the patient at the various couch angles, an experiment was performed with a mannequin training head in the open face mask (i.e., a patient lying motionless). The OSD system reference surface was captured, and the couch was rotated to 0°, 45°, 90°, 315°and 270° couch angles respectively. The mean ± SD

values for the translational vector displacements for the different couch angles 0°, 45°, 90°, 315°, and 270° obtained from the repeated monitoring sessions are presented in **Table 5.1**. Deviations larger than 0,5 mm were obtained for couch rotations 45º and 90º. These values corroborate the results presented in this thesis, since the 4th test also showed greater offsets in couch rotations from 30º to 90º.

Table 5.1 Comparison between the results obtained in the 4th test in this study and the results presented in the literature by *Ans Swinnen et al*[155]. Mean vector displacements to the isocenter ± SD (mm) per couch rotation with gantry at 0º.

	Couch Rotations								
	0º	**30º**	**45º**	**60º**	**90º**	**270º**	**300º**	**315º**	**330º**
This study	0,1±0,0	0,8±0,5	-	0,8±0,4	1,7±1,2	0,6±0,4	0,6±0,4	-	0,6 ±0,4
Ans Swinnen et al[155]	0,4±0,2	-	0,6±0,1	-	0,6±0,1	0,3±0,1	-	0,2±0,0	-

As non-coplanar treatments become more widely used, there is a need for an accurate and efficient method to measure and adjust the alignment between the treatment beam axis, couch axis, and OSD system axis. The HexaPOD couch calculates its isocenter shifts in relation to the isocenter, and the OSD system calculates its isocenter shifts in relation to the couch. That's the reason why OSD system isocenter shifts are inversely calculated by c4D software due to its geometric displacement in the treatment room. Since non-coplanar SRS treatments require perfect alignment between systems, QA procedures are essential to verify small couch rotation offsets and alignment between the isocenter of the OSD system and the treatment isocenter.

The 5th test aimed to assess the positional error agreement between the OSD System and HexaPOD couch at non-coplanar angles – with gantry and couch rotation concomitantly.

When the anterior oblique non-coplanar angles were performed, the isocenter shifts calculated by HexaPOD couch seemed to be reproducible in each couch rotation independent of the gantry angulation. The HexaPOD couch within this study detected larger offsets for bigger couch rotations, which can be related due to the drift of the table itself. The largest offset occurred with 45º gantry angulation with 270º couch rotation, with 1,8 mm in the lateral direction. The smaller offset occurred in the smaller couch rotations, 30º and 60º respectively. Shifts with bigger magnitude were seen in the lateral and longitudinal directions corresponding to a median displacement and SD of 0,4±0,9 mm and 0,4±0,5 mm respectively. Deviations with bigger magnitude are mostly seen in lateral and longitudinal rather than the vertical axis and may occur due to the insubstantial phantom surface occlusion since the HexaPOD frame and Fraxion headframe are placed above it.

Regarding the OSD system isocenter shift calculation based on the phantom surface, the suggested corrections seem to vary independently of the gantry angulation and couch rotation. The OSD system within this study showed larger offsets for gantry angulations where the gantry occludes one or two camera pods. Larger offsets were seen at 315° gantry angulation with 90º couch rotation with the major offset of -1,6 mm occurring in the lateral direction. The smaller offsets occurred at 45º gantry angulation with 30º couch rotation. Shifts with bigger magnitude were seen in the lateral and longitudinal directions corresponding to a median displacement and SD of -0,6±0,6 mm and 0,4±0,3 mm respectively. These results suggest that the OSD system has a better performance in detecting the anthropomorphic head phantom surface when there is no oblique angle camera pod occlusion, corroborating the results in the 3rd test.

Regarding all tests performed, the final step was to calculate and define the overall OSD system uncertainty. To calculate the OSD system uncertainty regarding the isocenter alignment at non-coplanar angles, the couch was rotated manually inside the treatment room to 270º. The HexaPOD couch and OSD system calculated isocenter shifts were registered. After the registration of the values, the couch isocenter was corrected manually at 270º inside the treatment room through the HexaPOD couch controller, and after manual correction, was rotated manually to 0º - standard position. A confirmation CBCT acquisition was conducted. The positional error calculated by the XVI corresponded to the isocenter shift calculated previously by HexaPOD iGUIDE software at couch rotation 270º. This methodology was reproduced five times. This test proved that the HexaPOD couch calculated isocenter shifts at the different couch rotations are in agreement with the expected XVI positional error if was possible to acquire CBCT with couch rotation ≠ 0°, as proved previously in the 2nd test. These results confirm that the manual correction of the HexaPOD executed inside the treatment room after couch rotations before an SRS treatment is reliable and should be performed.

Overall, the uncertainty of the OSD system corresponds to the difference between the HexaPOD couch and OSD system calculated isocenter shift, which is within 1 mm agreement for gantry angulations without camera pod occlusions. For gantry angulations where one or two of the camera pods are occluded, the uncertainty is within 2 mm. Although the results in this project do not corroborate the Catalyst HD™ position accuracy in the literature, which is within 0,5 mm for rigid bodys[147], *Ans Swnnen et al*[155] achieved deviations from rotational and translational isocenter corrections for CBCT and OSD system within 0,2° (pitch, roll, yaw), and 0,5 mm (lateral, longitudinal, vertical). Nevertheless, the setteled tolerance for the implementation of SRS treatments is within 1 mm submilimter accuracy.[147]

6. Conclusions

If an SRS treatment was considered to be planned, accordingly to a non-coplanar angle arrangement, the best gantry and couch configuration to perform the treatment concomitantly with the OSD system is the one with minimal camera pod occlusion, for a better patient detection and consecutive reading during treatment. Respecting the OSD system performance, the posterior oblique gantry angles - 135º and 225º - exhibited better results regarding phantom surface reading due to the minimal lateral camera pod occlusion in this study. When the gantry was at 0º angulation, the OSD system showed better phantom surface reading offsets in left couch rotations, 270º, 300º and 330º respectively. These results suggest that right couch rotations suffer larger drifts, due to table fluctuation.

Regarding the results obtained, it is recommended before an SRS treatment to perform XVI imaging and apply the isocenter deviations through HexaPOD submillimeter couch correction. After acquiring the volumetric image, the XVI detector and XVI X-Ray tube should be both retracted for a better OSD system reading.

It is also recommended to apply HexaPOD manual couch correction after each couch rotation performed inside the treatment room, and only after, acquiring a new 3D scan image of the patient surface with the OSD system. These steps are fundamental to minimize reading errors during treatment.

It has been also concluded that the overall OSD system uncertainty corresponds to the difference between the HexaPOD couch and OSD system calculated isocenter shift, which is within 1 mm agreement for gantry angulations with minimal camera pod occlusion. For gantry angulations where are more camera limitation, the uncertainty is within 2 mm.

The implementation of a maskless immobilization approach with only a vacuum mouthpiece suction system for head fixation in patients with CNS tumors who will undergo SRS treatment under the guidance of an OSD system coupled with 6-DOF robotic couch for submillimetric position correction it is viable. The results in this master thesis demonstrate that it’s possible to use the OSD system as a tracking tool during treatments with coplanar and non-coplanar angles through a precision below 1 mm in the majority of the clinical settings and arrays, even in extreme conditions.

Due to system configuration and study limitations, some treatment settings can only be used with accuracies below 2 mm. This is a subject to be explored in future tests.

This study did not evaluate the precision of the maskless immobilization approach since the tests were conducted in phantoms. Further investigation is necessary to achieve more conclusions regarding the utilization of the Fraxion system, firstly with verification tests on volunteers, before implementing the immobilization system in patients during SRS treatments.

7. Future Work

The research presented in this thesis is the preparatory work for a clinical implementation of a new SRS protocol using the optical surface detecting system and the maskless immobilization approach. These systems aim to position and monitor patients with CNS tumors with specific inclusion criteria. The OSD system presented in this work has already been implemented in the Radiotherapy Department at Hospital CUF Descobertas for other pathologies, such as breast treatments, but before it could be implemented for SRS treatments with non-coplanar couch arrangement, it had to be validated that the system provided sufficient accuracy for that purpose.

The OSD system in this study provided sufficient accuracy for a phantom, and the Hospital is now prepared to initiate a patient study and collect data from patient positioning using the OSD system and thus be able to directly compare setup errors with open-faced masks.

This phantom experiment was a crucial step before implementing a new protocol, since the implementation of SRS with non-coplanar angles using the OSD system with maskless approach hasn't been validated in the literature. The future research on SRS frameless implementation is to calculate the setup error associated with the use of Elekta Fraxion system with a vacuum mouthpiece for head immobilization and determine an optimal CTV-PTV margin for SRS.

8. Proposed Protocol for SRS Treatment with Catalyst HD™

A suggested protocol based on the Catalyst HD™ User Guide and flowchart for SRS treatment with Catalyst HD™ is presented in the Appendix for the implementation of the technique in the Radiotherapy Department at Hospital CUF Descobertas. This protocol is based on a series of instructions that gives the user guidance on the appropriate actions to be taken at all stages of the process, from the Routine QA to the treatment delivery. It should identify and manage all possible scenarios (what to image, when and how often) and the corrective suggestions.

9. References

1. Abbas, Z. & Rehman, S. (2018). An Overview of Cancer Treatment Modalities. In *IntechOpen*, Chapter 6.
2. Carl, G., Reitz, D., Schönecker, S., Pazos, M., Freislederer, P., Reiner, M., … Corradini, S. (2018). Optical surface scanning for patient positioning in radiation therapy: A prospective analysis of 1902 fractions. *Technology in Cancer Research and Treatment*, *17*.
3. Vaibhav, M. (2017). Quality assurance for clinical implementation of an Optical Surface monitoring system. *IOSR Journal of Applied Physics*, 2278-4861.Volume 9, Issue 6 Ver. II, PP 15-22.
4. De Los Santos J, Popple, R., Agazaryan, N. (2013). Image guided radiation therapy (IGRT) technologies for radiation therapy localization and delivery. *Int J Radiat Oncol Biol Phys*. 87(1):33-45.
5. Willoughby, T., Lehmann, J., Bencomo, JA. (2012) Quality assurance for nonradiographic radiotherapy localization and positioning systems: report of Task Group 147. *Med Phys*.39(4):1728-1747.
6. Fior, R., & Zilhão, R. (2019). *Molecular and Cell Biology of Cancer: When Cells Break the Rules and Hijack Their Own Planet (Learning Materials in Biosciences)* (1st ed. 2019 ed.). Springer.
7. Reya, T., Morrison, S. J., Clarke, M. F., & Weissman, I. L. (2001). Stem cells, cancer, and cancer stem cells. *Nature*, *414*(6859), 105–111. https://doi.org/10.1038/35102167
8. Taipale, J., & Beachy, P. A. (2001). The Hedgehog and Wnt signalling pathways in cancer. *Nature*, *411*(6835), 349–354. https://doi.org/10.1038/35077219
9. Zhu, Y., & Parada, L. F. (2002). The Molecular and Genetic Basis of Neurological Tumours. *Nature Reviews Cancer*, *2*(8), 616–626. https://doi.org/10.1038/nrc866
10. Pardal, R., Clarke, M. F., & Morrison, S. J. (2003). Applying the principles of stem-cell biology to cancer. *Nature Reviews Cancer*, *3*(12), 895–902. https://doi.org/10.1038/nrc1232
11. Ames, B. N., Gold, L. S., & Willett, W. C. (1995). The causes and prevention of cancer. *Proceedings of the National Academy of Sciences*, *92*(12), 5258–5265. https://doi.org/10.1073/pnas.92.12.5258
12. Abbas, Z., & Rehman, S. (2018). An Overview of Cancer Treatment Modalities. *Neoplasm*. https://doi.org/10.5772/intechopen.76558
13. Buckner, J. C., Brown, P. D., O'Neill, B. P., Meyer, F. B., Wetmore, C. J., & Uhm, J. H. (2007). Central Nervous System Tumors. *Mayo Clinic Proceedings*, *82*(10), 1271–1286. https://doi.org/10.4065/82.10.1271
14. Mucignat-Caretta, C. (2020). Tumors of the Central Nervous System: An Update. *Cancers*, *12*(9), 2507. https://doi.org/10.3390/cancers12092507
15. Louis, D. N., Perry, A., Reifenberger, G., von Deimling, A., Figarella-Branger, D., Cavenee, W. K., Ohgaki, H., Wiestler, O. D., Kleihues, P., & Ellison, D. W. (2016). The 2016 World Health Organization Classification of Tumors of the Central Nervous System: a summary. *Acta Neuropathologica*, *131*(6), 803–820. https://doi.org/10.1007/s00401-016-1545-1
16. *WHO Classification of Tumors Editorial Board.* World Health Organization Classification of Tumor of the Central Nervous System. 5th ed. Lyon: International Agency for Research on Cancer; 2021.
17. Louis, D. N., Perry, A., Wesseling, P., Brat, D. J., Cree, I. A., Figarella-Branger, D., Hawkins, C., Ng, H. K., Pfister, S. M., Reifenberger, G., Soffietti, R., von Deimling, A., & Ellison, D. W. (2021). The 2021 WHO Classification of Tumors of the Central Nervous System: a summary. Neuro-Oncology, 23(8), 1231–1251. https://doi.org/10.1093/neuonc/noab106
18. Battista, J. J., Rider, W. D., & van Dyk, J. (1980). Computed tomography for radiotherapy planning. *International Journal of Radiation Oncology*Biology*Physics*, *6*(1), 99–107. https://doi.org/10.1016/0360-3016(80)90211-4

19. Orton, C. (2013). *Progress in Medical Radiation Physics (Progress in Medical Radiation Physics, 1)* (Softcover reprint of the original 1st ed. 1982 ed.). Springer.

20. Pereira, G. C., Traughber, M., & Muzic, R. F. (2014). The Role of Imaging in Radiation Therapy Planning: Past, Present, and Future. *BioMed Research International*, *2014*, 1–9. https://doi.org/10.1155/2014/231090

21. Vordermark, D. (2011). Ten years of progress in radiation oncology. *BMC Cancer*, *11*(1). https://doi.org/10.1186/1471-2407-11-503

22. Steenbakkers, R. J., Duppen, J. C., Fitton, I., Deurloo, K. E., Zijp, L. J., Comans, E. F., Uitterhoeve, A. L., Rodrigus, P. T., Kramer, G. W., Bussink, J., de Jaeger, K., Belderbos, J. S., Nowak, P. J., van Herk, M., & Rasch, C. R. (2006). Reduction of observer variation using matched CT-PET for lung cancer delineation: A three-dimensional analysis. *International Journal of Radiation Oncology*Biology*Physics*, *64*(2), 435–448. https://doi.org/10.1016/j.ijrobp.2005.06.034

23. Li, J., & Xiao, Y. (2013). Application of FDG-PET/CT in Radiation Oncology. *Frontiers in Oncology*, *3*. https://doi.org/10.3389/fonc.2013.00080

24. Grégoire, V., Bol, A., Geets, X., & Lee, J. (2006). Is PET-Based Treatment Planning the New Standard in Modern Radiotherapy? The Head and Neck Paradigm. *Seminars in Radiation Oncology*, *16*(4), 232–238. https://doi.org/10.1016/j.semradonc.2006.04.006

25. Kron, T., Lehmann, J., & Greer, P. B. (2016). Dosimetry of ionising radiation in modern radiation oncology. *Physics in Medicine and Biology*, *61*(14), R167–R205. https://doi.org/10.1088/0031-9155/61/14/r167

26. Mukherji, A. (2018). *Basics of Planning and Management of Patients during Radiation Therapy*. Springer Publishing.

27. Njeh, C. (2008). Tumor delineation: The weakest link in the search for accuracy in radiotherapy. *Journal of Medical Physics*, *33*(4), 136. https://doi.org/10.4103/0971-6203.44472

28. Mendes, G., Ongaratti, B., Lima, J. (2014) Epidemiologia de uma série de tumores primários do sistema nervoso central. *Arq Bras Neurocir* 33(4): 279-83.

29. Martino, F., Clemente, S., Graeff, C., Palma, G., & Cella, L. (2021). Dose Calculation Algorithms for External Radiation Therapy: An Overview for Practitioners. *Applied Sciences*, *11*(15), 6806. https://doi.org/10.3390/app11156806

30. Minniti, G., Capone, L., Alongi, F., Figlia, V., Nardiello, B., el Gawhary, R., Scaringi, C., Bianciardi, F., Tolu, B., Gentile, P., & Paolini, S. (2020). Initial Experience With Single-Isocenter Radiosurgery to Target Multiple Brain Metastases Using an Automated Treatment Planning Software: Clinical Outcomes and Optimal Target Volume Margins Strategy. *Advances in Radiation Oncology*, *5*(5), 856–864. https://doi.org/10.1016/j.adro.2020.06.008

31. *An Introduction to Current Radiation Therapy Treatment Planning Systems*. (2021, October 3). Imaging Technology News. https://www.itnonline.com/article/introduction-current-radiation-therapy-treatment-planning-systems

32. Schlegel, W. (2010). If you can't see it, you can miss it: the role of biomedical imaging in radiation oncology. *Radiation Protection Dosimetry*, *139*(1–3), 321–326. https://doi.org/10.1093/rpd/ncq022

33. Ahn, P. H., & Garg, M. K. (2008). Positron Emission Tomography/Computed Tomography for Target Delineation in Head and Neck Cancers. *Seminars in Nuclear Medicine*, *38*(2), 141–148. https://doi.org/10.1053/j.semnuclmed.2007.11.002

34. Haynes-Outlaw, E. D., & Grigsby, P. W. (2010). The Role of FDG-PET/CT in Cervical Cancer: Diagnosis, Staging, Radiation Treatment Planning and Follow-Up. *PET Clinics*, *5*(4), 435–446. https://doi.org/10.1016/j.cpet.2010.07.004

35. Simpson, D. R., Lawson, J. D., Nath, S. K., Rose, B. S., Mundt, A. J., & Mell, L. K. (2009). Utilization of Advanced Imaging Technologies for Target Delineation in Radiation Oncology. *Journal of the American College of Radiology*, *6*(12), 876–883. https://doi.org/10.1016/j.jacr.2009.08.006

36. Glatstein, E., Lichter, A. S., Fraass, B. A., Kelly, B. A., & Geijn, J. V. D. (1985). The imaging revolution and radiation oncology: Use of CT, ultrasound, and nmr for localization, treatment planning and treatment delivery. *International Journal of Radiation Oncology*Biology*Physics*, *11*(2), 299–314. https://doi.org/10.1016/0360-3016(85)90152-x

37. Grosu, A. L., Piert, M., Weber, W. A., Jeremic, B., Picchio, M., Schratzenstaller, U., Zimmermann, F. B., Schwaiger, M., & Molls, M. (2005). Positron Emission Tomography for Radiation Treatment Planning. *Strahlentherapie Und Onkologie*, *181*(8), 483–499. https://doi.org/10.1007/s00066-005-1422-7

38. Hunter, K. U., & Eisbruch, A. (2011). Advances in Imaging. *The Cancer Journal*, *17*(3), 151–154. https://doi.org/10.1097/ppo.0b013e31821d7e35

39. Ahmad, I., Chufal, K. S., Bhatt, C. P., & Rathour, S. (2017). Treating patients with brain metastases has evolved: scalp-sparing, hippocampal avoidance whole brain radiotherapy with simultaneous integrated boost. *BMJ Case Reports*, bcr-2017. https://doi.org/10.1136/bcr-2017-223449

40. Paliwal, B., & Tewatia, D. (2009). Advances in radiation therapy dosimetry. *Journal of Medical Physics*, *34*(3), 108. https://doi.org/10.4103/0971-6203.54842_

41. *NCCN CNS Treatment Guidelines*. (2022). NCCN. Retrieved 2022, from https://www.nccn.org/guidelines/guidelines-detail?category=1&id=1425

42. Yakar, M., & Etiz, D. (2021). Artificial intelligence in radiation oncology. *Artificial Intelligence in Medical Imaging*, *2*(2), 13–31. https://doi.org/10.35711/aimi.v2.i2.13

43. International Atomic Energy Agency. (2005). *Radiation Oncology Physics: A Handbook for Teachers and Students*. International Atomic Energy Agency.

44. A. H. Vitoria, M. C. L. Arroyo, and C. P. Olmos. (2012) Fundamentos de Física Médica Volume 3 *Radioterapia Externa I: Bases Físicas, Equipamentos, determinação da dose absorvida e programa de garantia de qualidade.* ADI Serviços Editorales.

45. Gazda, J. M. M. S., & Coia, L. R., MD. (2020, November 10). *Principles of Radiation Therapy*. Cancer Network. Retrieved 2022, from https://www.cancernetwork.com/view/principles-radiation-therapy

46. Cherry, P., & Duxbury, A. M. (2019). *Practical Radiotherapy: Physics and Equipment* (3rd ed.). Wiley-Blackwell.

47. Sandle, T. (2014). *Sterility, Sterilisation and Sterility Assurance for Pharmaceuticals: Technology, Validation and Current Regulations*. Woodhead Publishing.

48. Zeman, E. M., Schreiber, E. C., & Tepper, J. E. (2014). Basics of Radiation Therapy. *Abeloff's Clinical Oncology*, 393–422.e3. https://doi.org/10.1016/b978-1-4557-2865-7.00027-8

49. Ahmad, S. S., Duke, S., Jena, R., Williams, M. V., & Burnet, N. G. (2012). Advances in radiotherapy. *BMJ*, *345*(dec04 1), e7765. https://doi.org/10.1136/bmj.e7765

50. Scaringi, C., Agolli, L., & Minniti, G. (2018). Technical Advances in Radiation Therapy for Brain Tumors. *Anticancer Research*, *38*(11), 6041–6045. https://doi.org/10.21873/anticanres.12954

51. Choi, W. H., & Cho, J. (2016). Evolving Clinical Cancer Radiotherapy: Concerns Regarding Normal Tissue Protection and Quality Assurance. *Journal of Korean Medical Science*, *31*(Suppl 1), S75. https://doi.org/10.3346/jkms.2016.31.s1.s75

52. Lewis, B. C., Snyder, W. J., Kim, S., & Kim, T. (2018). Monitoring frequency of intra-fraction patient motion using the ExacTrac system for LINAC-based SRS treatments. *Journal of Applied Clinical Medical Physics*, *19*(3), 58–63. https://doi.org/10.1002/acm2.12279

53. Márquez-Graña, C., McGowan, P., Cotterell, M., & Ares, E. (2017). Qualitative feasibility research to develop a novel approach for a design of a head support for radiosurgery or stereotactic radiosurgery (SRS). *Procedia Manufacturing*, *13*, 1344–1351. https://doi.org/10.1016/j.promfg.2017.09.112

54. Andrews, DW., Scottl, CB., Sperduto, PW., Flanders, AE., Gaspar, LE., Schell, MC., Werner-Wasik, M., Demas, W., Ryu, J., Bahary, JP., Souhami, L., Rotman, M., Mehta, MP., Curran, WJ. (2004).

Whole brain radiation therapy with or without stereotactic radiosurgery boost for patients with one to three brain metastases: Phase III results of the RTOG 9508 randomised trial. *The Lancet.* 363(9422):1665-1672.

55. Kano, H., Flickinger, JC., Tonetti, D., Hsu, A., Yang, HC., Flannery, TJ., Niranjan, A., Lunsford, LD. (2017). Estimating the risks of adverse radiation effects after gamma knife radiosurgery for arteriovenous malformations. *Stroke*. 48(1):84-90.

56. Abbas, Z. & Rehman, S. (2018). An Overview of Cancer Treatment Modalities. In *IntechOpen*, Chapter 6.

57. Gopan, O., & Wu, Q. (2012). Evaluation of the Accuracy of a 3D Surface Imaging System for Patient Setup in Head and Neck Cancer Radiotherapy. *International Journal of Radiation Oncology*Biology*Physics*, *84*(2), 547–552. https://doi.org/10.1016/j.ijrobp.2011.12.004

58. Konradsson E. (2018) Surface guided radiotherapy for high precision treatments of brain metastases. *Master of Science Thesis*, Lund University.

59. Kondziolka, D., Shin, S. M., Brunswick, A., Kim, I., & Silverman, J. S. (2014). The biology of radiosurgery and its clinical applications for brain tumors. *Neuro-Oncology*, *17*(1), 29–44. https://doi.org/10.1093/neuonc/nou284

60. Kerin, M. J. (2001). Cancer principles and practice of oncology. *Surgical Oncology*, *6*(2), 125.

61. Great Ormond Street Hospital. (2018). *Gamma Knife® stereotactic radiosurgery*. GOSH Hospital Site. Retrieved 2022, from https://www.gosh.nhs.uk/conditions-and-treatments/procedures-and-treatments/gamma-knife-stereotactic-radiosurgery/

62. Ruggieri, R., Naccarato, S., Mazzola, R., Ricchetti, F., Corradini, S., Fiorentino, A., & Alongi, F. (2018). Linac-based VMAT radiosurgery for multiple brain lesions: comparison between a conventional multi-isocenter approach and a new dedicated mono-isocenter technique. *Radiation Oncology*, *13*(1). https://doi.org/10.1186/s13014-018-0985-2

63. Aoyama, H., Shirato, H., Tago, M., Nakagawa, K., Toyoda, T., Hatano, K., Kenjyo, M., Oya, N., Hirota, S., Shioura, H., Kunieda, E., Inomata, T., Hayakawa, K., Katoh, N., & Kobashi, G. (2006). Stereotactic Radiosurgery Plus Whole-Brain Radiation Therapy vs Stereotactic Radiosurgery Alone for Treatment of Brain Metastases. *JAMA*, *295*(21), 2483. https://doi.org/10.1001/jama.295.21.2483

64. Yamamoto, M., Serizawa, T., Shuto, T., Akabane, A., Higuchi, Y., Kawagishi, J., Yamanaka, K., Sato, Y., Jokura, H., Yomo, S., Nagano, O., Kenai, H., Moriki, A., Suzuki, S., Kida, Y., Iwai, Y., Hayashi, M., Onishi, H., Gondo, M., . . . Tsuchiya, K. (2014). Stereotactic radiosurgery for patients with multiple brain metastases (JLGK0901): a multi-institutional prospective observational study. *The Lancet Oncology*, *15*(4), 387–395. https://doi.org/10.1016/s1470-2045(14)70061-0

65. Kocher, M., Wittig, A., Piroth, M. D., Treuer, H., Seegenschmiedt, H., Ruge, M., Grosu, A. L., & Guckenberger, M. (2014). Stereotactic radiosurgery for treatment of brain metastases. *Strahlentherapie Und Onkologie*, *190*(6), 521–532. https://doi.org/10.1007/s00066-014-0648-7

66. Aoyama, H., Shirato, H., Tago, M., Nakagawa, K., Toyoda, T., Hatano, K., Kenjyo, M., Oya, N., Hirota, S., Shioura, H., Kunieda, E., Inomata, T., Hayakawa, K., Katoh, N., & Kobashi, G. (2006). Stereotactic Radiosurgery Plus Whole-Brain Radiation Therapy vs Stereotactic Radiosurgery Alone for Treatment of Brain Metastases. *JAMA*, *295*(21), 2483. https://doi.org/10.1001/jama.295.21.2483

67. Chang, E. L., Wefel, J. S., Hess, K. R., Allen, P. K., Lang, F. F., Kornguth, D. G., Arbuckle, R. B., Swint, J. M., Shiu, A. S., Maor, M. H., & Meyers, C. A. (2009). Neurocognition in patients with brain metastases treated with radiosurgery or radiosurgery plus whole-brain irradiation: a randomised controlled trial. *The Lancet Oncology*, *10*(11), 1037–1044. https://doi.org/10.1016/s1470-2045(09)70263-3

68. Li. W. (2014) Determining Rational Planning Target Volume Margins for Intracranial Stereotactic Radiotherapy. *Master Thesis. Department of Institute of Medical Science University of Toronto*

69. Ramakrishna, N., Rosca, F., Friesen, S., Tezcanli, E., Zygmanszki, P., & Hacker, F. (2010). A clinical comparison of patient setup and intra-fraction motion using frame-based radiosurgery versus a frameless image-guided radiosurgery system for intracranial lesions. *Radiotherapy and Oncology*, *95*(1), 109–115. https://doi.org/10.1016/j.radonc.2009.12.030

70. Otto, K., & Fallone, B. (1998). Frame Slippage Verification in Stereotactic Radiosurgery. *International Journal of Radiation OncologyBiologyPhysics*, *41*(1), 199–205. https://doi.org/10.1016/s0360-3016(98)00005-4

71. Nath, S. K., Lawson, J. D., Wang, J. Z., Simpson, D. R., Newman, C. B., Alksne, J. F., Mundt, A. J., & Murphy, K. T. (2009). Optically-guided frameless linac-based radiosurgery for brain metastases: clinical experience. *Journal of Neuro-Oncology*, *97*(1), 67–72. https://doi.org/10.1007/s11060-009-9989-y

72. Guckenberger, M., Baier, K., Guenther, I., Richter, A., Wilbert, J., Sauer, O., Vordermark, D., & Flentje, M. (2007). Reliability of the Bony Anatomy in Image-Guided Stereotactic Radiotherapy of Brain Metastases. *International Journal of Radiation Oncology*Biology*Physics*, *69*(1), 294–301. https://doi.org/10.1016/j.ijrobp.2007.05.030

73. Fuss, M., Salter, B. J., Cheek, D., Sadeghi, A., Hevezi, J. M., & Herman, T. S. (2004). Repositioning accuracy of a commercially available thermoplastic mask system. *Radiotherapy and Oncology*, *71*(3), 339–345. https://doi.org/10.1016/j.radonc.2004.03.003

74. Ramakrishna, N., Rosca, F., Friesen, S., Tezcanli, E., Zygmanszki, P., & Hacker, F. (2010). A clinical comparison of patient setup and intra-fraction motion using frame-based radiosurgery versus a frameless image-guided radiosurgery system for intracranial lesions. *Radiotherapy and Oncology*, *95*(1), 109–115. https://doi.org/10.1016/j.radonc.2009.12.030

75. Lamba, M., Breneman, J. C., & Warnick, R. E. (2009). Evaluation of Image-Guided Positioning for Frameless Intracranial Radiosurgery. *International Journal of Radiation Oncology*Biology*Physics*, *74*(3), 913–919. https://doi.org/10.1016/j.ijrobp.2009.01.008

76. Solberg, T. D., Medin, P. M., Mullins, J., & Li, S. (2008). Quality Assurance of Immobilization and Target Localization Systems for Frameless Stereotactic Cranial and Extracranial Hypofractionated Radiotherapy. *International Journal of Radiation Oncology*Biology*Physics*, *71*(1), S131–S135. https://doi.org/10.1016/j.ijrobp.2007.05.097

77. Linthout, N., Verellen, D., Tournel, K., & Storme, G. (2006). Six dimensional analysis with daily stereoscopic x-ray imaging of intrafraction patient motion in head and neck treatments using five points fixation masks. *Medical Physics*, *33*(2), 504–513. https://doi.org/10.1118/1.2165417

78. Spadea, M. F., Tagaste, B., Riboldi, M., Preve, E., Alterio, D., Piperno, G., Garibaldi, C., Orecchia, R., Pedotti, A., & Baroni, G. (2011). Intra-fraction setup variability: IR optical localization vs. X-ray imaging in a hypofractionated patient population. *Radiation Oncology*, *6*(1). https://doi.org/10.1186/1748-717x-6-38

79. Grusell, E., Montelius, A., Russell, K. R., Blomquist, E., Pellettieri, L., Lilja, A., Moström, U., & Jakobsson, P. (1994). Patient positioning for fractionated precision radiation treatment of targets in the head using fiducial markers. *Radiotherapy and Oncology*, *33*(1), 68–72. https://doi.org/10.1016/0167-8140(94)90088-4

80. Tsai, J. S., Engler, M. J., Ling, M. N., Wu, J. K., Kramer, B., Dipetrillo, T., & Wazer, D. E. (1999). A non-invasive immobilization system and related quality assurance for dynamic intensity modulated radiation therapy of intracranial and head and neck disease. *International Journal of Radiation Oncology*Biology*Physics*, *43*(2), 455–467. https://doi.org/10.1016/s0360-3016(98)00398-8

81. Ryken, T. C., Meeks, S. L., Pennington, E. C., Hitchon, P., Traynelis, V., Mayr, N. A., Bova, F. J., Friedman, W. A., & Buatti, J. M. (2001). Initial clinical experience with frameless stereotactic radiosurgery: analysis of accuracy and feasibility. *International Journal of Radiation Oncology*Biology*Physics*, *51*(4), 1152–1158. https://doi.org/10.1016/s0360-3016(01)01756-4

82. Murphy, M. J. (2002). Fiducial-based targeting accuracy for external-beam radiotherapy. *Medical Physics*, *29*(3), 334–344. https://doi.org/10.1118/1.1448823

83. Li, S., Liu, D., Yin, G., Zhuang, P., & Geng, J. (2006). Real-time 3D-surface-guided head refixation useful for fractionated stereotactic radiotherapy. *Medical Physics*, *33*(2), 492–503. https://doi.org/10.1118/1.2150778

84. Bova, F. J., Meeks, S. L., Friedman, W. A., & Buatti, J. M. (1998). Optic-guided stereotactic radiotherapy. *Medical Dosimetry*, *23*(3), 221–228. https://doi.org/10.1016/s0958-3947(98)00017-x

85. Yan, Y., Song, Y., & Boyer, A. L. (2002). An investigation of a video-based patient repositioning technique. *International Journal of Radiation Oncology*Biology*Physics*, *54*(2), 606–614. https://doi.org/10.1016/s0360-3016(02)02934-6

86. Kim, K. H., Cho, M. J., Kim, J. S., Kim, J. S., Song, C. J., Song, S. H., Kim, S. H., Myers, L., & Kim, Y. E. (2003). Isocenter accuracy in frameless stereotactic radiotherapy using implanted fiducials. *International Journal of Radiation Oncology*Biology*Physics*, *56*(1), 266–273. https://doi.org/10.1016/s0360-3016(03)00088-9

87. Li, S., Liu, D., Yin, G., Zhuang, P., & Geng, J. (2006). Real-time 3D-surface-guided head refixation useful for fractionated stereotactic radiotherapy. *Medical Physics*, *33*(2), 492–503. https://doi.org/10.1118/1.2150778

88. Baroni, G., Garibaldi, C., Riboldi, M., Spadea, M. F., Catalano, G., Tagaste, B., Tosi, G., Orecchia, R., & Pedotti, A. (2006). 3D optoelectronic analysis of interfractional patient setup variability in frameless extracranial stereotactic radiotherapy. *International Journal of Radiation Oncology*Biology*Physics*, *64*(2), 635–642. https://doi.org/10.1016/j.ijrobp.2005.07.964

89. Ma, J., Chang, Z., Wang, Z., Jackie Wu, Q., Kirkpatrick, J. P., & Yin, F. F. (2009). ExacTrac X-ray 6 degree-of-freedom image-guidance for intracranial non-invasive stereotactic radiotherapy: Comparison with kilo-voltage cone-beam CT. *Radiotherapy and Oncology*, *93*(3), 602–608. https://doi.org/10.1016/j.radonc.2009.09.009

90. Peng, J. L., Kahler, D., Li, J. G., Samant, S., Yan, G., Amdur, R., & Liu, C. (2010). Characterization of a real-time surface image-guided stereotactic positioning system. *Medical Physics*, *37*(10), 5421–5433. https://doi.org/10.1118/1.3483783

91. Willner, J., Flentje, M., & Bratengeier, K. (1997). CT simulation in stereotactic brain radiotherapy — analysis of isocenter reproducibility with mask fixation. *Radiotherapy and Oncology*, *45*(1), 83–88. https://doi.org/10.1016/s0167-8140(97)00135-7

92. A Comparison of Two Different Wrist Immobilization Methods. (2019). *Case Medical Research*. https://doi.org/10.31525/ct1-nct04213352

93. Zhao, B., Maquilan, G., Jiang, S., & Schwartz, D. L. (2017). Minimal mask immobilization with optical surface guidance for head and neck radiotherapy. *Journal of Applied Clinical Medical Physics*, *19*(1), 17–24. https://doi.org/10.1002/acm2.12211

94. Wiant, D., Squire, S., Liu, H., Maurer, J., Lane Hayes, T., & Sintay, B. (2016). A prospective evaluation of open face masks for head and neck radiation therapy. *Practical Radiation Oncology*, *6*(6), e259–e267. https://doi.org/10.1016/j.prro.2016.02.003

95. *Fraxion™ Elekta*. (2020). Elekta. Retrieved 2022, from https://ecatalog.elekta.com/oncology/oncology/fraxion/products/0/22325/22313/20231/fraxion.aspx

96. Verellen, D., Ridder, M. D., & Storme, G. (2008). A (short) history of image-guided radiotherapy. Radiotherapy and Oncology, 86(1), 4–13. https://doi.org/10.1016/j.radonc.2007.11.023

97. Dawson, L. A., & Jaffray, D. A. (2007). Advances in Image-Guided Radiation Therapy. Journal of Clinical Oncology, 25(8), 938–946. https://doi.org/10.1200/jco.2006.09.9515

98. Xu, H., Brown, S., Chetty, I. J., & Wen, N. (2016). A Systematic Analysis of Errors in Target Localization and Treatment Delivery for Stereotactic Radiosurgery Using 2D/3D Image Registration.

Technology in Cancer Research & Treatment, 16(3), 321–331. https://doi.org/10.1177/1533034616664425

99. Wu, Q. J., Li, T., Wu, Q., & Yin, F. F. (2011). Adaptive Radiation Therapy. *The Cancer Journal*, *17*(3), 182–189. https://doi.org/10.1097/ppo.0b013e31821da9d8

100. Goyal, S., & Kataria, T. (2014). Image Guidance in Radiation Therapy: Techniques and Applications. Radiology Research and Practice, 2014, 1–10. https://doi.org/10.1155/2014/705604~

101. Ely, B., Ely, B., & Kazumba, P. (2022, May 10). Patient positioning and motion management, SGRT. C-RAD. Retrieved 2022, from https://c-rad.com/clinical-usage/sigrt/

102. Van Herk, M. (2007). Different Styles of Image-Guided Radiotherapy. Seminars in Radiation Oncology, 17(4), 258–267. https://doi.org/10.1016/j.semradonc.2007.07.003

103. Gupta, T., & Narayan, C. (2012). Image-guided radiation therapy: Physician′s perspectives. Journal of Medical Physics, 37(4), 174. https://doi.org/10.4103/0971-6203.103602

104. Kaul, D., Budach, V., Wurm, R., Gruen, A., Graaf, L., Habbel, P., & Badakhshi, H. (2014). Linac-based stereotactic radiotherapy and radiosurgery in patients with meningioma. Radiation Oncology, 9(1). https://doi.org/10.1186/1748-717x-9-78

105. Ma, J., Chang, Z., Wang, Z., Jackie Wu, Q., Kirkpatrick, J. P., & Yin, F. F. (2009). ExacTrac X-ray 6 degree-of-freedom image-guidance for intracranial non-invasive stereotactic radiotherapy: Comparison with kilo-voltage cone-beam CT. Radiotherapy and Oncology, 93(3), 602–608. https://doi.org/10.1016/j.radonc.2009.09.009

106. Ding, A. P. X. (2018). *Image Guidance in Radiation Therapy: Techniques, Accuracy, and Limitations, Mono No. 39* (1st ed.). Medical Physics Pub Corp.

107. American Association of Physicists in Medicine (2009). The Role of In-Room kV X-Ray Imaging for Patient Setup and Target Localization. *Report of AAPM Task Group 104*.

108. Jaffray, D. (2007). Kilovoltage volumetric imaging in the treatment room. *Frontiers of Radiation Therapy and Oncology*, vol. 40, pp.116–131.

109. McBain, C. A., Henry, A. M., Sykes, J., Amer, A., Marchant, T., Moore, C. M., Davies, J., Stratford, J., McCarthy, C., Porritt, B., Williams, P., Khoo, V. S., & Price, P. (2006). X-ray volumetric imaging in image-guided radiotherapy: The new standard in on-treatment imaging. *International Journal of Radiation Oncology*Biology*Physics*, *64*(2), 625–634. https://doi.org/10.1016/j.ijrobp.2005.09.018

110. Morin, O., Gillis, A., Chen, J., Aubin, M., Bucci, M. K., Roach, M., & Pouliot, J. (2006). Megavoltage cone-beam CT: System description and clinical applications. *Medical Dosimetry*, *31*(1), 51–61. https://doi.org/10.1016/j.meddos.2005.12.009

111. Pouliot, J., Bani-Hashemi, A., Josephine Chen, Svatos, M., Ghelmansarai, F., Mitschke, M., Aubin, M., Xia, P., Morin, O., Bucci, K., Roach, M., Hernandez, P., Zheng, Z., Hristov, D., & Verhey, L. (2005). Low-dose megavoltage cone-beam CT for radiation therapy. *International Journal of Radiation Oncology*Biology*Physics*, *61*(2), 552–560. https://doi.org/10.1016/j.ijrobp.2004.10.01

112. Johnson, L., Milliken, B., Hadley, S., Pelizzari, C., Haraf, D., & Chen, G. (1999). Initial clinical experience with a video-based patient positioning system. *International Journal of Radiation Oncology*Biology*Physics*, *45*(1), 205–213. https://doi.org/10.1016/s0360-3016(99)00182-0

113. Batista, V., Meyer, J., Kügele, M., & Al-Hallaq, H. (2020). Clinical paradigms and challenges in surface guided radiation therapy: Where do we go from here? *Radiotherapy and Oncology*, *153*, 34–42. https://doi.org/10.1016/j.radonc.2020.09.041

114. *Introduction to Surface Guided Radiation Therapy (SGRT)*. (2022, April 26). Vision RT. Retrieved 2022, from https://www.visionrt.com/technology/sgrt/

115. Hattel, S. H., Andersen, P. A., Wahlstedt, I. H., Damkjær, S., Saini, A., & Thomsen, J. B. (2019). Evaluation of setup and intrafraction motion for surface guided whole-breast cancer radiotherapy. *Journal of Applied Clinical Medical Physics*, *20*(6), 39–44. https://doi.org/10.1002/acm2.12599

116. Ely, B., Ely, B., & Kazumba, P. (2022, March 15). *Catalyst HD*. C-RAD. Retrieved 2022, from https://c-rad.com/products/catalyst-plus-hd/

117. Pan, H., Cerviño, L. I., Pawlicki, T., Jiang, S. B., Alksne, J., Detorie, N., Russell, M., Carter, B. S., Murphy, K. T., Mundt, A. J., Chen, C., & Lawson, J. D. (2012). Frameless, Real-Time, Surface Imaging-Guided Radiosurgery. *Neurosurgery*, *71*(4), 844–852. https://doi.org/10.1227/neu.0b013e3182647ad5

118. Wagner, T. H., Meeks, S. L., Bova, F. J., Friedman, W. A., Willoughby, T. R., Kupelian, P. A., & Tome, W. (2007). Optical Tracking Technology in Stereotactic Radiation Therapy. *Medical Dosimetry*, *32*(2), 111–120. https://doi.org/10.1016/j.meddos.2007.01.008

119. Yang, C. C. J., Ting, J. Y., Markoe, A., Bova, F. J., Mendenhall, W. M., & Friedman, W. A. (1999). A comparison of 3-D data correlation methods for fractionated stereotactic radiotherapy. *International Journal of Radiation Oncology*Biology*Physics*, *43*(3), 663–670. https://doi.org/10.1016/s0360-3016(98)00444-1

120. Shoup, T.E. & Mistree, F. (1987) Optimization Methods with Applications for Personal Computers. Englewood Cliffs, NJ: Prentice-Hall.

121. Bouchet, L. G., Meeks, S. L., Goodchild, G., Bova, F. J., Buatti, J. M., & Friedman, W. A. (2001). Calibration of three-dimensional ultrasound images for image-guided radiation therapy. *Physics in Medicine and Biology*, *46*(2), 559–577. https://doi.org/10.1088/0031-9155/46/2/321

122. Horn, B. K. P. (1987). Closed-form solution of absolute orientation using unit quaternions. *Journal of the Optical Society of America A*, *4*(4), 629. https://doi.org/10.1364/josaa.4.000629

123. American Association of Physicists in Medicine. (1994) Physical Aspects of Quality Assurance in Radiation Therapy. *AAPM Report No. 13*

124. American Association of Physicists in Medicine. (1995) Stereotactic Radiosurgery. *AAPM Report No. 54*

125. Yeung, T. K., Bortolotto, K., Cosby, S., Hoar, M., & Lederer, E. (2005). Quality assurance in radiotherapy: evaluation of errors and incidents recorded over a 10 year period. *Radiotherapy and Oncology*, *74*(3), 283–291. https://doi.org/10.1016/j.radonc.2004.12.003

126. Ishikura, S. (2008). Quality Assurance of Radiotherapy in Cancer Treatment: Toward Improvement of Patient Safety and Quality of Care. *Japanese Journal of Clinical Oncology*, *38*(11), 723–729. https://doi.org/10.1093/jjco/hyn112

127. Ku H.H. (1969). Precision Measurement and Calibration. *MBS Special Publication 300*. Vol.1. Washington DC.

128. Seung, S. K., Larson, D. A., Galvin, J. M., Mehta, M. P., Potters, L., Schultz, C. J., Yajnik, S. V., Hartford, A. C., & Rosenthal, S. A. (2013). American College of Radiology (ACR) and American Society for Radiation Oncology (ASTRO) Practice Guideline for the Performance of Stereotactic Radiosurgery (SRS). *American Journal of Clinical Oncology*, *36*(3), 310–315. https://doi.org/10.1097/coc.0b013e31826e053d

129. Report 91. (2014). *Journal of the ICRU*, *14*(2), 1–160. https://doi.org/10.1093/jicru_ndx017

130. International Atomic Energy Agency (2017). Dosimetry of small static fields used in external beam radiotherapy. IAEA technical reports series, vol 483

131. Zheng, D., Zhu, X., Zhang, Q. et al (2016). Target dose conversion modeling from pencil beam (PB) to Monte Carlo (MC) for lung SBRT. Radiat Oncol 11:83

132. Keall, PJ., Mageras, GS., Balter, JM. et al (2006). The management of respiratory motion in radiation oncology Report of AAPM Task Group 76. Med Phys 33(10):3874–3900

133. Benedict, S. H., Yenice, K. M., Followill, D., Galvin, J. M., Hinson, W., Kavanagh, B., Keall, P., Lovelock, M., Meeks, S., Papiez, L., Purdie, T., Sadagopan, R., Schell, M. C., Salter, B., Schlesinger, D. J., Shiu, A. S., Solberg, T., Song, D. Y., Stieber, V., . . . Yin, F. F. (2010). Stereotactic body

radiation therapy: The report of AAPM Task Group 101. *Medical Physics*, *37*(8), 4078–4101. https://doi.org/10.1118/1.3438081

134. Halvorsen, P. H., Cirino, E., Das, I. J., Garrett, J. A., Yang, J., Yin, F., & Fairobent, L. A. (2017). AAPM - RSS Medical Physics Practice Guideline 9.a. for SRS - SBRT. *Journal of Applied Clinical Medical Physics*, *18*(5), 10–21. https://doi.org/10.1002/acm2.12146

135. Wilke, L., Andratschke, N., Blanck, O., Brunner, T. B., Combs, S. E., Grosu, A. L., Moustakis, C., Schmitt, D., Baus, W. W., & Guckenberger, M. (2019). ICRU report 91 on prescribing, recording, and reporting of stereotactic treatments with small photon beams. *Strahlentherapie Und Onkologie*, *195*(3), 193–198. https://doi.org/10.1007/s00066-018-1416-x

136. Fraass, B., Doppke, K., Hunt, M., Kutcher, G., Starkschall, G., Stern, R., & van Dyke, J. (1998). American Association of Physicists in Medicine Radiation Therapy Committee Task Group 53: Quality assurance for clinical radiotherapy treatment planning. *Medical Physics*, *25*(10), 1773–1829. https://doi.org/10.1118/1.598373

137. Li, G., Ballangrud, S., Kuo, L. C., Kang, H., Kirov, A., Lovelock, M., Yamada, Y., Mechalakos, J., & Amols, H. (2011). Motion monitoring for cranial frameless stereotactic radiosurgery using video-based three-dimensional optical surface imaging. *Medical Physics*, *38*(7), 3981–3994. https://doi.org/10.1118/1.3596526

138. Cervino, L., Taylor, M., Lawson, J., Pan, H., Murphy, K., Mundt, A., & Pawlicki, T. (2010). Initial Clinical Experience with a Frameless and Maskless Stereotactic Radiosurgery Treatment. *International Journal of Radiation Oncology*Biology*Physics*, *78*(3), S779. https://doi.org/10.1016/j.ijrobp.2010.07.1803

139. Zhao, B., Maquilan, G., Jiang, S., & Schwartz, D. L. (2017). Minimal mask immobilization with optical surface guidance for head and neck radiotherapy. *Journal of Applied Clinical Medical Physics*, *19*(1), 17–24. https://doi.org/10.1002/acm2.12211

140. Gopan, O., & Wu, Q. (2012). Evaluation of the Accuracy of a 3D Surface Imaging System for Patient Setup in Head and Neck Cancer Radiotherapy. *International Journal of Radiation Oncology*Biology*Physics*, *84*(2), 547–552. https://doi.org/10.1016/j.ijrobp.2011.12.004

141. Li, G., Lovelock, D. M., Mechalakos, J., Rao, S., Della-Biancia, C., Amols, H., & Lee, N. (2013). Migration from full-head mask to "open-face" mask for immobilization of patients with head and neck cancer. *Journal of Applied Clinical Medical Physics*, *14*(5), 243–254. https://doi.org/10.1120/jacmp.v14i5.4400

142. Wei, W., Ioannides, P. J., Sehgal, V., & Daroui, P. (2020). Quantifying the impact of optical surface guidance in the treatment of cancers of the head and neck. *Journal of Applied Clinical Medical Physics*, *21*(6), 73–82. https://doi.org/10.1002/acm2.12867

143. GE Reports, *Discovery RT Designed to Improve Accuracy for Radiation Therapy Planning.* (2015). Recovered in 2022 from: https://www.genewsroom.com/press-releases/discovery-rt-designed-improve-accuracy-radiation-therapy-planning

144. Elekta, *Elekta Versa HD™ - Our most advanced & versatile platform making SRS & SBRT easy.* (2020). Recovered in 2022 from: https://www.elekta.com/radiotherapy/treatment-delivery-systems/versa-hd/

145. HexaPOD™ evo RT System; iGUIDE® 2.2 User Manual P10603-928; iGUIDE 2.2.2 Elekta. © 2017 Medical Intelligence Medizintechnik GmbH.

146. Elekta, *XVI.* (2020). Recovered in 2022 from:https://www.elekta.com/radiotherapy/treatmentsolutions/imaging/xvi/?utm_source=xvi&utm_medium=redirect&utm_campaign=redirects

147. Catalyst User's Guide © 2019 C-RAD Positioning AB

148. ModusQA. *State-of-the-art breathing simulator using patient respiratory waveforms.* (2020) Recovered in 2022 from: https://modusqa.com/motion/phantom

149. Russo, M., Owen, R., Bernard, A., Moutrie, V., & Foote, M. (2015). Evaluation of accuracy and reproducibility of a relocatable maxillary fixation system for fractionated intracranial stereotactic radiation therapy. *Journal of Medical Radiation Sciences*, *63*(1), 41–47. https://doi.org/10.1002/jmrs.142

150. *QUASAR™ Penta-Guide Phantom*. (2022). Modus Medical Devices. Retrieved 2022, from https://modusqa.com/products/quasar-penta-guide-phantom/

151. The British Institute of Radiology (2003). Geometric Uncertainties in Radiotherapy: Defining the Planning Target Volume. London: BIR.

152. Cerviño, L. I., Pawlicki, T., Lawson, J. D., & Jiang, S. B. (2010). Frame-less and mask-less cranial stereotactic radiosurgery: a feasibility study. *Physics in Medicine and Biology*, *55*(7), 1863–1873. https://doi.org/10.1088/0031-9155/55/7/005

153. Klein, E. E., Hanley, J., Bayouth, J., Yin, F. F., Simon, W., Dresser, S., Serago, C., Aguirre, F., Ma, L., Arjomandy, B., Liu, C., Sandin, C., & Holmes, T. (2009). Report No. 142 - Task Group 142 report: Quality assurance of medical accelerators. *Medical Physics*, *36*(9Part1), 4197–4212. https://doi.org/10.1118/1.3190392

154. Barber, J., Sykes, J. R., Holloway, L., & Thwaites, D. I. (2016). Comparison of automatic image registration uncertainty for three IGRT systems using a male pelvis phantom. *Journal of Applied Clinical Medical Physics*, *17*(5), 283–292. https://doi.org/10.1120/jacmp.v17i5.6332

155. Swinnen, A. C. C., Öllers, M. C., Loon Ong, C. & Verhaegen, F. (2020). The potential of an optical surface tracking system in non-coplanar single isocenter treatments of multiple brain metastases. *Journal of Applied Clinical Medical Physics*, *21*(6), 63-72. https://doi.org/10.1002/acm2.12866

10. Appendix

Protocol for SRS Treatment with Catalyst HD

1. Daily Check and Routine QA

Purpose: The purpose of the quality assurance (QA) procedure is to align the Catalyst HD system to the radiation isocenter by aligning the routine QA phantom using verification imaging (MV/kV). The results are saved in the “Routine QA History” and can be viewed in Advanced mode. The routine QA is performed in two steps.

1. The first step is to align the three Catalyst cameras to the same coordinate system. The procedure for this step is the same as for a standard **Daily Check** using the daily check device and the room lasers.
2. In the second step the final adjustment of the Catalyst coordinate system is performed. This is accomplished by aligning the routine QA phantom using a reference image of the phantom and verification imaging (MV/kV). The frequency of the performed QA procedure is defined by the user. The QA of the linac verification imaging systems is recommended to be performed before the routine QA of the Catalyst system. If a patient synchronization event occurs during routine QA, that in a normal workflow would had send the user to c4D Welcome screen, c4D stays in the current routine QA workflow and an information dialog is displayed to the user.

Preparation: It is recommended to use a CT image of the routine QA phantom as a reference data set. In order to create such reference data set, the phantom is scanned with a conventional CT scanner using a slice thickness of high resolution, 1 or 1.5 mm. The CT data set is then sent to the treatment planning system, where the isocenter is carefully located and marked at the geometrical center of the cube. A QA plan is then created in the record and verify system and the reference image set including the structure and beam data is sent there. It is crucial to have the isocenter marked correctly in the reference data set.

Daily check can be performed by using the Daily Check device specially designed for this purpose. Make sure the Daily Check device is in a horizontal position, by adjusting the screws and checking the spirit levels. For the **Daily Check** device of model **HZ-023** perform the steps followed bellow:

1.1. Place the Daily Check device in the correct position and align the side marks on the device to the room laser.

1.2. Align the lines at the center of the spheres to the vertical room laser.

1.3. Restart c4D by selecting the "**Exit**" button in the Welcome screen. If you are an advanced user select "**Exit**" in Advanced mode.

1.4. Log on to the system as a clinical user by entering a username and a password. Select "**OK**".

1.5. Click on the symbol for "**Daily Check**" in the Welcome screen.

1.6. Select "**Check**" or press button "**Scan**" on the remote control to start the daily check.

1.7. Initially a test is performed to ensure the scanner's linearity. A progress bar indicates the progress of the operation.

1.8. The device is then scanned. The scan is automatically repeated five times to ensure highest possible accuracy. A progress bar indicates the progress of the scanning and algorithm calculation. The information displayed is:

- **Current deviation** - the system drift since the previous daily check or routine QA if a routine QA has been performed.
- **Total deviation** - the total drift since the last isocenter adjustment.
- Result:
  o **Daily Check OK** - the deviations are within the tolerance.

  o **Daily Check Outside Tolerance!** - highlighted in red if the deviations are outside the tolerance.

  o **Object not recognized!** - highlighted in red, if the object is not recognized. Make sure that you have the correct object and that the whole object is visible in the scanned image.

- **Accepted Deviation** - the tolerance values for the different deviations.
- **Last Daily Check** - date and time for the last Daily Check.

1.9. Specific information for Catalyst HD.

- The daily check is performed for all three cameras at the same time. A summary of the result is presented.
- To see the detailed result, select the different cameras one at the time (Left, Mid and Right).

1.10. Select "**Save**" to accept the Daily Check result. Depending on your calibration routine one of the following options will occur:

- Only daily Check relative the room lasers is used: The Daily check result is saved and will be used to align the Catalyst coordinate system to the isocenter and thereby compensate for any hardware drift. The result is saved in the "**Daily Check history**".

- A Routine QA relative radiation isocenter has been performed (only possible with Catalyst HD): The Daily Check result is saved but will not be used to align the Catalyst coordinate system. The last performed Routine QA is used for the alignment of the Catalyst system.

Select "**Cancel**" if you don't want to compensate for the drift with the current result. This may be the case when the current and total deviations are less than 0.5 mm which can be caused by the manual placement of the Daily check object. We recommend you to always press "**Save**" and compensate for any hardware drift when current and total deviations exceeds 0.5 mm.

If the result is out of tolerance you should perform the following steps.

1.10.1. Make sure that the object is properly aligned according to the room lasers and press “**Check**” again to calculate a new result.

1.10.2. If you are still out of tolerance make sure that the room lasers are calibrated and redo the Daily Check procedure.

1.10.3. If step 1 and 2 is performed but the result remains out of tolerance you should select “**Save**” to save the result. This will guarantee that you have the proper conditions to receive the best accuracy.

1.10.4. If you are using the Daily Check procedure in combination with Routine QA you need to redo the Routine QA to compensate for the result.

1.10.5. If the result is the same the next day you should contact the personnel authorized by C-RAD Positioning AB.

1.11. After selecting “**Save**” to accept the Daily Check result, the step for the radiation isocenter alignment in then presented.

1.12. Align the **Routine QA** phantom to the radiation isocenter by using verification imaging (MV, CBCT or kV). Adjust the couch according to the result.

1.13. Press "**Check**" when phantom is in the final position.

1.14. The deviation between the alignment to the room lasers and the alignment to the isocenter is presented.

1.15. Depending on the accuracy of the couch it could be a small difference between the optimal position according to verification imaging and the final position of the phantom after the couch adjustment. The difference is typically within **0.5 mm**, depending on the accuracy of the couch. If this is the case, you have the possibility to correct for this setup error. To do this follow the steps below:

- **a.** Acquire new verification images (MV, CBCT or kV) and match the images. Do not adjust the couch.
- **b.** Select "Add kV or MV couch correction".
- **c.** Enter the residual couch correction according to the verification imaging system and press "OK".
- **d.** The total deviation is the difference between the calculated deviation (from step 1.13 and the residual couch correction.

1.16. Press "**Verify**" to visually see the resulting correction. The Catalyst system is compensating the acquired images according to the final result.

1.17. Select "**Save**" to use the compensation. To cancel the alignment according to the verification imaging press "**Cancel**". Only the Daily Check procedure using the room lasers will then be used.

2. Patient Selection

The patient selection can be performed with R&V system or manually.

2.1. Patient Selection with R&V System

2.1.1. A patient and a field are selected in the external system. The Catalyst system verifies that the patient details from the external system correspond with information found in the Catalyst system.

2.1.2. A window for pre-setup is displayed, see section Pre setup for information about the next step in the workflow.

2.2. Select Patient Manually

2.2.1. From the Welcome screen you can proceed with the step for selecting a patient manually.

2.2.2. Click on the symbol  to select a patient manually.

2.2.3. A window with available patients is shown.

2.2.4. You can change the selected room or choose to display the patients for all room. If you change your choice of room the patient list will be updated.

2.2.5. The patient list can be sorted by Patient ID and Patient Name. The selected sorting with be used next time you enter the manual patient selection.

2.2.6. Select the desired patient and press “**OK**”.

2.2.7. A window for the “pre-setup” is displayed, see section Pre setup for information about the next step in the workflow.

3. Patient Pre-setup for SRS Workflow

3.1. A window for the “**pre-setup**” is displayed. On the screen you can see information about the patient's identification, name and site. Make sure the information is in compliance with the current patient.

3.2. The following information is specific for the SRS workflow:

- Treatment type: SRS TREATMENT
- Time for last performed Routine QA. A Routine QA must be performed prior to a SRS treatment. The maximum allowed time since last completed Routine QA is four hours.

3.3. If the time since the last performed Routine QA is exceeding four hours it is not possible to proceed with the Setup or Treatment step. The text "RQA has not been performed" is displayed in red and the pop-up message ‘’SRS Treatment cannot proceed, please Perform RQA before SRS Treatment’’ is presented.

3.4. Coarsely positioning the patient for the scheduled treatment. The screen shows the steps in the workflow, pre-setup, setup, treatment and summary of results. Selectable steps in the workflow is shown in yellow. The current step is shown in green. You cannot choose the steps in the workflow that are dimmed. You can choose to go forwards and backwards in the workflow.

Depending on whether the patient is configured for Position, Motion and/or Respiration various steps are selectable.

- Only the "**Setup**" is optional if the patient is configured for Position.
- Only "**Treatment**" is optional if the patient is not configured to Position but Motion and / or Respiration.

3.5. Check camera settings - a reminder to verify that the camera settings are optimal for the patient. Before each SRS treatment check that the settings are optimal for the patient. This can be done by pressing the "**Settings**" button.

3.6. The settings view is presented.

3.7. Specific for SRS treatments:

o **Scan volume** - adjust the scan volume to only include the opening of the mask.

o **Edit Reference** - If a CT image has been imported as Position reference use the "Edit reference" function to crop the Position reference to include a surface as similar as possible to the opening of the mask.

o **Camera settings** - For treatments involving non-coplanar fields it is important that the camera settings are equivalent for the three cameras. Always use the predefined levels if possible.

Note! If the exposure time setting is very high, the update rate of the 3D surface images will be slower.

Select the cameras Left/Mid and Right one at the time and inspect the surface and image view (for overexpose and underexpose indication). If required adjust the camera settings one at the time. For the mid camera, it is sometimes required to rotate the couch to set the camera settings. Make sure that the surface is not overexposed, see examples below.

o **Optimal settings** - no or very small red (overexposed) and blue (underexposed) areas in the relevant section of the camera image.

o **Overexposed** - Red areas in the camera image (overexposed). If this is the case you should decrease the time and/or gain. Start by decreasing the time.

o **Underexposed** - Blue or dark areas in the camera image (underexposed). If this is the case, you should increase the time and/or gain. Start by increasing the time.

The settings for Registration HD and target result in submillimeter are always selected for SRS treatments type and is not possible to unselect. Averaging from 1 second can be used to reduce the noise in the image. A time of 2-3 seconds is recommended.

4. Patient Positioning for SRS Workflow

Specific for SRS patients is that the image is scanned with high image resolution. The patient has been selected manually or via synchronization and one of the following cases has occurred:

- During the step of pre- setup, you have chosen to proceed with the next step “Setup”. This requires that the patient is configured for the Position module.
- While in Setup, a field of another Site within a Site Group is loaded and the Sites of the corresponding fields have the same Frame of Reference, Patient Position, Isocenter position and are configured for the same application modules and Beam Control Settings.

During the positioning step the gating box (Response control module) indicates that any beam radiation is on hold. It is not possible to disable the gating box (Response control module) during the Setup step.

Follow the steps below to perform positioning:

4.1. A window for positioning is displayed. The continuously measurement of the patient’s surface is started. On the screen, and projected on the patient, you can see the latest positioning result. This result is based on the current reference image. The description of the current reference image is displayed on the screen. Catalyst continuously reads the current table coordinates from iCOM and the results are presented in absolute and relative coordinates.

The following information is displayed on the screen:

- **Reference image** – green colored. A new reference image can be taken by clicking the camera button. This image will be used as reference for this- and the upcoming fractions.
- **Distance map** – The live image is colored by how the patient's posture should be corrected.
  - o **No Color** - the area is in the correct position.
  - o **Highlighted in yellow/red** – The area should be moved in the direction from the area marked in red to the yellow.
- **Target/isocenter correction**, shown as follows:
  - o Target visualized in the form of a sphere. The correct position according to the reference image is displayed with a black sphere and the current position is shown with a green sphere if the result is within the tolerance and with a red sphere if the result is outside tolerance.
  - o Suggested absolute correction / absolute couch coordinates

    Lat – Lateral translation (mm/cm)
    Long – Longitudinal translation (mm/cm)
    Vert – Vertical translation (mm/cm)
    Rot – Rotation around the z-axis (°)
  - o Suggested relative correction – if any value is outside the tolerance it is highlighted in red.

    Lat – Lateral translation (mm/cm)
    Long – Longitudinal translation (mm/cm)
    Vert – Vertical translation (mm/cm)
    Rot – Rotation around the z-axis (°)
    Roll – Rotation around the y-axis (°)

Pitch – Rotation around the x-axis (°)

Note! The correction must be performed in the same order as shown on the screen. Start with the translation corrections. You can perform the translations of the couch in any order you want. You can then adjust for the rotations. Start with "Rot" followed by "Roll" and then "pitch".

o If the expected accuracy of target correction calculation is not obtained the text "Out of range" is displayed and the result is presented in gray color.

o If the system detects unexpected movements the result is calculated in a high speed mode. The correction result is then displayed with a grey color. See section Target result during unexpected movements for more information.

Note! If possible, always make sure that no warning for movements is displayed when you continue to treatment mode.

The information projected onto the patient is:

- **Distance map** – The current position is colored by how the patient's posture should be corrected.

  o **No Color** - the area is in the correct position.

  o **Highlighted in yellow/red** – The area should be moved in the direction from the area marked in red to the yellow. See separate section for example.

- Point / line - shows how a point should be moved to get into the correct position. When there is a posture error a line colored from red to yellow is displaced onto the patient. The yellow end of the line shows the accurate location and the red end of the line the current position. When the patient posture is correct, points instead of lines are projected onto the patient. (This information is optional).
- Suggested relative correction. The same information is also presented on the screen. (This information is optional.)
- Progress bar for the high precision calculation (This information is optional.)
- The boundaries of the reference are projected on the patient with a green color (This information is optional.)

4.2. Adjust for the patient's posture by following the distance map projected on the patient.

4.3. Adjust the treatment couch according to the correction.

- If you have Couch Control with Mosaiq enabled use the following procedure to adjust the treatment couch: Press the "**Adjust couch**" button. The couch correction will be sent to Mosaiq Couch Control. It is not

possible to adjust the couch in the same time as an unexpected movement is detected. When

all values are within tolerance the treatment button is activated and you can proceed to treatment.

- If you do NOT have Couch Control with Mosaiq enabled move the treatment couch to the proposed absolute coordinates.

4.4. As long as the patient's position deviates more than the set tolerance, it is not possible to proceed to treatment. Repeat the step 2-3 until all values are within tolerance. This activates the treatment button and you can proceed to treatment.

4.5. To end the positioning and move on without making the proposed adjustment of the patient's position press the symbol for override. A warning is displayed with the following message ''Are you sure you want to override?'' If you really want to move on choose "Yes", otherwise select "No".

4.6. Press the symbol for the treatment to proceed to the next step. If the Catalyst system detects unexpected movements when you select to continue to treatment mode a warning is displayed. Select "No" to remain in positioning mode and check the result. To proceed with treatment anyway, press "Yes".

4.7. Projection on the patient stops. The current positioning results are saved and a window for the treatment mode is displayed.

5. SRS Treatment

The patient has been selected manually or through synchronization with an external R&V/LINAC system. You have chosen to proceed with the treatment mode During treatment, it is possible to use the applications for both patient monitoring (cMotion) and respiratory gating (cRespiration), depending on your licenses and the patient configuration, one or both modules are active. For SRS patients, only the Motion application is usually selected for the treatment step. However, it is possible to use the Respiration application. If Respiration is used it is recommended to set a gating window to hold the beam if unexpected movements is detected (exception gating).

The following steps are specific for the SRS workflow:

5.1. The patient is scanned with high image resolution.

5.2. After setup correction with HexaPOD based on XVI verification imaging (kv/MV), reset the treatment step to create a new motion reference in the final treatment position.

5.3. To obtain the best accuracy the imaging system should be retracted on the Linac as much as possible. By retracting the imaging systems, it will be avoided the blocking of both Catalyst side systems at the same time when rotating the gantry.

5.4. The Catalyst system supports treatments with couch rotations. Each treatment field is associated with a specific couch rotation. The field is selected manually or with an R&V system. The selected field with corresponding couch rotation is displayed on the screen.

5.5. Perform the rotation of the couch.

5.6. Press "OK" in the dialog when the couch rotation is adjusted.

5.7. The motion and/or gating reference is rotated according to the rotation information on the selected field. An information dialog is displayed. Move the couch to the new rotation angle. During this time no result is presented in the graph. Any beam delivery is on hold if beam control with c4D is active.

5.8. The result is updated in the graph. If the Catalyst HD and the HexaPOD isocenter shifts are within 1 mm agreement in all translation axes proceed to beam delivery.

5.9. If the Catalyst HD and the HexaPOD isocenter shifts are >1 mm of agreement in all translation axes, proceed to HexaPOD manual correction and create a new Catalyst HD patient motion reference in the final treatment position for beam deliver

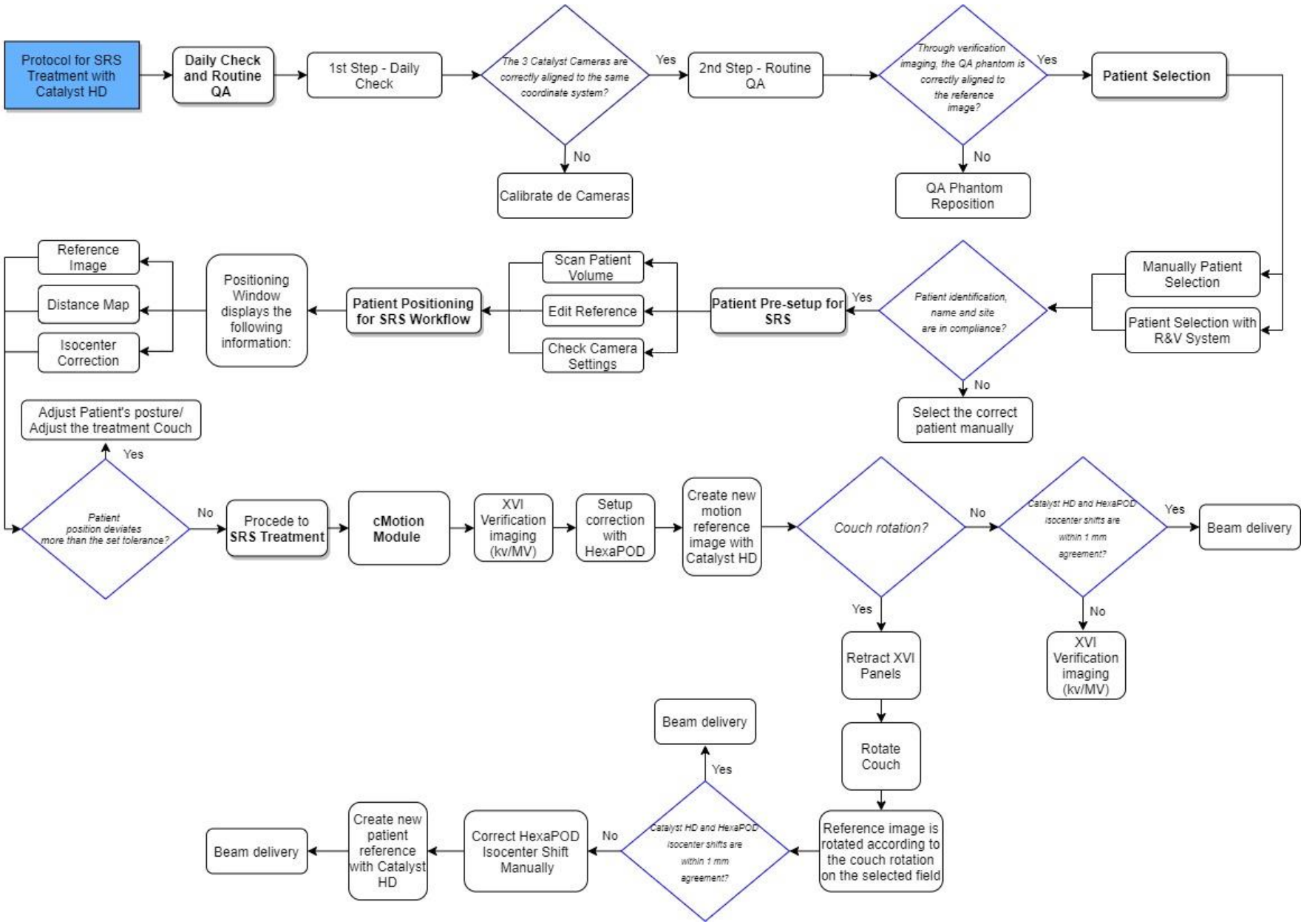
Protocol for SRS Treatment with Catalyst HD
Daily Check and Routine QA
1st Step - Daily Check
The 3 Catalyst Cameras are correctly aligned to the same coordinate system?
Yes
No
Calibrate de Cameras
2nd Step - Routine QA
Through verification imaging, the QA phantom is correctly aligned to the reference image?
Yes
No
QA Phantom Reposition
Patient Selection
Manually Patient Selection
Patient Selection with R&V System
Patient identification, name and site are in compliance?
Yes
No
Select the correct patient manually
Patient Pre-setup for SRS
Scan Patient Volume
Edit Reference
Check Camera Settings
Patient Positioning for SRS Workflow
Positioning Window displays the following information:
Reference Image
Distance Map
Isocenter Correction
Adjust Patient's posture/ Adjust the treatment Couch
Yes
Patient position deviates more than the set tolerance?
No
Procede to SRS Treatment
cMotion Module
XVI Verification imaging (kv/MV)
Setup correction with HexaPOD
Create new motion reference image with Catalyst HD
Couch rotation?
No
Catalyst HD and HexaPOD isocenter shifts are within 1 mm agreement?
Yes
Beam delivery
No
XVI Verification imaging (kv/MV)
Yes
Retract XVI Panels
Rotate Couch
Reference image is rotated according to the couch rotation on the selected field
Catalyst HD and HexaPOD isocenter shifts are within 1 mm agreement?
Yes
Beam delivery
No
Correct HexaPOD Isocenter Shift Manually
Create new patient reference with Catalyst HD
Beam delivery